Photo-physical Properties of Single Semiconductor Nanostructures Using Fluorescence Correlation Spectroscopy

A thesis

Submitted in partial fulfilment of the requirements

of the degree of

Doctor of Philosophy

by

A. V. R. Murthy

20083017

INDIAN INSTITUTE OF SCIENCE EDUCATION AND RESEARCH, PUNE

MARCH, 2014

DEDICATION

Mother, Father and Teachers

ఎవ్వని చే జనించు జగ మెవ్వని లోపల నుండు లీనమై
ఎవ్వని యందు డిందు పరమేశ్వరుడెవ్వడు? మూల కారణం
బెవ్వ? డనాది మధ్య లయుడెవ్వడు సర్వము తానె యైన వా
డెవ్వడు వాని నాత్మ భవు నీశ్వరు నే శరణంబు వేడెదన్

"Who is the reason for the creation, process and destruction, who can control the entire world, who is omnipresent, who is everything, who is the past, present and future; I adore myself to him"

CERTIFICATE

Certified that the work incorporated in this thesis entitled **Photo-physical Properties of Single Semiconductor Nanostructures Using Fluorescence Correlation Spectroscopy** submitted by **A. V. R. Murthy** was carried out by the candidate, under my supervision. The work presented here or any part of it has not been included in any other thesis submitted previously for the award of any degree or diploma from any other University or institution.

Dr. Shivprasad Patil

Supervisor

DECLARATION

I declare that, this written submission represents my ideas in my own words and where other's ideas have been included, I have adequately cited and referenced the original sources. I also declare that I have adhered to all principles of academic honesty and integrity and have not misrepresented or fabricated or falsified any idea / data / fact / source in my submission. I understand that violation of the above will be cause for disciplinary action by the Institute and can also evoke penal action from the sources which have thus not been properly cited or from whom proper permission has not been taken when needed.

A. V. R. Murthy

20083017

ACKNOWLEDGEMENTS

This thesis would have not been in its current shape without the help and support of many individuals whom I have met during my PhD. I would like to take this opportunity to thank each and every individual.

First of all, I am very grateful to my supervisor Dr.Shivprasad Patil for his continuous help and support throughout my Ph.D. I should specially thank him for the freedom and independence that he provided in the lab and work. I have enjoyed most of the time in the lab. The unique opportunity that I have got here is active involvement of lab setting.

Apart from my supervisor, I must mention special thanks to an inspiring personality whom I have met- Dr. Sudipta Maiti. I would like to mention a Chinese saying before I acknowledge him "Give a man a fish and he will eat for a day. Teach a man to fish and he will eat for a lifetime." to convey my deep sense of gratitude. I should thank him to teach me the FCS technique on which this thesis stands today.

I would like to thank our collaborators. Prof. M.Jayakannan and Dr. Shouvik Datta. I would like to thank my student friends Mahima and Padmashri who have initiated this successful scientific collaboration.

I thank my RAC members- Dr. Umakant Rapol and Dr. Girish Ratnapharki for their support. I am also thankful to many of the first phase of IISER faculty who are my well wishers irrespective of the scientific commons. I can only mention some of the people like Dr. T.S.Mahesh, Dr.V.G.Anand, Dr. Pavan Kumar, Dr.Sudarshan Ananth and many others. I am thankful to Prof. K. N. Ganesh for providing academic and residential facilities at IISER. I thank Dr. V. S. Rao for all his help whenever I needed, be it academic or non-academic. I am highly grateful to IISER for the graduate fellowship that I received during my PhD.

I also thank all my lab members Vinod, Arpit, Karan, Vibham and Amandeep with

whom I have interacted and shared my experiences. It is really inspiring and refreshing experience to attend FCS workshops at various places in India. I also thank Department of Science and Technology(DST) to sponsor my visit to Berlin to attend the Single Molecule Spectroscopy Workshop.

Other than the Lab, I had a really comfortable stay at IISER. I thank all friends, physics friends and especially 2008 batch mates. I thank Arthur, Arun, Somu, Kanika, Padu and Mayur for their friendly support and encouragement. I am especially thankful to my cooking partners Arthur, Resmi, Padmashri, Ramya, Anuradha and many other friends occasionally joined with me in cooking. I should express my deep gratitude to Tamil mess for providing undisturbed meals. Other than department, I have to thank many people like Amar, Harsha, and many other Telugu friends, Gopal, Satish, Ganesh, Pranith.

I am very lucky to have found my life partner Shweta at IISER who is also my wife now. Her continuous cooperation in the second half of my Ph.D life has really helped me in completing my thesis.

I thank my teachers, Sri K.V Subbarao, Sri N. Madhusudana Rao and Prof. G. Markendayulu who are my "Gurus" and ever inspiring for me throughout my life. I thank all my long-time and long-distance friends- Vijay, Satya, Satish, Pavan, Srikant, Ravi, Uma and many other friends for their support and encouragement. Conversations were always cheerful and motivating with them.

My research career would have not been possible without the active support of my family. I thank my mother, father and brother for their love, support and encouragement throughout all the time.

A.V.R.Murthy

Abstract

Tuning photophysical properties of luminescent semiconductor nanostructues is crucial for their device applications. In nano scale, the electrical and optical properties are highly sensitive to the size due to quantum confinement of electrons in nanostructures. This led to various technological applications and boosted the field of nano science in the past years. Novel synthesis methods of inorganic, metal and organic nanostructures have offered excellent control on size, composition, and crystal structure, surface chemistry increased range of their applications. Currently, they are used in light-emitting diodes, photo-voltaics, sensors/biosensors, nano-electronics and nano-photonics.

Quantum Dots (QDs) are semiconductor nano materials composed of groups II-VI or III-V elements (e.g. PbS, CdTe). They are defined as particles with physical dimensions smaller than the exciton Bohr radius. At this smaller size, quantum confinement effects in QDs plays a key role and gives rise to unique optical and electronic properties. This offers numerous advantages in influencing fluorescence behavior, and therefore in bio-labeling applications. The broad excitation spectra, narrow emission spectra and the photo-stability of QDs allows using as FRET pairs and fluorescent markers.

Similarly, the field of π-conjugated polymers which are organic semiconductor materials has developed parallel to inorganic and metal nanotechnology and has led to major advances in device applications. The fundamental understanding of their diverse electronic, optoelectronic, and photonic properties played a key role in this field by enabling their applications. Understanding the photo-physical properties of the organic semiconducting materials has led to development of organic light-emitting diodes (OLEDs) for colorful display technology, photo-voltaics and for solar energy applications.

Despite of their several advantages, QDs lack the fundamental understanding of some optical properties. For example, fluorescence intermittency or "blinking"' is most common

property in many of the QDs and limits their applications for single molecule studies such as biomarkers. Similarly, in conjugated polymers, molecular aggregation, conformational changes in various solvent conditions play key role limits their applications.

We have addressed the above mentioned problems using a single molecule technique Fluorescence Correlation Spectroscopy (FCS) and presented in this thesis. Chapter 1 presents the motivation to this work and need to address such problem. Chapter 2 explains the importance of single molecule technique like FCS along with theory and applications. It also provides the complete instrumentation of the home built FCS setup used for these studies. In Chapter 3, we present the photo-luminescence blinking effects in QDs, and estimation of photo darkened fraction and photo darkening probability of QDs. In Chapter 4, we present the work about the diffusion dynamics of conjugated polymers and role of the chain length in molecular aggregation. Finally, we present development of an experimental technique by combining the FCS with Electrostatic Force Microscopy to directly measure the relationship between the photo ionization and photo darkening along with other future plans.

Contents

List of Figures

List of Tables

Chapter 1

Introduction

1.1 Motivation

Technology has played a key role in revolutionizing the human civilization. From telephones to mobile phones and smart phones, from type-writers to computer and laptops, almost all the fields have been transformed to a superior and advanced stage from their inception. These technological revolutions have resulted in remarkable improvement in the quality of life and have eventually led to the transformation of the human society. The human curiosity is continuing to develop better technologies. Today, nanotechnology has a great impact in almost every sector and believed to be the next stage of technological revolution. Since nanomaterials possess unique chemical, physical and mechanical properties, they can be used for a variety of applications[1]. As name suggests the dimensions of these materials are typically from 1-10 nm. At this scale, the properties of the materials drastically differ from their bulk properties. Nanomaterials appears in different forms and can be classified as zero dimensional(0D), one dimensional(1D), two dimensional(2D), and three dimensional(3D) structures. Common types of nanomaterials include nanotubes, nanorods(e.g.carbon nanotubes), nanoparticles(e.g. metallic and semiconductor), and fullerenes[2].

Semiconductor nanomaterials are class of materials with interesting electrical and optical properties as compared to conventional bulk materials. Narrow and intense emis-

sion spectra, continuous absorption bands and photo-stability are attractive properties of these nanomaterials. Various synthesis methods and strategies have helped in improving the photophysical properties of these semiconductor nanoparticles. For example, spatial quantum confinement effect results in significant change in optical properties of semiconductor nanomaterials. The effect of high surface-to-volume ratio on physical and chemical properties of the semiconductor has major influence on their optical and surface properties. As a result, semiconductor nanomaterials are in the focus of research from last 20 years and have attracted significant interest in diverse disciplines such as solid-state physics, physical chemistry, colloid chemistry, materials science, engineering and recently in biological sciences. The electrons and holes in semiconductor nanomaterials primarily govern the electrical and optical properties and are largely affected by the size, shape, and geometry [3, 4, 5]. The specific surface area and surface-to-volume ratio increases dramatically as the size of material decreases and affects the photophyscial properties. Parameters such as size, shape, and surface characteristics can be varied to control their properties for different applications [6, 7]. These novel properties of semiconductor nanomaterials have given rise to emerging technologies such as nanoelectronics, nanophotonics, biophotonics, imaging and sensor devices, solar cells.

Among nano-structures semiconductor nanocrystals, also known as Quantum Dots (QDs), are light absorbing luminescent nanoparticles with size tunable emission properties. These nanocrystals are typically in the size range of 2-8 nm in diameter and are formed by II-VI and III-V elements in the periodic table. Due to smaller size of QDs (which is below their Bohr exciton radius) they exhibit quantum confinement effects. Their excitonic wave functions are confined in all three spatial dimensions and hence QDs show dramatic consequences in their electronic properties. Below a certain size, properties of semiconductors are significantly different from their bulk counterparts and resemble those of single molecules. QDs are also called as artificial atoms because of their discrete energy levels, similar to that of atoms, and exhibit the unique optical properties. This makes it possible to optically excite a broad spectrum of quantum dot and tune the emission wavelength. This offers QDs for many potential applications [8, 9, 10].

Quantum dots were first discovered by A. Eklimov et al. in early 80s [11, 12, 13]. For the first time, they had provided theoretical and experimental description of quantum confinement in three dimensions in semiconductor nanocrystals. The word "Quantum Dot" was first coined by Reed et al. due to the electronic transport in three dimensional confined quantum well [14]. In 1990s, Murray et al., had shown a new method to synthesize highly mono dispersed CdSe quantum dots [15]. Later, Margret et al. synthesized the strongly luminescent ZnS-capped CdSe quantum dots with a stable band-edge luminescence and 50 percent quantum yield at room temperature[16]. Since then, various new protocols are used to synthesize different quantum dots with high luminescence quantum yield which are also commercially available[17, 18].

π-conjugated polymers,known as conducting polymers, are another class of semiconductor nanomaterials for light emitting and photovoltaic applications. The discovery of first conducting polymer (polyacetylene) was in 1970s. It was found that polyacetylene exhibits increase in electrical conductivity when exposed to halogen vapor [19]. Since the discovery of conjugated polymers, this class of materials have gained a lot of attention due to their wide applications. The conductive nature, electro-luminescence properties or light-induced charge generation, of these polymers made them a suitable choice in applications such as wide displays, photovoltaics, solar cells and sensors

In 2000, Alan Heeger, Alan MacDiarmid, and Hideki Shirakawa won the Nobel Prize in chemistry for their discovery of conducting polymers. After their pioneering work, several conjugated polymers were developed including polythiophene, polypyrrole, poly(paraphenylene), polyaniline, poly(phenylene vinylene), polyfluorene etc [20]. The conjugated polymers are a modern class of organic materials with good conductivity. Advantage of organic polymer materials is that they exhibit metallic conductivity along with retaining properties of plastics such as mechanical flexibility, easy processing and low production costs. They behave like semiconductors in their neutral state and exhibit increased conductivity upon oxidation or reduction. As a result, they have received

considerable technological attention, leading applications in sensors, organic field effect transistors (OFETs), organic photovoltaic (OPV) devices and organic light emitting-diodes (OLEDs) [21, 22, 23]. Among many conjugated polymers, Poly-(para-phenylene) vinylene (PPV) and its derivatives are widely studied polymers for their semiconducting and luminescent properties. Within this class of PPVs, poly(2-methoxy-5(2-ethylhexyl)-1,4-phylenevinylene) (MEH-PPV) is extensively studied polymer as it has important characteristics like enhanced solubility in common solvents, easy processing and better luminescence which makes it favorable for device fabrication [24].

Despite many advantages, some of the basic properties of these semiconductor nanostructures are still far from understood. Discontinuous and random emission of light from single fluorescent species is called fluorescence intermittency or "blinking". This is commonly observed in almost all QDs and not yet understood [25-28]. Quantum dot blinking was traditionally believed to be the result of a light-induced charging process. When the electron is photo excited it enters the surface trap state and leaves QD charged. It was thought that, the the charged QDs are responsible for fluorescence intermittency resulting in low quantum yield. However, there is no clear picture yet about what is the mechanism of blinking in QDs? How to control and quantify this blinking behavior? Addressing such questions can shed light on fundamental photophysical properties of QDs. This will enable QDs not only for a better bio-labeling and imaging applications, but also for solar and QD laser technologies. Similarly, in conjugated polymers, it is not known how chain morphology affects the molecular aggregation process and what is its effect on the photo-physical properties. Understanding how the chain length dynamics alters photo-physical properties, molecular aggregation and conformational morphology can provide new insights about these polymers which enable better device applications.

The difficulty in addressing such issues of individual semiconductor nanostructures is that, these properties are masked or become indeterminate in its bulk form. Hence, the bulk measurements or ensemble averaged measurements cannot effectively sense and distinguish these properties. But, blinking behavior in QDs or a polymer chain mor-

phology becomes a serious concern in single molecule scale where one or a few of them are used. Therefore, it is necessary to use single molecule techniques to understand the photophysical properties of single semiconductor nanostructures. Single molecule fluorescence technique like Fluorescence correlation spectroscopy (FCS) can be used to address these problems of semiconductor nanomaterials.

Fluorescence correlation spectroscopy (FCS) is a noninvasive detection technique that can measure the fluorescence fluctuations from single particles. Statistical analysis of fluorescence fluctuations can provide important information about the emitting species. FCS can measure the average number of luminescent particles in the detection volume and their diffusion coefficient. Also, the average luminescence intensity and the Per Particle Brightness (PPB) can be measured based on count rate and the number of bright particles [29, 30]. As a result, the use of FCS offers an unique opportunity to study changes in photo-luminescence on the surface properties as well as morphology in semiconductor nanostructures.

The concept of fluorescence correlation spectroscopy (FCS) emerged in the early 1970s and has been used to measure the rate kinetics and diffusion dynamics [31, 32]. After Rigler et al. adopted the confocal detection system; this technique has reached to single molecule sensitivity and gained importance in many fields [33]. Conventionally, FCS is used to study the diffusion, size, aggregation and chemical kinetics in bio-macro-molecules and similar studies in materials science as well. Here we explored the single molecule sensitivity of the FCS to address the important aspects of single semiconductor nanostructures.

As mentioned earlier, quantum dots suffer from fluorescence intermittency called "blinking". This blinking behavior depends on many parameters like excitation intensity, size of the QD, surface chemistry and defects, local vicinity and temperature [27]. All of these quantities can influence the photo-luminescence and emission quantum yield of a single QD. However, a systematic study of this blinking behavior in QDs can be addressed by single molecule techniques such as FCS. Similarly, role of the molecular

weight (or chain length) in aggregation process of conjugated polymer can be addressed using a narrow molecular weight distributed polymers and by FCS technique. We have addressed the above mentioned problems using Fluorescence Correlation Spectroscopy (FCS) and presented in this thesis.

1.2 Scope of the thesis:

Understanding various photophysical properties of single semiconductor nanostructures requires a sensitive single molecule detection technique. Here we have employed FCS technique to address the above mentioned problems. Chapter 2 presents background and theory involved in FCS measurements and interpretation along with special cases. We further describe the technical requirements and experimental realization of our home-built FCS set up. Unlike conventional application of FCS as a diffusion measurement tool, we have used FCS to investigate the blinking dynamics of single QDs. We have also measured molecular aggregation in conjugated polymers.

The interaction of light with semiconductor quantum dots is a central process that determines its use in variety of applications such as single quantum dot lasers, photo-voltaic cells and a biomarker. It is well established fact that photo-luminescence from a single quantum dot exhibits intermittency known as "blinking". Addition of thiols such as Dithiothreitol (DTT) or β-mercaptoethanol (BME) is known to suppress blinking. The physical origin of blinking as well as its suppression is not understood yet.

In chapter 3, we present measurement of fraction of photo-darkened CdTe quantum dots in aqueous solution due to blinking. We used FCS to measure number of luminescent quantum dots before and after addition of sufficient amount of BME to suppress blinking completely. This provides a new approach towards measuring photo-induced dark fraction in blinking QDs. Here, we describe methodology of this measurement. Further, from intensity dependence of this fraction we compute photo-darkening probability at band-edge photo-excitation ($\approx 10^{-6}$). We interpret the reaction rate used in conventional FCS

analysis as the electron transfer rate that causes "on-off" states of luminescence. We demonstrate that measurement of this rate can become a method to reveal the electron transfer mechanism in blinking QDs.

Conjugated polymers are emerging as an important class of materials due to their potential applications in electronic devices such as light emitting diodes, photo-voltaics, and field effect transistors. In general, π-conjugated polymers have a tendency towards aromatic π- stacking via inter- or intra-chain interactions, which leads to formation of micrometer- to nanometer- sized aggregated species. This aggregation depends on molecular weight or chain length. It is challenging to determine the aggregation dynamics in solution state.

In chapter 4, we describe the use of FCS and a fitting algorithm based on maximum entropy method to understand aggregation dynamics. We have studied the role of chain length in molecular aggregation in π-conjugated polymers. To measure dependence of chain length on aggregation of π-conjugated polymers, we used a standard polymer MEH-PPV (poly (2-methoxy-5(2-ethylhexyl)-1,4-phylenevinylene). We observed that longer chains form a self-collapsed conformation and diffuse faster, whereas shorter chains have larger inter-particle interaction and diffuse slowly.

In chapter 5, we describe our understanding of photophysical properties using FCS. We discuss some of the future plans such as measurement of photo-darkening probability in various core/shell QDs using FCS.

A long-standing hypothesis to understand "blinking" of single dots is called charging hypothesis. According to this hypothesis, the charged QD core stops emission of photons and becomes dark. The luminescence is retrieved when the core becomes neutral again. There is no direct experimental evidence confirming this hypothesis. A combination of FCS like measurement and Electric Force Microscopy (EFM) for the charge measurement on QDs under illumination is proposed.

Bibliography

[1] Textbook of Nanoscience and Nanotechnology by B.S.Murthy et al. Springer,2013 pp 107.

[2] Nano materials hand book by yury gogotsi, Taylor and Francis 2006.

[3] Iijima, S. Nature 1991, 354, 56.

[4] Alexander, E. Angew. Chem.Int. Ed. 2005, 44, 4839.

[5] Alivisatos, A. P. J. Phys. Chem. 1996, 100, 13226.

[6] Alivisatos, A. P. Science 1996, 271, 933.

[7] Li J.; Jin Z. Z. Coordination Chemistry Reviews, 2009, 253,3015.

[8] Burda, C.; Chen, X.; Narayanan, R.; El-Sayed, M. A. Chem. Rev. 2005, 105, 1025.

[9] Murray, C. B.; Kagan, C. R.; Bawendi, M. G. Annu. Rev. Mater. Sci. 2000, 30, 545.

[10] Chen, X.; Lou, Y.; Dayal, S.; Qiu, X.; Krolicki, R.; Burda, C.; Zhao, C.; Becker. J. Nanosci. Nanotechnol. 2005, 5, 1408.

[11] A.I. Ekimov, A. A. O. JETP Lett., 1981, 34, 309

[12] Al.L. Efros, A. L. E. Soviet Phys. Semiconductorsâ“USSR 1982, 16, 772.

[13] Rossetti, R., S. Nakahara, and L. E. Brus. J. Chem. Phy. 1983, 79, 1086.

[14] M. A. Reed, J. N. Randall, R. J. Aggarwal, R.J. Matyi, T. M. Moore, and A. E. Wetsel, phys.Rev.Letts.,1988, 60, 535.

[15] Murray, C. B., M. Nirmal, D. J. Norris, and M. G. Bawendi. Z. Phys. D: At. Mol. Clusters 1993, 26,231.

[16] Hines, M. A., and P. Guyot-Sionnest. J. Phys. Chem. 1996, 100, 468.

[17] Peng, Z. A., and X. Peng. J. Am. Chem. Soc., 2001, 123, 183.

[18] Reiss, P., J. Bleuse, and A. Pron. Nano Lett., 2001, 2, 781.

[19] Shirakawa, H.; Louis, E. J.; MacDiarmid, A. G.; Chiang C. K.; Heeger, A. J. J. Chem. Soc. Chem. Commun., 1977, 474, 578.

[20] Skotheim, T. A.; Reynolds, J. R. Eds.; Handbook of Conducting Polymers, 3rd ed., CRC Press: Boca Raton, FL, 2007.

[21] Perepichka, I. F.; Perepichka, D. F. Eds Handbook of Thiophenebased Materials, John Wiley Sons: Hoboken, NJ, 2009.

[22] Roncali, J. Chem. Rev., 1992, 92, 711.

[23] Monk, P.; Mortimer, R.; Rosseinsky, D. Electrochromism and Electrochromic Devices, Cambridge University Press, 2007.

[24] Rasmussen, S. C.; Ogawa, K.; Rothstein, S. D, Handbook of Organic Electronics and Photonics, H. S. Nalwa, Ed.; American Scientific Publishers: Stevenson Ranch, CA, 2008.

[25] J. Yao, D. R. Larson, H. D. Vishwasrao, W. R. Zipfel, W. W. Webb, Proc. Natl. Acad. Sci. (U.S. A.) 2005, 102, 14284.

[26] M. Nirmal, B.O. Dabbousi, M. G. Bawendi, J. J. Macklin and J. K. Trautman, T. D. Harris, and L. E. Brus, Nature 1996, 383, 802.

[27] M. Kuno, D. P. Fromm, H. F. Hamann, A. Gallagher, and D. J. Nesbitt, J. Chem. Phys. 2001, 115, 1028.

[28] K. T. Shimizu, R. G. Neuhauser, C. A. Leatherdale, S. A. Empedocles, W. K. Woo, and M. G. Bawendi, Phys. Rev. B, 2001, 63, 205316(1).

[29] N. Thompson, in: J.R. Lakowicz (Ed.), Topics in Fluorescence spectroscopy,Plenum, New York, 1991, 1, 337.

[30] O. Krichevsky, and G. Bonnet, Rep. Prog. Phys. 2002, 65, 251.

[31] D. Magde, E. Elson, W. W. Webb, Phys. Rev. Lett. 1972, 29, 705.

[32] D. Magde, E. Elson, W. W. Webb, Biopolymers 1974, 13, 1.

[33] R. Rigler, U. Mets, J. Widengren, P. kask Eur.Biophys.J., 1993, 22, 169.

Chapter 2

Fluorescence Correlation Spectroscopy: Theory and Instrumentation

2.1 Introduction

Fluorescence is widely used phenomena in many techniques in different branches of science such as biology, medicine, chemistry and material science. In today's research, fluorescence based microscopic and spectroscopic techniques are indispensable while addressing scientific problems. Information from a typical fluorescence cycle such as fluorescence intensity, lifetime, wavelength provides a meaningful insight into the material of interest. Traditionally, various fluorescence based techniques like fluorescence spectroscopy, life time measurement, fluorescence microscopy, Fluorescence Recovery After Photo-bleaching (FRAP) are often used for quantitative measurements. All of these techniques require sample in high concentration (above μM) and measurement is ensemble averaged or also called as bulk measurement.

Recently, fluorescence has been used in single molecule regime where fluorescence from single molecules are precisely measured to characterize the material of interest. Techniques like Fluorescence Correlation Spectroscopy (FCS), confocal imaging, Fluo-

rescence Lifetime Imaging Microscopy (FLIM) single molecule Fluorescence Resonance Energy Transfer (smFRET) are some of the single molecule techniques that are popularly used. Each technique have its own importance in research areas and has been applied to understand the fluorescence itself.

Fluorescence Correlation Spectroscopy (FCS) is one such fluorescence based technique that offers single molecule sensitivity and can be used to monitor diffusion dynamics of molecules. FCS allows measurement of diffusion and associated processes such as size, aggregation, binding rates. In this chapter, we discuss phenomenon of fluorescence, theoretical aspects of FCS, instrumentation of home-built FCS setup and its calibration, operation and its importance in understanding the photo-physical properties of semiconductor nanostructures.

Fluorescence: Luminescence is the property of the material to emit photons with lower energy upon absorbing the higher energy photons. This emission of light from substance occurs due to transition between the electronically excited state to ground state. Depending on the nature of the excited state, luminescence can occur in two ways and divided into two categories fluorescence and phosphorescence. In the excited singlet states, the electron in the excited orbital is paired (by opposite spin) with electron in the ground-state orbital. Consequently, return to the ground state (spin allowed) occurs rapidly by emission of a photon that is called radiative emission. This radiative emission is called "Fluorescence" and the time taken for this to occur is called the fluorescence lifetime(τ) which is typically in nano seconds. If the excited electron has the same spin orientation of the ground-state electron then transition to the ground state is forbidden. Therefore the excited electron emits light from triplet excited states with a very slow emission rate (10^3 to $100s^{-1}$). This phenomenon is called "Phosphorescence" and the lifetimes are typically milliseconds to seconds [1, 2]. The schematic of the fluorescence phenomena explained by the Jablonski diagram as shown in the figure 2.1.

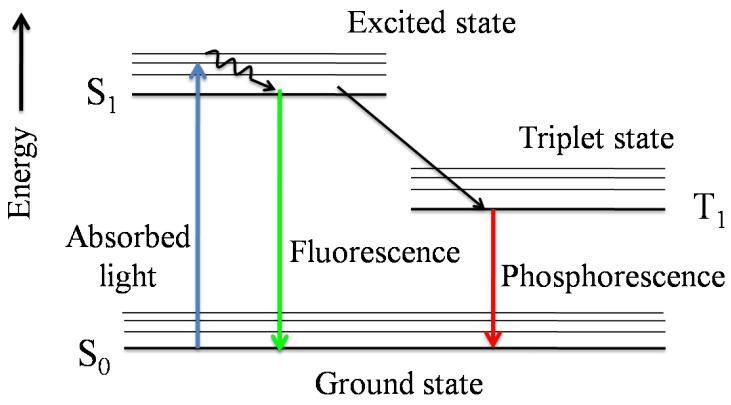

Figure 2.1: Jablonski Diagram

2.2 Fluorescence Correlation Spectroscopy

Fluorescence Correlation Spectroscopy (FCS) is a non-invasive technique to measure the diffusion coefficients based on fluorescence fluctuations in a small open volume under equilibrium conditions. At thermal equilibrium, particles or molecules in a medium have Brownian motion due to its thermal energy. Due to this, particles fluctuate freely in the medium. If the number of particles(N) are less then local fluctuations in N, then δN becomes a measurable quantity as $\delta N \propto 1/\sqrt{N}$. In FCS measurements, the fluorescence fluctuations can be measured by using dilute concentrations(nM) of the sample and using small detection volumes(fL). Therefore, FCS allows to compute the diffusion coefficient (hence size) from this Brownian motion. Here, we show the basic derivation of the autocorrelation fit that can be used to fit measured auto correlation of fluorescence intensities. These fit functions are different for variety of physical processes such as diffusion and chemical kinetics, transport[13]. The autocorrelation function of fluorescence fluctuations carries information about different dynamics of system at different time scales. Therefore, by choosing the appropriate model, different dynamics can be probed by its characteristic time scale. For example, diffusion dynamics, chemical rate kinetics having different time scales can be identified by FCS.

FCS was invented by Webb, Elson, Magde in 1972 to monitor the binding and unbinding rates of Ethidium Bromide(EtBr) to DNA [3-6]. From its inception, it was a well

established tool to measure coefficients of translational and rotational diffusion as well as the chemical rate kinetics [7]. Though, FCS had important applications, the technique was not well developed due to its poor sensitivity. The introduction of confocal illumination scheme in FCS by Rigler et al. in 1993 has greatly improved sensitivity [8-11]. FCS technique reached to single molecule level due to technological improvements in lasers, photon detectors and high efficiency dyes. Finally, FCS set ups are now manufactured in industries and are commercially available along with many confocal microscopes. Recent reviews on different aspects of FCS shows the popularity and importance of the technique [12-17].

Unlike bulk techniques where the measurement is ensemble averaged, FCS works at a single molecule level to obtain diffusion constants. FCS extracts information from the fluorescence fluctuations of the sample at extremely low concentration(nM) from a very small probe volume(fL) as described in figure(2.2a). The fluorescence from these molecules will be fluctuating around a mean value figure(2.1b). These fluorescence fluctuations may arise from molecules passing through the probe volume (Diffusion) or due to the conversion from non-fluorescent to fluorescent (Chemical kinetics) states with in the probe volume. In the next section, we describe the theoretical aspects of FCS to measure the diffusion dynamics and chemical kinetics.

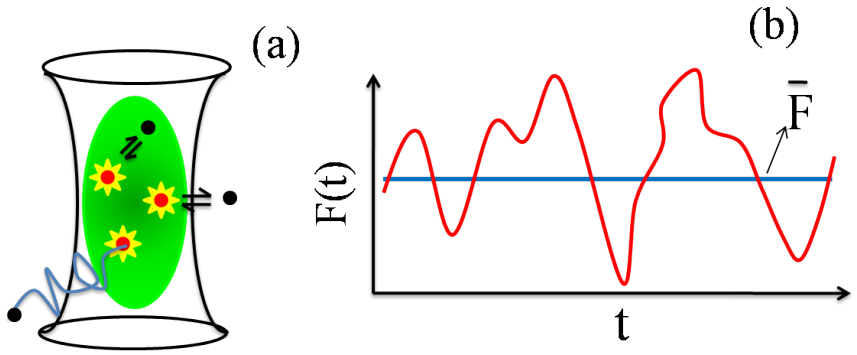

Figure 2.2: Schematic of fluorescence fluctuations in a small volume(fL) with a very low(nM) fluorephore concentration

2.3 Theory of FCS

2.3.1 Development of general formalism

Consider an ideal solution with "m" different chemical species or components. The local concentration of the j^{th} species is characterized by $C_j(\mathbf{r},t)$. Average concentration of the ensemble represented be $\bar{C_j}$. Then the fluctuation in the concentration will be $\delta C_j(\mathbf{r},t) = C_j(\mathbf{r},t) - \bar{C_j}$.

The different components in the system participate in diffusion and chemical reactions. This causes the deviations in local concentration. In the equilibrium situation, the relaxation in $\delta C_j(\mathbf{r},t)$ can be written as

$$\frac{\partial \delta C_j(\mathbf{r},t)}{\partial t} = D_j \nabla^2 \delta C_j(\mathbf{r},t) + \sum_{k=1}^{m} K_{jk} \delta C_k(\mathbf{r},t) \tag{2.1}$$

Where the first term represents the diffusion dynamics with diffusion constant D_j and the second term represents the dark-bright conversion rate with rate constant K_{jk}. Suppose these species are fluorescent in nature, then the emitted fluorescence will vary according to the concentration fluctuations. Also, the number of fluorescent photons emitted and collected $F(t)$ will depend on the excitation intensity, absorption cross section, fluorescence quantum yield, efficiency of the flurophore. Therefore, it can be written as

$$F(t) = \Delta t \int d^3\mathbf{r} I(\mathbf{r}) \sum_{k=1}^{m} Q_k C_k(\mathbf{r},t) \tag{2.2}$$

Where Q_k denotes the product of absorption cross section by quantum yield and fluorescence efficiency of the sample. $I(\mathbf{r})$ denotes excitation light intensity.

The deviation in the photon count from the mean is

$$\delta F(t) = \Delta t \int d^3\mathbf{r} I(\mathbf{r}) \sum_{k=1}^{m} Q_k \delta C_k(\mathbf{r},t) \tag{2.3}$$

In FCS experiments, autocorrelation function $G(\tau)$ will be calculated from the time av-

erage of fluorescence fluctuations. If $\delta F(t)$ is the deviation in fluorescence from the mean at time t and $\delta F(t+\tau)$ at a later time $t+\tau$ then $G(\tau)$ can be written as

$$G(\tau) = \frac{\langle \delta F(t) * \delta F(t+\tau) \rangle}{\langle F \rangle^2} \tag{2.4}$$

Considering the ergodicity of the system, above equation can be written as

$$G(\tau) = \frac{\langle \delta F(0) * \delta F(\tau) \rangle}{\langle F \rangle^2} \tag{2.5}$$

Substituting eqn. 2.3 in 2.5

$$G(\tau) = \frac{(\Delta t)^2}{\bar{F}^2} \int\int d^3\mathbf{r} d^3\mathbf{r}' I(\mathbf{r}) I(\mathbf{r}') \sum_{j,l} Q_j Q_l \langle \delta C_j(\mathbf{r},0) \delta C_l(\mathbf{r}',t) \rangle \tag{2.6}$$

The autocorrelation function of the fluorescence intensity fluctuations is a convolution of the auto and cross-correlation functions of the concentration changes with the excitation profile. To solve the above integral we will use the following initial conditions. At time t = 0 the correlation function is

$$\langle \delta C_j(r,0) * \delta C_k(r'',0) \rangle = \bar{C}_j \delta_{jk} \delta(r - r'') \tag{2.7}$$

To obtain the solution for $\delta C_j(r,t)$ We will solve the equation (2.1) in the Fourier space.

$$\frac{d\delta\tilde{C}_j(\mathbf{q},t)}{dt} = M_{jk} \delta\tilde{C}_k(\mathbf{q},t) \tag{2.8}$$

where $\tilde{C}_j(\mathbf{q},t) = (2\pi)^{-3/2} \int d^3r e^{iqr} \delta C_l(r,t)$ is a Fourier transform of $\delta C_l(r,t)$ and $M_{jk} = T_{jk} - D_l q^2 \delta_{lk}$. The solution can be represented in a standard way by using eigen values and eigen vectors of the matrix M as

$$\tilde{C}_l(q,t) = \sum X_l^s exp(\lambda^s t) \sum X^{(-1)}{}_k^s \tilde{C}_k(q,0) \tag{2.9}$$

Where X^{-1} is the inverse matrix of eigen vectors. Now, we can evaluate the average of the concentration fluctuation product

$$\delta C_j(r,0)\delta C_l(r',t) = (2\pi)^{-3/2}\int d^3q e^{-iqr'}\left\langle \delta C_j(r,0)\delta C_l(q,t)\right\rangle$$

$$\begin{aligned}
&= (2\pi)^{-3/2}\textstyle\int d^3q e^{-iqr'}\sum X_l^s exp(\lambda^s t)\sum (X^{-1})_k^s \left\langle \delta C_j(r,0)\delta \tilde{C}_k(q,0)\right\rangle \\
&= (2\pi)^{-3/2}\textstyle\int d^3q e^{-iqr'}\sum X_l^s exp(\lambda^s t)\sum (X^{-1})_k^s \times \int d^3q e^{-iqr''}\left\langle \delta C_j(r,0)\delta \tilde{C}_k(r'',0)\right\rangle \\
&= (2\pi)^{-3/2}\bar{C}_j\int d^3q e^{-iqr'}\sum X_l^s exp(\lambda^s t)\sum (X^{-1})_k^s
\end{aligned} \tag{2.10}$$

substituting the above equation into the equation 2.6 and integrating we obtain

$$G(\tau) = \frac{(\Delta t)^2}{\bar{F}^2}\int d^3q\,|I(q)|^2\sum Q_j Q_l \tilde{C}_j \sum X_l^s exp(\lambda^s t)\sum (X^{-1})_k^s \tag{2.11}$$

Where $I(q) = (2\pi)^{-3/2}\int d^3r e^{-iqr}\ I(\mathbf{r})$ us the Fourier transform of $I(\mathbf{r})$
The average number of collected photons can be represented by

$$\begin{aligned}
\bar{F} &= \Delta t\int d^3r I(\mathbf{r})\sum q_i\bar{C}_i \\
&= (2\pi)^{-3/2}\tilde{I}(0)\Delta t\sum q_i\tilde{C}_i
\end{aligned} \tag{2.12}$$

The autocorrelation function $G(\tau)$ can be evaluated from the experimental parameters like excitation profile, standard diffusion coefficients and known concentrations. In many of the FCS experiments, the laser illumination profile assumed as Gaussian profile.

$$I(\mathbf{r}) = I_0 exp\left(-\frac{2(x^2+y^2)}{\omega_{xy}^2} - \frac{2(z^2)}{\omega_z^2}\right) \tag{2.13}$$

where ω_{xy} and ω_z are the radial and axial dimensions of the excitation profile. The Fourier

transform of this excitation profile is

$$I(q) = I_0 \frac{\omega_{xy}^2 \omega_z}{8} exp\left(-\frac{\omega_{xy}^2(q_x^2+q_y^2)}{8} - \frac{(\omega_z^2 q_z^2)}{8}\right) \tag{2.14}$$

Therefore, final autocorrelation function will be

$$G(\tau) = \frac{(2\pi)^{-3/2}}{(\sum Q_i \bar{C})^2} \int d^3q exp\left(-\frac{\omega_{xy}^2(q_x^2+q_y^2)}{4} - \frac{(\omega_z^2 q_z^2)}{4}\right) \times \sum Q_j Q_l \tilde{C}_j \sum X_l^s exp(\lambda^s t) \sum (X^{-1})_j^s \tag{2.15}$$

This is the general form of the autocorrelation. Depending on the physical process we can compute the relevant autocorrelation function.

2.3.2 Single-component diffusion

Let us solve the diffusion equation in the case of a single species diffusion in all three dimensions in a very dilute situation. The generalized differential equation 2.1 can be written as.

$$\frac{\partial \delta C(r,t)}{\partial t} = D\nabla^2 \delta C(\mathbf{r},t) \tag{2.16}$$

This equation can be solved by considering the Fourier transform of $\delta C(\mathbf{r},t)$ as $\delta C(q,t) = \delta C(q,0) exp(-Dq^2 t)$
Now the matrix M will have one Eigen value and an Eigen vector as $\lambda = Dq^2$ and $X = 1$ substituting these values in the equation 2.15 we get

$$G(\tau) = \frac{(2\pi)^{-3/2}}{(\sum Q_i \bar{C})^2} \int d^3q exp\left(-\frac{\omega_{xy}^2(q_x^2+q_y^2)}{4} - \frac{(\omega_z^2 q_z^2)}{4} - D\tau(q_x^2+q_y^2+q_z^2)\right) = \frac{1}{\bar{C}V}\left(1+\frac{\tau}{\tau_D}\right)^{-1}\left(1+\frac{\tau}{\tau_D'}\right)^{-1/2} \tag{2.17}$$

Where the effective sampling volume $V = \pi^{-3/2}\omega_{xy}^2\omega_z$ and characteristic times in the illumination volume also known as average residence times are $\tau_D = \omega_{xy}^2/4D$ and $\tau_D' = \omega_z^2/4D$. Also the product of average concentration and the sampling volume is the average number of molecules within the detection volume and can be represented by "N" and $\omega = \omega_z/\omega_{xy}$

Therefore the above equation can be rewritten as

$$G(\tau) = \frac{1}{N}\left(1 + \frac{\tau}{\tau_D}\right)^{-1}\left(1 + \frac{\tau}{\omega^2\tau_D}\right)^{-1/2} \tag{2.18}$$

2.3.3 Chemical reaction along with diffusion

If the fluorescence fluctuations in the detection volume are also arising from a chemical reaction along with diffusion.

Let A represent the species and A* represents the fluorescent species of the same and diffusing with a diffusion coefficient D then the differential equation can be written as

$$\begin{aligned}\frac{\partial \delta C_A(\mathbf{r},t)}{\partial t} &= D\nabla^2\delta C_A(\mathbf{r},t) - k_{AA^*}\delta C_A + k_{A^*A}\delta C_{A^*} \\ \frac{\partial \delta C_{A^*}(\mathbf{r},t)}{\partial t} &= D\nabla^2\delta C_{A^*}(\mathbf{r},t) + k_{AA^*}\delta C_A - k_{A^*A}\delta C_{A^*}\end{aligned} \tag{2.19}$$

The matrix corresponding to above equation

$$M = \begin{bmatrix} -(Dq^2 - kAA^*) & k_{A^*A} \\ k_{AA^*} & -(Dq^2 - kA^*A) \end{bmatrix}$$

The eigenvalues of the matrix are $-q^2D$ and $-q^2D - k_{AA^*} - k_{A^*A}$ and the eigen vectors are $X_1 = \begin{pmatrix} 1 \\ -1 \end{pmatrix}$ and $X_2 = \begin{pmatrix} 1 \\ k_{AA^*}/k_{A^*A} \end{pmatrix}$

Substituting these values in the generalized autocorrelation equation (2.15) and solving we obtain

$$G(\tau) = \frac{1}{N}\left(1 + \frac{\tau}{\tau_D}\right)^{-1}\left(1 + \frac{\tau}{\omega^2\tau_D}\right)^{-1/2}\left(1 + Kexp\left(\frac{-\tau}{\tau_r}\right)\right) \tag{2.20}$$

Here $K = k_{AA^*}/k_{A^*A}$ is the rate constant of the reaction. Various autocorrelation fit functions are listed in the following table depending on the physical process involved.

Physical Process	Equation
1D Diffusion	$\mathbf{G}(\tau) = \frac{\mathbf{1}}{\mathbf{N}} \frac{\mathbf{1}}{\sqrt{(\mathbf{1}+(\mathbf{r}/\mathbf{l})^{\mathbf{2}}(\frac{\tau}{\tau_{\mathbf{D}}})}}$
2D Diffusion	$\mathbf{G}(\tau) = \frac{\mathbf{1}}{\mathbf{N}} \frac{\mathbf{1}}{(\mathbf{1}+\frac{\tau}{\tau_{\mathbf{D}}})}$
3D Diffusion	$\mathbf{G_{diff}}(\tau) = \frac{\mathbf{1}}{\mathbf{N}} \frac{\mathbf{1}}{(\mathbf{1}+\frac{\tau}{\tau_{\mathbf{D}}})\sqrt{(\mathbf{1}+(\mathbf{r}/\mathbf{l})^{\mathbf{2}}(\frac{\tau}{\tau_{\mathbf{D}}}))}}$
3D Diffusion + Triplet term	$\mathbf{G}(\tau) = (\mathbf{1} + \frac{\mathbf{T}}{(\mathbf{1}-\mathbf{T})}\mathbf{e}^{(-\tau/\tau_{\mathbf{T}})}) \frac{\mathbf{1}}{\mathbf{N}} \frac{\mathbf{1}}{(\mathbf{1}+\frac{\tau}{\tau_{\mathbf{D}}})\sqrt{(\mathbf{1}+(\mathbf{r}/\mathbf{l})^{\mathbf{2}}(\frac{\tau}{\tau_{\mathbf{D}}}))}}$
3D Diffusion + Rev. Reac.	$\mathbf{G}(\tau) = \frac{\mathbf{1}-\mathbf{F}+\mathbf{F}\mathbf{e}^{-(\tau/\tau_{\mathbf{R}})}}{\mathbf{1}-\mathbf{F}} * \mathbf{G_{diff}}(\tau)$
3D Diffusion + Directed flow	$\mathbf{G}(\tau) = \mathbf{G_{diff}} * \mathbf{e}^{\frac{-\tau/\tau_{\mathbf{V}}}{\mathbf{1}+\tau/\tau_{\mathbf{D}}}}$
2Comp-3D Diffusion	$\mathbf{G}(\tau) = \frac{\mathbf{f}}{(\mathbf{N})(\mathbf{1}+\frac{\tau}{\tau_{\mathbf{D1}}})(\mathbf{1}+(\mathbf{r}/\mathbf{l})^{\mathbf{2}}(\frac{\tau}{\tau_{\mathbf{D1}}}))^{\mathbf{0.5}}} + \frac{\mathbf{1}-\mathbf{f}}{(\mathbf{N})(\mathbf{1}+\frac{\tau}{\tau_{\mathbf{D2}}})(\mathbf{1}+(\mathbf{r}/\mathbf{l})^{\mathbf{2}}(\frac{\tau}{\tau_{\mathbf{D2}}}))^{\mathbf{0.5}}}$

Table 2.1: List of autocorrelation $G(\tau)$ fit-functions corresponding to the physical process.

Here, τ_D - Diffusion time

τ_T - Triplet life time

τ_R - Relaxation time of the forward and backward reaction rates

τ_V - Particle velocity

T-Triplet state fraction

F- dark fraction in a bright dark equilibrium

f- fraction of the first species in a two component system

N- average number of molecules

r, l- radial dimension and axial dimensions of the detection volume

2.3.4 Statistical accuracy of FCS

In this section, we discuss the statistical accuracy of the FCS measurement. The problem was first addressed by Koppel et al. in 1974 [18]. In FCS measurements, the rate of photon emission is directly proportional to the number of molecules(N) in the detection volume. Hence, Larger N contributes to a better photon statistics reducing the noise. On the other hand, the amplitude of autocorrelation function is inversely proportional to N indicating the better signal for small N. Therefore, it is critical to find the optimal concentration for accurate FCS measurements [19].

Let 'n' is the number of detected photons per unit time and the photons were collected for an experimental time interval T.

The signal to noise ratio is defined as $G(\tau)/\sqrt{var(G(\tau))}$ and computed by the following equations.

$$G(\tau) = \frac{1}{T}\sum_{i=0}^{T-1}\frac{\delta n_i \delta n_{i+m}}{\bar{n}^2} = \frac{\langle \delta n_0 \delta n_m \rangle}{\bar{n}^2} \tag{2.21}$$

and

$$varG(\tau) = \frac{1}{T^2} var\left(\sum_{i=0}^{T-1}\frac{\delta n_i \delta n_{i+m}}{\bar{n}^2}\right) = \frac{1}{T\bar{n}^4} var(\langle \delta n_0 \delta n_m \rangle) \tag{2.22}$$

In FCS measurement, fluctuations in $\delta n(t)$ occur from two main sources. 1) the statistical nature of the system itself (the diffusing species) 2) the statistical nature of the photon emission and detection process from the emitting species.

In the first case, relative fluctuation in the photon count (for understanding, represented by $\delta n^{(1)}$) is directly proportional to the average number of molecules N. Therefore, $\sqrt{var\delta n^1}/\bar{n} = \sqrt{var\delta N}/\bar{N} = 1/\sqrt{N}$. These fluctuations contribute to both signal $G(\tau)$ and the noise var$(G(\tau))$

In second case,relative fluctuation in the photon count is from a given "N".(for understanding, represented by $\delta n^{(2)}$) Now, $\sqrt{var\delta n^{(2)}/\bar{n}} = 1/\sqrt{\bar{n}} = 1/\sqrt{\upsilon \bar{N}}$

where υ is the average number of photons per molecule per sampling interval also

known as Per Particle Brightness (PPB).

$$
\begin{aligned}
varG(\tau) &\approx \frac{1}{T\bar{n}^4} var\left(\delta n_0 \delta n_m\right) \\
&= \frac{1}{T\bar{n}^4}\left(\left\langle(\delta n_0 \delta n_m)^2\right\rangle - \langle \delta n_0 \delta n_m\rangle^2\right) \\
&= \frac{var(\delta n)^2}{T\bar{n}^4} = \frac{1}{T(\upsilon N)^2}
\end{aligned} \tag{2.23}
$$

and considering the fact that $G(\tau) \propto 1/N$. Finally, the signal to noise ratio in the FCS measurement is

$$
S/N = \frac{G(\tau)}{\sqrt{var(G(\tau))}} \approx G(\tau)\upsilon N\sqrt{T} \propto \upsilon\sqrt{T} \tag{2.24}
$$

The above mentioned equation has the following consequences. Firstly, for $N >> 1$ the statistics of FCS is independent of the number of molecules and depends only on per particle brightness and the total acquisition time. Secondly, the S/N depends strongly on ν than on the experimental time interval. This means it is extremely important to optimize photon detection in the FCS experiment.

Qian (1990)and Kask et al.(1997) carried out statistical fluorescence intensity fluctuations as an extension to Koppel work. In this paper, they have derived a more generalized quantitative expression for Signal-to-Noise ratio for FCS measurements.

$$
S/N = \frac{G(\tau)}{\sqrt{var(G(\tau))}} = \sqrt{\frac{U}{TR}} \tag{2.25}
$$

Where U = data collection time. T - dwell time and R is

$$
\begin{aligned}
R = 2(1+2K_2) + \frac{4}{QT} + \frac{2}{(QT)^2} + \\
\frac{1}{m}\left[\frac{1}{\gamma_4}(1+2K_1) + \frac{4}{\gamma_3 QT} + \frac{2}{(QT)^2}\right]
\end{aligned} \tag{2.26}
$$

Where m is mean number of particles per sample volume. γ_3, γ_4 are parameters represent the Gaussian beam profile. Q - per particle brightness.

Depending on the values of m and QT, different terms on the right hand side in the above equation dominate and decide the signal to noise ratio in FCS experiments.
for m»1 and QT«1

$$S/N = Q\sqrt{\frac{UT}{2}} \tag{2.27}$$

This is similar to the equation 2.24.
for m«1 and QT«1

$$S/N = Q\sqrt{\frac{UTm}{2}} \tag{2.28}$$

In this case, the Signal-to-Noise ratio has a square root dependence on the mean number of particles per sample volume. This results in the signal-to-noise ratio decreases monotonously with decreasing with N. [20, 21].

In addition, S/N might be limited by different short comings of in the experimental system and contributes to background noise and correlated laser noise[18]. Increasing the concentration of the molecules diminishes these noise components and improves the overall signal. However, the concentration cannot be increased indefinitely, since the amplitude of the correlation function decreases with increasing N.

2.4 FCS instrumentation

Commercially, Fluorescence Correlation Spectroscopy(FCS) set up is available as an additional feature with confocal microscope. Confocal microscope mainly consists of different laser lines, optics and scanning stages. FCS requires a collimated laser beam which is passed through a high Numerical Aperture (NA) objective and focused to a tiny volume. Molecules in the volume absorb light and emit fluorescence. This fluorescent photons from the sample are collected back using the same objective and separated from the excitation light. Further this is focused to a pinhole at the detector end. Together with the pinhole and the lens combination, photons are collected from small volume called probe volume. The photo detector generates the electrical signal corresponds to number of photons. This electrical signal is further processed to obtain the autocorrelation curve. Schematic diagram of FCS is shown in the figure 2.3. FCS can be realized in the desired experimental geometry and can be built in the lab. It requires a laser, suitable optics, opto-mechanical components, detector and, a correlator card. This approach is cost effective and can achieve better sensitivity compared to commercial instruments. In this section, we describe briefly the constituent parts and construction of FCS [9, 10].

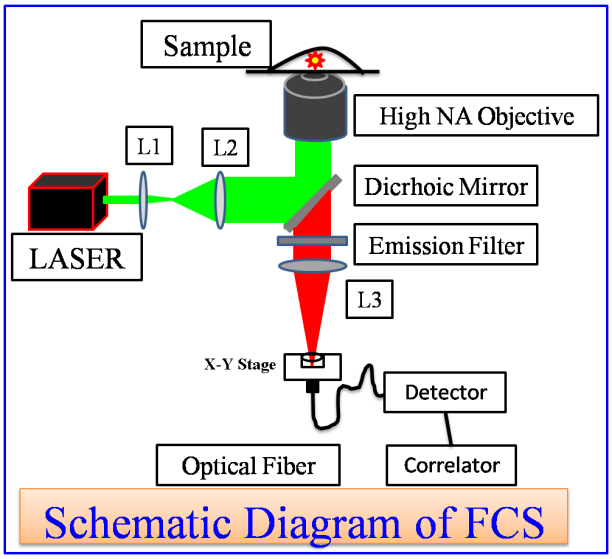

Figure 2.3: Schematic of FCS

2.4.1 Technical Details

Lasers: Laser is used as an excitation source in FCS. The choice of wavelength depends on the probe fluorophore used for experiments. A basic requirement of the laser is that it should have a TEM_{00} mode or a Gaussian intensity profile. This is because the basic derivation of the autocorrelation function assumes that the excitation intensity profile is Gaussian. Secondly, A very low intensity, in the of range 10-100 μW is required to avoid undesirable effects like photo-bleaching of the sample. Different types of laser are used in FCS such as diode lasers, DPSS lasers, Argon ion lasers, He-Ne Lasers. However, solid state lasers are preferred as they are compact and occupy less experimental space.

Figure 2.4: DPSS Lasers with 532 nm and TEM_{00} mode

Optics: A good quality optics is important in building FCS. We require a high reflectivity mirrors(99%) can be used to steer the laser beam in a desired geometry. A combination of lenses is used to expand and collimate the laser beam to overfill the back aperture of the microscope objective. In our FCS set up, we used a combination of lenses having focal length f1 = 20cm and f2 =2.54cm. The lenses are fixed in the initial laser path maintaining the distance between the two lenses as f1+f2 (22.54cm) to obtain the expanded and collimated laser beam at the other end.

A dichroic mirror is used to reflect the collimated laser beam on to the microscope objective. This dichroic mirror has a property of reflecting certain band(the excitation light) and transmitting another color (the emitted light). After the excitation of the sample, the emitted photons can be collected using the same optical path. Now the emitted photons are transmitted through the dichroic mirror and further filtered using a band pass filter.

Using an achromatic lens, filtered fluorescent light is focused on to a pinhole. A careful selection of optical fiber is required to collect maximum number of photons at the pinhole as it depends on the detection volume. We have used a multi-mode optical fiber of 25 μm core diameter. Following figure describes characteristics of all optics used in FCS.

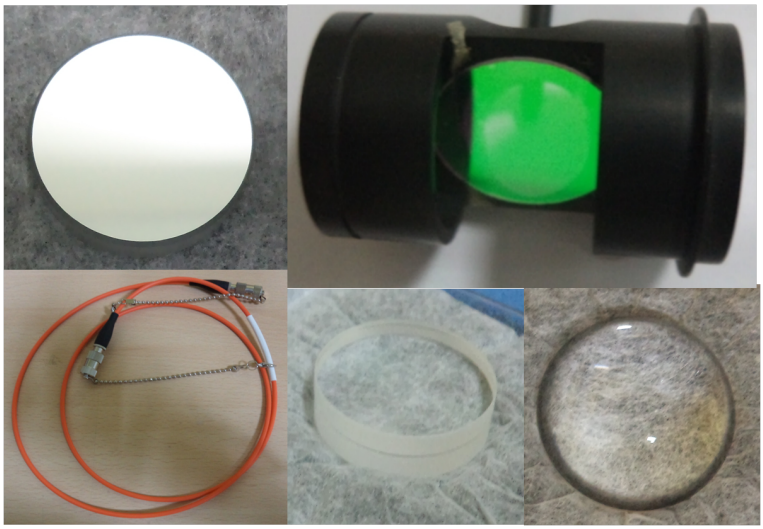

Figure 2.5: Optics for FCS. Mirror,dichoric filter, lenses, emission band pass filter and optical fiber

Mircoscope Objective: Objective is very important part of FCS. FCS detects signal from a very small open volume(fL) and a very tight focus is required. It can be achieved by High NA objective. Generally, oil immersion (1.33NA) or water immersion (1.2NA) objectives can provide a tight focus. However, many of the FCS studies are in aqueous solution. Therefore, to avoid refractive index mismatch water immersion objective is preferred for FCS measurement. In certain cases, where large focal volumes are required one can choose objective with less numerical aperture.

Opto-mechanical components: FCS instrument also requires a good quality opto-mechancial components which makes the entire instrument stable. There are mirror mounts, lens mounts,bread board, various size posts, post holders, base plates, dichroic mirror mount, cube, XY positioning stage, Micrometers, cage plates, Iris, fiber connector, screws etc. Following picture shows some of these parts.

Figure 2.6: Olympus Water immersion objective with NA 1.2

Detectors: The signal in FCS comes from fluctuations in fluorescence from single fluorophores and detecting the optimum number of emitted photons is critical in FCS measurements. Therefore, FCS requires a sensitive detector with high quantum efficiency(QE). Two kinds of detectors, photomultiplier tubes(PMT) and avalanche photo diodes(APD) are commercially available. APD has 70 percent QE whereas PMT have only 26 percent. Therefore, APD is preferable for FCS experimental set up. Other technical parameters to be considered about APDs are dark count, maximum light count,dead time and after-pulse time.After pulsing time is the minimum time between to electrical pulses which is a response of detected photons. If more number of photons reached below this time there will be a pile-up of photons at the detector. This may contribute to the artifacts using a single detector. However using two detectors and cross-correlation scheme this effect was nullified at they are uncorrelated). Typical values of the APD(from Perkin Elmer) used in our FCS setup are; dark count: 250Hz, maximum light count:10MHz, dead time: 65ns, after pulsing: 100ns-500ns. For a typical FCS measurement where the time scales are from "1" μs to few ms, commercially available APDs with the above mentioned parameters are suitable to for detection. However, for detecting processes in ns - μs time scales, one can choose a cross-correlation of emission light collected from two detectors to avoid after pulsing affects. The cross correlated data of this two detectors will not

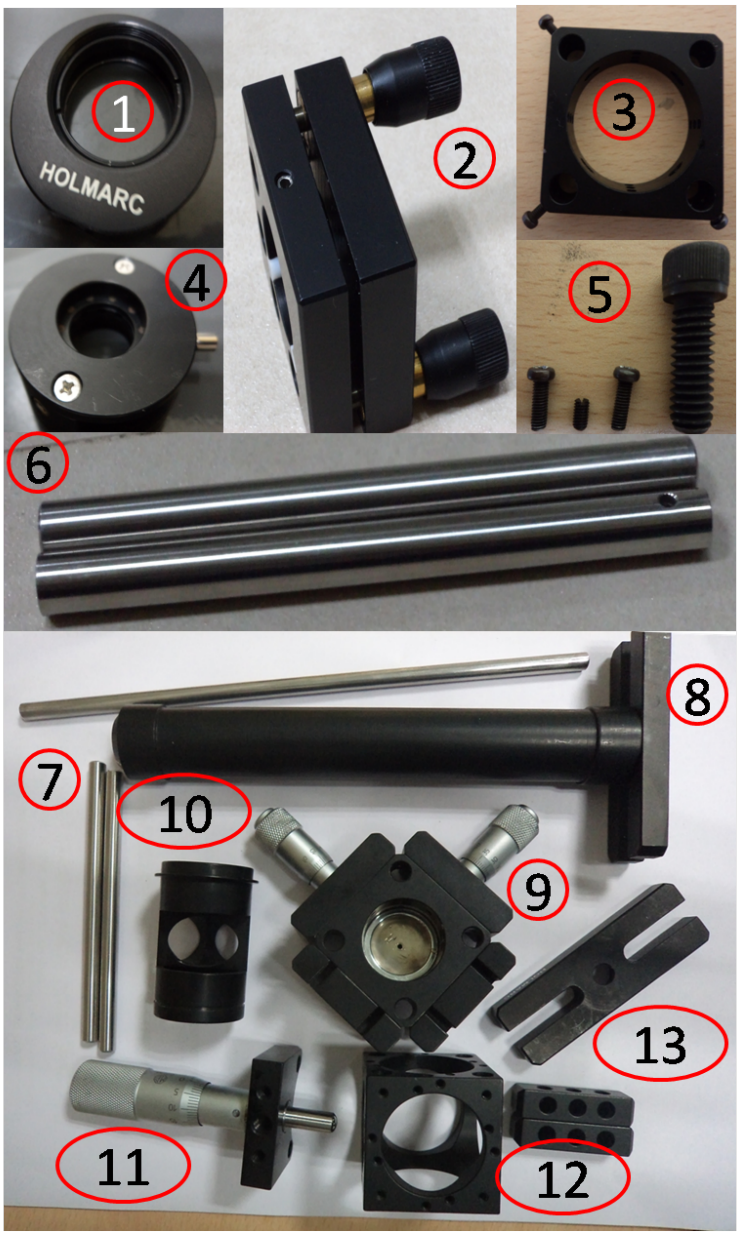

Figure 2.7: Optomechanical components used in FCS

show any signal of after pulsing effect. This is extremely useful to study fast chemical kinetics(sub micro second) along with diffusion.

Figure 2.8: Single Photon Counting Module(SPCM) from Perkin Elmer

Correlator Card: Correlator card is an essential component of FCS instrument that actually generates the final autocorrelation curve. It is an external hardware electronic device that computes autocorrleation curve and communicates with the computer. Correlator card consists of many real time input channels that receives the electrical signals from the detector.It measures fluctuations in the signal and an average signal and performs mathematical operation like multiplexing in real-time from each input channels. Finally, it generates output autocorrelation data which can be saved.

Mainly, Two types of linear (with linear time scales) and logarithmic (with logartihmic time scales) correlator cards are available with various multichannel input options. For FCS measurements, logarithmic correlator is preferred because it spans a broad range of (ns to minutes) time scales. In our FCS measurements, we use the Multiple Tau correlator from correlator.com (model no: flex99oem-12) which can perform auto/cross correlations. In this correlator card, there are 288 real time channels with minimum sampling time of t = 12.5 ns.The autocorrelation data will be recorded in logarithmic time scales.(first 16 channels with 12.5ns(t) interval and second 16 channels with 25ns(2t) and so on up to

288 channels)

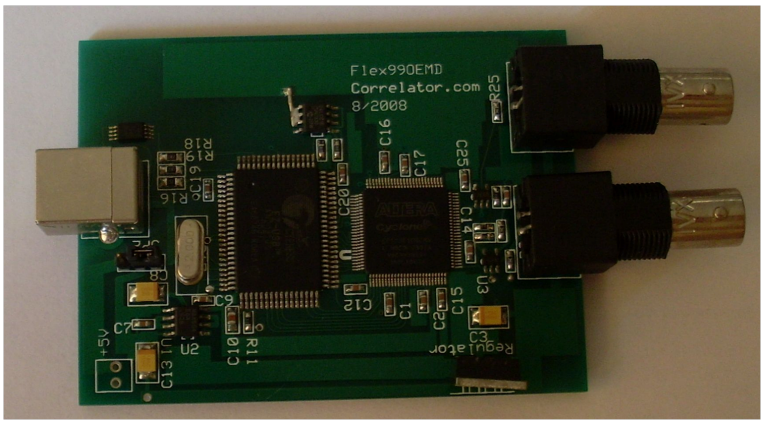

Figure 2.9: Multiple Tau correlator

2.4.2 Construction of FCS instrument

In the previous section, all the technical details are discussed. With the choice of right components FCS can be constructed in the desired geometry following the schematic as in figure(2.1).

A Laser is fixed on the optical bread board and is used as an excitation source. Two mirrors M1 and M2 were used to direct laser onto a beam expanding optics. The laser beam was expanded and collimated to approximately to 10 times using combination of lenses(L1, L2) to back-fill the objective. This collimated laser beam was directed into the micro cage assembly (see Figure 2.10) by another two mirrors M3 and M4. In the micro cage assembly, the laser light was reflected by a Dichroic Mirror and passes through an objective to focus into the sample. The fluorescence collected from the same objective was separated from the excitation light using the same dichroic filter and further filtered by an emission filter. This light was focused to a confocal pinhole with an achromatic lens. The multi-mode fiber is needed as a pinhole to collect the fluorescent light and carries it to a Single Photon Counting Module (SPCM) which converts optical signal to electrical signal. A correlator card was used to calculate the autocorrelation of this

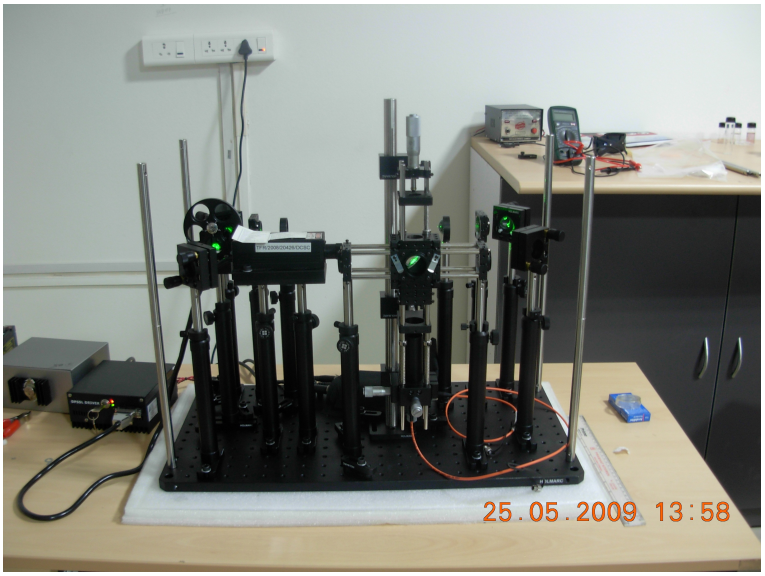

Figure 2.10: Home-built FCS Setup

electrical signals and can be connected to computer to record the same.

A photograph of home-built instrument is shown in the figure2.10. A DPSS laser (532 nm, 15 mW from Dream lasers,China) is used as an excitation source along with a set of neutral density filters to reduce the power as per the requirement. The laser beam is expanded and collimated to 10 mm using a combination of lenses having a focal length of 20 and 2.4 cm. A water immersion objective (1.2 NA, 60X from Olympus, Japan) is used to focus the light. The emitted fluorescent light separated from the excitation light using a dichroic filter (560DCLP, omega optics, USA) and by a band pass filter.This light is focused by and achromatic lens(f= 15cm) (Thorlabs, USA) into a multi-mode fiber (25μm inner diameter, OZ optics Canada) coupled to a single photon counting module (Perkin-Elmer Optoelectronics, Canada). A correlator card (Flex99oem-12D, correlator.com, USA) was used to calculate the autocorrelation of the intensities.

Data Analysis and software: Correlator card can be directly connected to the computer using an USB port. Data acquisition can be done by Labview programming and can be saved. However, a full length data from the correlator card will be saved. This may contain unwanted data points. User have to choose right data range that cor-

responds to observed physical phenomenon. Generally from one micro seconds to few hundreds of ms. Following figure shows the front panel of the FCS Labview software. This software is provided by Prof. Maiti group from TIFR, India.

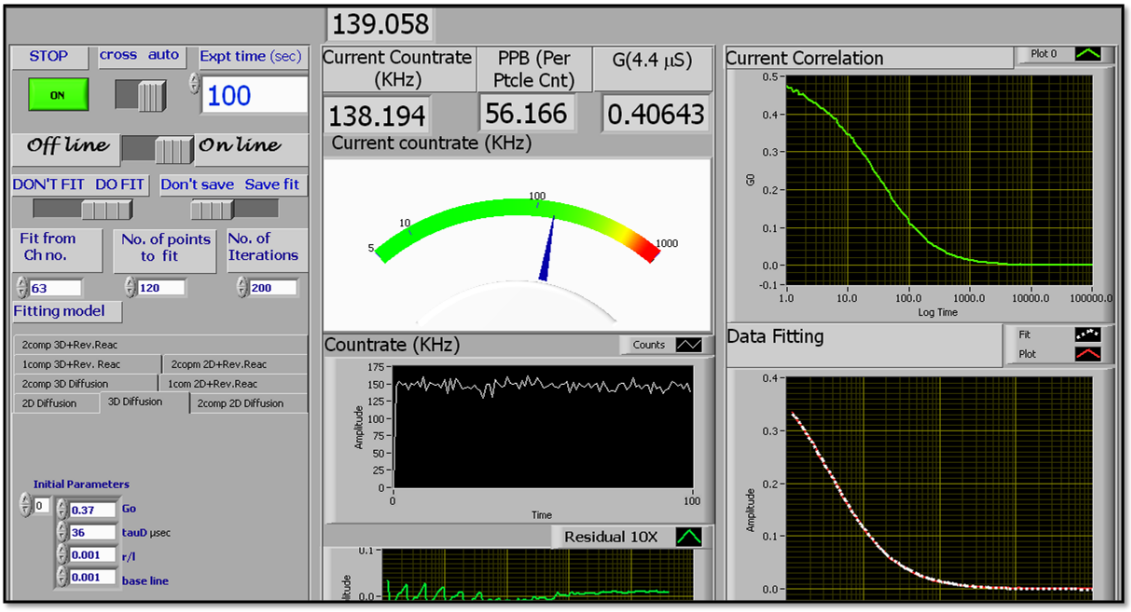

Figure 2.11: Front panel of data analysis software(Labview

Power supply: FCS laser requires electrical power supply as per specifications of the laser. Secondly, APD requires a constant DC voltage. We use a DC battery of 12V connected with electronic step-down circuit which can produce an accurate 5V output which can be used as a power supply to the APD.

2.4.3 Other Considerations

Several other important factors need to be considered before starting the FCS experiments.

Light Isolation: In FCS, the detected signal is much less than emitted light by a single molecule. So, small amount of stray light can overwhelm the measurement and can damage the ultra-sensitive detector. Black beam tubes are used to cover the space between the optics holders. The whole instrument with the detector is put inside a black box not to allow any light from outside. However, it is better to perform experiments in a dark room to avoid accidents.

Vibration Isolation: In FCS, we measure the fluctuation in fluorescence caused by diffusive movement of molecules in a small volume. This demands a complete vibration isolation system that can produce a stationary excitation laser spot and the sample at stationary equilibrium. Therefore, FCS instrument is mounted on a vibration isolated optical table. In case of unavailability of such tables, FCS setup can be placed on the table (with thick foam in between) is well insulated from most vibrations.

Electrical isolation: This is important if the laboratory electrical supply is noisy. A precautionary check is required before switching the laser power supply to prevent the damage. However, detector is more sensitive and prone to damage even by very small light and electrical surges. Therefore, we use a home-built 12- to 5-V DC-to-DC converter power supply to avoid such damages.

2.4.4 Calibration of FCS and Measurements

Calibration of the FCS instrument is required prior to actual experiments. Standard florescent dyes with known diffusion coefficient is used for FCS calibration. A fluorescent dye should be chosen according to the laser excitation wavelength. Depending on the physical processes, suitable fit function is used to fit the measured autocorrelations. Radial and axial dimensions of the detection volume are estimated using the following relation.

$$\omega_{xy}^2 = 4D\tau_D \tag{2.29}$$

Using these parameters diffusion coefficient of the sample estimated. Further, average size (hydrodynamic radius) of the molecules or particles are estimated following Stokes-Einstein relation ship.

$$R_H = \frac{kT}{6\pi\eta D} \tag{2.30}$$

Here, R_H - hydrodynamic radius, k - Boltzmann constant, T - Temperature, η - viscocity of the medium.

The autocorrelation curves are recorded with standard fluorescent dyes (Rhodamine 6G for 532 nm excitation and Coumarin for 446 nm excitation wavelengths) of the home-built FCS and shown in the following figure.

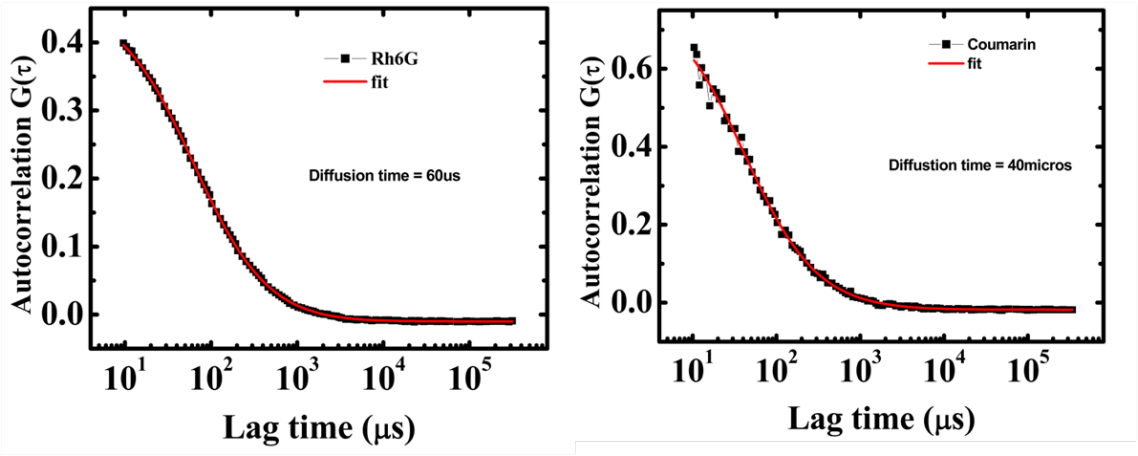

Figure 2.12: Autocorrelation curves of Rhodamine 6G and Coumarin

As discussed earlier, the signal-to noise ratio in FCS measurements depends strongly on the Per Particle Brightness(PPB) than the acquisition time (T). Therefore, it is important to maximize PPB for a better measurement. In FCS setup, the detection pinhole can be adjusted in XYZ direction using micrometer. PPB is optimized by adjusting the detection pinhole. Further, we can also confirm the quality of the FCS measurement by concentration dependence experiment with a standard fluorophore.This should vary linearly in allowed concentration limits(nM) of FCS measurements.

2.4.5 Applications of Fluorescence Correlation Spectroscopy

Because of its single molecule detection capability, applications of FCS have been extended to many research fields. Fluorescence Correlation Spectroscopy has been extensively used for many research applications in biology, chemistry, medicines and material science. FCS has become an established tool for biophysical studies such as protein aggregation, conformational dynamics, folding unfolding studies, ligand-receptor binding and photo dynamics of proteins. FCS has also been employed to investigate the molecular motion and receptor density in live cells and tissues [20-27]. Here, we provide a brief note on applications of FCS.

Concentration and aggregation measurements: We have seen in the theory section that G(0) equals to the reciprocal number of molecules (N) in the sampling volume. Therefore, from an autocorrelation function one can estimate the number of molecules or the local concentrations. Such measurements are extremely useful in quantifying and controlling the fluorescent protein expression in intracellular environments. On the other hand, we can also estimate the Per Particle Brightness from the average fluorescence intensity. Depending on decrease/increase in PPB, we can study fluorescent quenching effects or the aggregation effects along with the size measurements.

Average Residence time and Mobility: Mobility is important parameter to interrogate many the biological processes. It is essential to distinguish various types of mobility such as diffusion, active transport, anomalous diffusion or convection.

Diffusion analysis: Average residence time in FCS measurement is affected by any of these processes. We can measure the diffusion constants of bio molecules with external

stimuli such as pH, Temperature, viscosity. We can also compare such measurements both in vitro and intracellular environments.

It was known that membrane-bound receptors often exhibit anomalous sub-diffusion. Among possible reasons for such a non-Brownian behavior are environmental inhomogeneities and non-specific interactions with other particles or local confinement. FCS is useful for such studies and can provide and insight about membrane - receptor binding. In the 2D diffusion case, where the membrane is on the surface and a protein bounds to specific cites of the membrane, such anomalous behavior can be captured by sudden changes in the average residence time form the FCS measurements.

Active transport: Besides diffusion measurements, FCS can be applied to profile flow properties through the confocal detection. Flow properties of fluorescent particles in a micro capillary channels like effect of flow velocity and optical forces produced by laser beam can be investigated. Experiments like how do flow properties can affect the chemical kinetics in a binary mixture of interacting particles can be performed with FCS.

Molecular interactions: From the successive recording of FCS curves, it is possible to monitor continuous phenomenal changes by accessing parameters like diffusion time, molecular brightness and concentration. In an ideal reaction system, small and fluorescent labeled ligand interaction with a comparatively large, non-fluorescent counterpart. There will be a significant change in the diffusion time upon the binding and unbinding in such interaction and analyzing such system is especially easy in FCS studies. Therefore, it is possible to determine the diffusion time of the labeled ligand from a reference measurement.

Conformational changes: In the protein folding-unfolding studies, and protein denaturation (by external denaturation agent) studies, FCS can efficiently measure the change in hydrodynamic radius and change in fluorescence corresponds to the photo dynamics of protein. Therefore, FCS is extremely useful in monitoring the conformational changes.

Application of FCS in nanomaterials: Other than the biophysical applications, the field that has been benefited from FCS most is nanotechnology. Even though FCS

has been mainly applied to biological systems, recently, there is increasing number of FCS studies in nanomaterials demonstrating the enormous potential of the technique as well as the field. The two major fields of the material science where this technique has been significantly used are colloidal systems and polymer science. The recent reviews on FCS in measuring photophysical properties of QDs and in polymer science emphasize the importance of FCS [28, 29].

2.4.6 Maximum Entropy Method analysis of FCS data

As we seen in the theory section, using FCS fit function we can determine diffusion constant of a species present in the system by its fluorescence fluctuations. We can also determine diffusion constants of the two or more species present in the system by considering the multi-component fit function. However, this fitting holds good for only two component system. As the number of components increase, the number of fit parameters will increase and may lead to the estimation of erroneous diffusion constants. To address this problem, Sengupta et al. developed a different fitting algorithm called Maximum Entropy Method analysis of FCS data also known as MEMFCS. This kind of fitting algorithm is extremely useful to study heterogeneous system with size distribution such as polymers. In this section, we briefly describe the working methodology of MEMFCS algorithm

MEMFCS algorithm can fit for more number of (upto 41) diffusing species present in the system. This fitting algorithm is very much useful if heterogeneous size distribution is present in the system. MEMFCS works on the principle of maximum entropy method and it is proposed by Skilling and Bryan in 1984. This is used for reconstruction of astronomical images and has the virtue of preserving the maximum uncertainty in the estimation of parameters that is consistent with the data. This method can be adopted in the context of FCS, it provides a bias-free fitting of data with a quasi continuous distribution for large number of diffusing components present in the system [25]. Here, we briefly explain about MEMFCS alogorithm.

Assume that there is a distribution in diffusion time and each diffusion time associated with an amplitude α. for example, the i^{th} species will have a diffusion time of τ_{D_i} and its amplitude is α_i. Then we can write the autocorrelation fit function for all the species present in the system

$$G(\tau) = \sum_{i=1}^{n} \alpha_i \left(1 + (\frac{\tau}{\tau_{D_i}})\right)^{-1} \left(1 + ((r/l)^2 \frac{\tau}{\tau_{D_i}})\right)^{-1/2} \tag{2.31}$$

The amplitude α_i have to satisfy the condition that the experimental data $G(\tau)$ is correctly fitted, i.e., the value of calculated $G_c(\tau_i)$ should agree with the experimental value $G_e(\tau_i)$ for all data. As the experimental data is noisy, standard methods for evaluating the goodness of fit are as followed.

One such conventional method is to calculate the weighted residual for each data and examine the residuals (r_i) both qualitatively and quantitatively.

$$r_i = \frac{G_c(\tau_i) - G_e(\tau_i)}{\sigma_i} \tag{2.32}$$

σ_i is the inverse of weight for the i^{th} data. For a good fit, a random distribution of residuals about the mean value of zero is required for a qualitative estimation. When weights are properly known then the quantitative parameter χ^2 is useful, where

$$\chi^2 = \frac{1}{M} \sum_{i=1}^{M} r_i^2 \tag{2.33}$$

In above equation, M is the number of FCS data points. For a good fit, χ^2 is approximately equal to unity when M is sufficiently large. It is often possible that the good fit criterion is satisfied for many different distributions of α_i, especially when the data is noisy. Such distributions may also include solutions for specific models, such as, one or more fixed value for τ_D. The experimental data is then consistent with any of these distributions and thus any model that predicts such a distribution is acceptable.

But, in the maximum entropy method, acceptable distribution is the one for which the value of entropy S is maximum. S is defined as

$$S = -\sum p_i ln p_i \tag{2.34}$$

where $p_i = \alpha_i / \sum \alpha_i$. According to this principle, a discrete solution for τ_D is the least acceptable solution for noisy data because S will be lowest for such a distribution. Therefore, it seeks a distribution for which S is maximum and χ^2 is minimum. This method is employed to FCS data as following.

The analysis begins with equal values for all α_i at all τ_{D_i}. The distribution is improved in successive iterations: $\alpha_i(new)$ =α_i(old) + x$\Delta\alpha_i$. The correction factor $\Delta\alpha_i$ (an n-dimensional vector) is determined by the optimization procedure in three search directions constructed using the derivatives, $\nabla\chi^2, \nabla S$ and $\nabla\nabla\chi^2$. The procedure ensures that χ^2 is minimized in successive iterations and S is maximum for that χ^2. The multiplication factor "x" is determined by the "$\alpha - chop$ and $p - chop$" technique to achieve an aimed value of χ^2. Care is taken to avoid negative value for α_i, by using only a fraction of "x" and by equating negative values to zero. Successive iterations give distributions with reduced χ^2. The analysis is terminated when χ^2 does not change in successive iterations.

2.5 Summary

In this chapter, we have introduced the single molecule technique FCS and discussed the basic theory involved in FCS measurements. We have derived various autocorrelations fit functions in the case of 3D diffusion and for the rate kinetics. We discussed the statistical accuracy of FCS measurements. Instrumentation of FCS set up along with the details of technical requirements of each component has been discussed in this chapter. Furthermore, we have discussed calibration and measurement procedures along with necessary precaution in operation the instruments has been discussed. Finally, we have presented the details of a robust fitting algorithm based on maximum entropy method for fit the measured autocorrelation data in the case of more than two component systems. This has been used further in study of conjugated polymers.

Bibliography

[1] Principles of Fluorescence Spectroscopy Third Edition by Joseph R. Lakowicz.Springer

[2] Molecular fluorescence:Principles and applications by B Valeur, Wiley 2001

[3] D. Magde, E. Elson, W.W. Webb, Phys. Rev. Lett. 1972, 29, 705.

[4] Magde, D.; Elson E. Biopolymers, 1974, 13, 1.

[5] D. Magde, E. Elson, W.W. Webb, Biopolymers, 1974, 13, 29.

[6] S.R. Aragon, R. Pecora, J.Chem.Phys., 1976, 64, 1791.

[7] D. Magde, Quart. Rev. Biophys., 1976, 9, 35.

[8] R. Rigler, U. Mets, J widengren,P.Kask Eur.Biophys.J., 1993, 22 169.

[9] Ü. Mets, R. Rigler. J. Fluorescence, 1994, 4, 25.

[10] J. Widengren, R. Rigler, Ü. Mets, J. Fluorescence, 4, 1994, 255.

[11] J. Widengren, Ü. Mets, R. Rigler, J. Phys. Chem. 1995, 99, 13368.

[12] N. Thompson, in: J.R. Lakowicz (Ed.), Topics in Fluorescence spectroscopy, Plenum, New York, 1991, 1, 337.

[13] O. Krichevsky, and G. Bonnet, Rep. Prog. Phys. 2002, 65, 251.

[14] Kim, S.A. and Schwille, P., Curr. Op. Neurobiol. 2003, 13, 583.

[15] Elke Haustein and Petra Schwille, Annu. Rev. Biophys. Biomol. Struct. 2007, 36, 151.

[16] Mütze, J., Ohrt, T. and Schwille, P. Laser Photonics Rev., 2011, 5, 52.

[17] Pramit K Chowdhury, Journal of Protiens and Proteomics 2011, 2, 145.

[18] D.E. Koppel, Phys. Rev. 1974, 10, 1938.

[19] H. Qian Biophys. Chem. 1990, 30, 49.

[20] P. Kask, R. Günther, P. Axhausen Eur. Biophys. J., 1997, 25, 163.

[21] E. Van Craenenbroeck, G. Matthys, J. Beirlant and Y. Engelborghs, Journal of Fluorescence, 1999, 9, 325.

[22] P. Sengupta, J. Balaji, S. Maiti, 2002, 27, 374.

[23] W.W. Webb Quart. Rev. Biophys. Methods, 1976, 9, 49.

[24] S. Maiti, U. Haupts, W.W. Webb Proc. Natl. Acad. Sci. USA 1997, 94, 11753.

[25] Sengupta, P.; Garai, K.; Balaji, J.; Periasamy, N.; Maiti, S. Biophys. J., 2003, 84, 1977.

[26] K. Starchev, J. Buffle, E. Perez J. Colloid and Interface Science 1999, 213, 479.

[27] K. Starchev, J. Zhang, C. Buffle J. Colloid and Interface Science 1998, 203, 189.

[28] Romey F. Heuff, Jody L. Swift and David T. Cramb, Phys. Chem. Chem. Phys., 2007, 9, 1870.

[29] Dominik Woll, RSC Adv., 2014, 4, 2447.

Chapter 3

Photo-induced Blinking effects in CdTe Quantum Dots

3.1 Introduction

The emission wavelength of colloidal Quantum Dots (QDs) depends on its band-gap energy and can be tuned by varying its size. Due to excellent wavelength tunability and high photo-stability compared to conventional organic fluorescent dyes, QDs are being explored as efficient markers for biological imaging applications [1-9]. Despite having tremendous applications in bio-imaging and devices such as tunable lasers, solar cells and LEDs, [10, 11] luminescence intermittency known as "blinking" [12, 13, 14] restricts advances in QD technology where a single QD is used [15]. The random "on" and "off" states in luminescence blinking occur at all time scales [12-14]. The "off" state also affects ensemble quantum yield [16] and it is important to understand photo-physics of luminescence blinking from single QD in aqueous solution [3]. Although there is no clear physical picture of blinking mechanism yet [12, 17-20], researchers have found that blinking can be suppressed by addition of thiols to a colloidal solution of QDs [21]. It has also been demonstrated that thiolates, formed due to dissociation of thiols in aqueous medium, suppresses blinking [16].

Fluorescence Correlation Spectroscopy (FCS) is emerging as a useful single molecule

tool for investigating photo-physical properties of QDs [3, 22-29]. Blinking affects FCS measurements and many researchers have tried to model this effect using Monte Carlo simulations [3], stretched exponents [24, 25] and multiple exponents [29]. In general, FCS can measure average number of luminescent particles in its detection volume [30-33] and it can be used to measure number of luminescent QDs before and after thiol addition such as β-Mercaptoethanol (BME) and Dithiothreitol (DTT). Since addition of thiols to solution of colloidal QDs is known to suppress blinking [21, 16], this provides a new approach towards measuring photo-induced dark fraction in blinking QDs. In this chapter, we describe methodology of such a measurement. Further, from intensity dependence of this fraction we compute photo-darkening probability at band-edge photo-excitation (10^{-6}). We interpret the reaction rate used in conventional FCS analysis as the electron transfer rate that causes the "on-off" states of luminescence[32]. We demonstrate that measurement of this rate can become a method to reveal the electron transfer mechanism in blinking QDs.

3.2 Materials and Methods

3.2.1 Synthesis of CdTe Quantum Dots

All chemicals were used as purchased without further purification. Cadmium chloride, sodium borohydride, mercaptosuccinic acid and boric acid were purchased from Merck, sodium telluride was purchased from LobaChemie, trisodium citrate was purchased from Thomas Baker. 18 MΩ de-ionized water was used as solvent.

Mercaptosuccinic Acid (MSA) capped CdTe QDs were synthesized by modifying procedure developed by E. Ying et al. [34]. All reactions proceed in buffer solutions of boric acid and trisodium citrate. 15mM of boric acid and 15 mM of trisodium citrate is used in 50 ml milipore water to make buffer of pH 8. Precursor solution for CdTe QDs was made by adding cadmium chloride (1 mM), sodium telluride Na_2TeO_3 (0.25 mM), and mercaptosuccinic acid (3 mM) in 50 ml of buffer solution at pH 8 at 25 ^oC. After vigorous

stirring of precursors for 5 min, 20 mg of sodium borohydride $NaBH_4$ was added in to the precursor solution. After reaction proceeds for 10 min at room temperature the flask was attached to a condenser and refluxed at 80 ^oC under open air condition and shown in figure 3.1. Aliquots were collected at different time intervals after starting the reaction. Figure 3.1 shows the synthesis scheme. These QDs are synthesized by Ms. Padmashri Patil from Dr. Shovik Datta Group at IISER Pune.

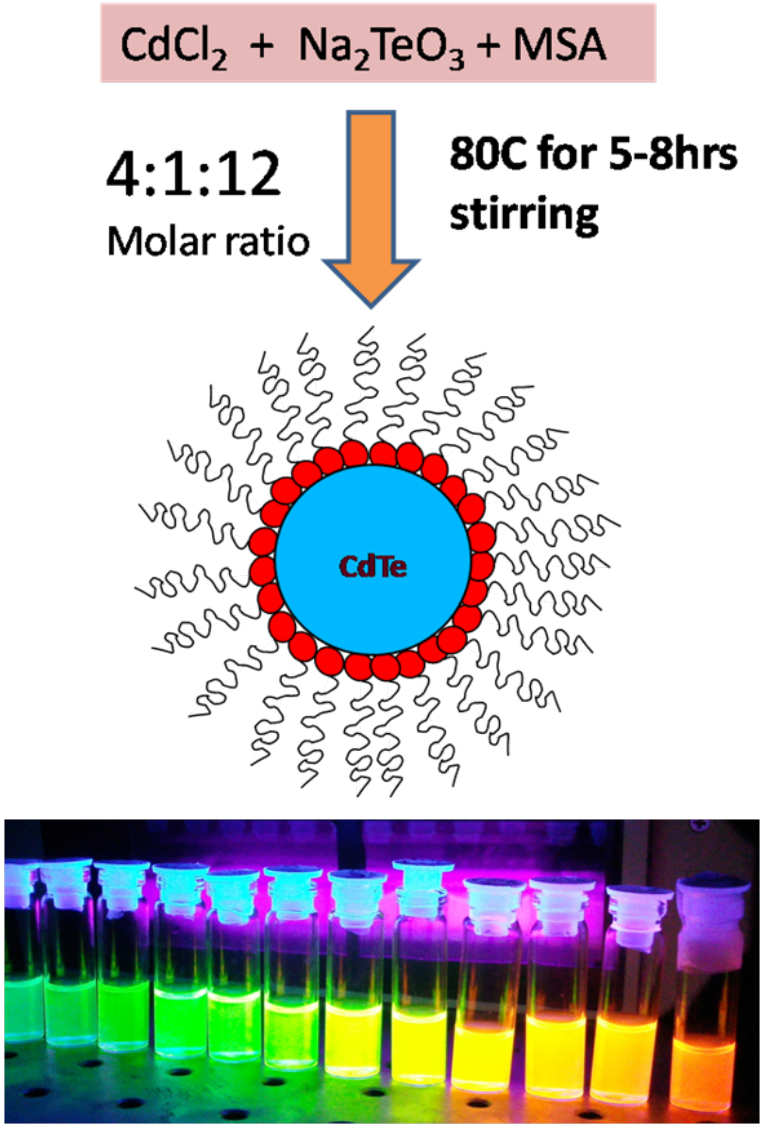

Figure 3.1: Synthesis scheme of CdTe Quantum Dots

3.2.2 Photophyscial Properties

All aliquots are first characterized by UV/VIS/NIR spectrometer (Lambda 950 Perkin Elmer) and then photoluminescence spectrometer (Flurolog3, HORIBA). QDs having four different diameters corresponding to absorption peaks at 456 nm, 535 nm, 546 nm and 565 nm were synthesized. They are referred to as QD456, QD535, QD546 and QD565. Figure 3.2 shows the absorption and emission spectra of four different quantum dot sets labeled with the wavelength of absorption peak. Size of QDs were calculated from the "effective mass approximation" formula.

Absorption cross section calculation: QD546 is used to calculate absorption cross section. A series of absorption spectra were recorded at various dilutions. Molar extinction coefficient of 5.6×10^4 mol^{-1}cm^{-1} was measured from the concentration versus peak absorbance data. Absorption cross section is determined following ref. 35. The absorption cross section of QD546 is 2 $\times 10^{-16}$ cm^2.

3.3 Results and Discussion

3.3.1 Excitation Intensity Dependence on Quantum dots in FCS experiments

We measured auto-correlation curves for QD546 in extremely dilute aqueous solution at different excitation intensities. We fit an analytical expression describing diffusion for all intensities. As mentioned in chapter 2, the expression for auto-correlation fit function for 3D diffusion is given by

$$G(\tau) = \frac{1}{\bar{N}} \left(1 + \frac{\tau}{\tau_D}\right)^{-1} \left(1 + (r/l)^2 \frac{\tau}{\tau_D}\right)^{-1/2} \tag{3.1}$$

Here, N is the average number of fluorescent particles and τ_D is the diffusion time or average residence time spent by luminescent QDs in the detection volume. r and l are radial and axial dimensions of the detection volume respectively. This analytical expres-

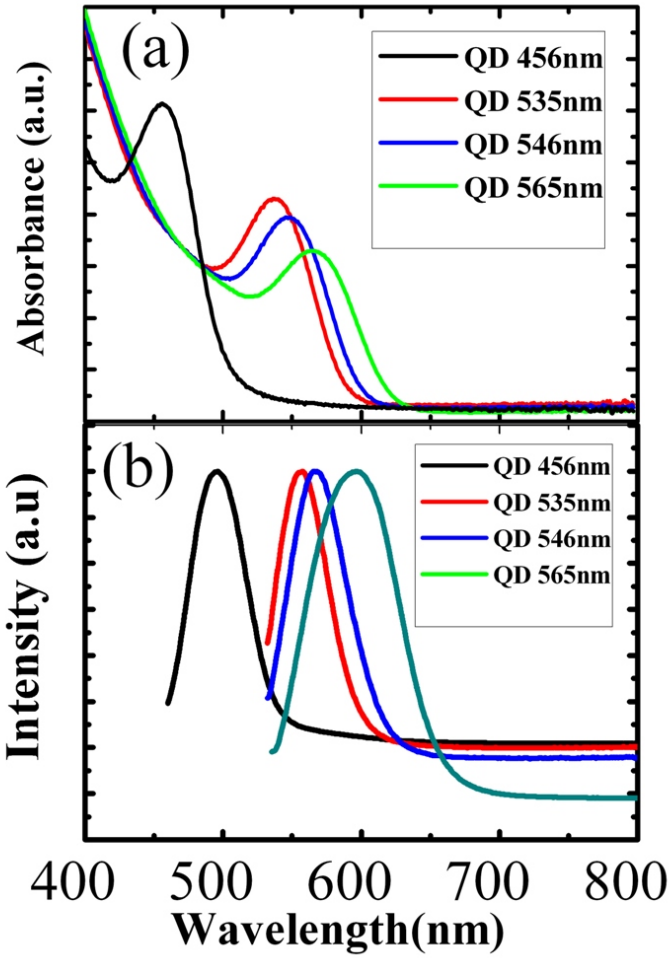

Figure 3.2: UV/VIS absorption spectra for CdTe samples. The peak absorption wavelengths are 456 nm, 535 nm, 546 nm and 565 nm corresponding to four different QD diameters. b)Photo-luminescence spectra for QD456, QD535, QD546 and QD565.

sion was chosen to fit autocorrelations as $\tau_r << \tau_D$ in the case of colloidal QD solution alone. Figure 3.3a shows measured auto-correlations and fits to equation 3.1 at different excitation intensities. The residual plot for a representative fit at 145 kW/cm^2 shows quality of the fit.

An important parameter for subsequent analysis and conclusion in this work is N, the average number of QDs in the detection volume. Figure 3.3b shows N at various intensities obtained from the fit. Unexpectedly, N initially decreases with intensity and further remains constant. We argue that blinking QDs under FCS measurement will show effectively less average number of QDs in the detection volume than actual number. We refer this number as apparent average number of QDs and represent it by N_{app}. But the actual number of QDs could be higher than this number. We refer the actual number of QDs as N_{actual} which we will discuss in the later part. The measurements in figure 3.3a provide us only N_{app}.

Figure 3.3c shows the values of τ_D obtained by fitting equation 3.1 for both QD and Rh6G. In contrast to Rh6G, τ_D for QDs reduces with increasing excitation intensity. We attribute this reduction in τ_D due to the "apparently reduced detection volume" for blinking QDs. The cartoon in figure 3.4 describes this concept. When a QD enters into the detection volume it starts to blink. While calculating autocorrelation, a QD becoming dark is not different from a QD leaving the detection volume. Similarly a QD becoming luminescent again is identical to a QD entering the detection volume. Therefore, the effective detection volume seen by a blinking QD is less than actual detection volume. This actual detection volume is usually measured using a standard fluorophore (Rh6G) with known diffusion coefficient in a given medium. Due to apparently reduced detection volume, the measured average residence time of blinking QD is less than its actual value. A close inspection of Figure 3.3b reveals that at low excitation intensity, the τ_D does not change much with intensity and remains constant around 200 μs. From this value of τ_D and using Stokes-Einstein relationship we determined the hydrodynamic radius to be 3 nm. This matches well with estimated radius of these QDs (2.2 nm) using effective mass

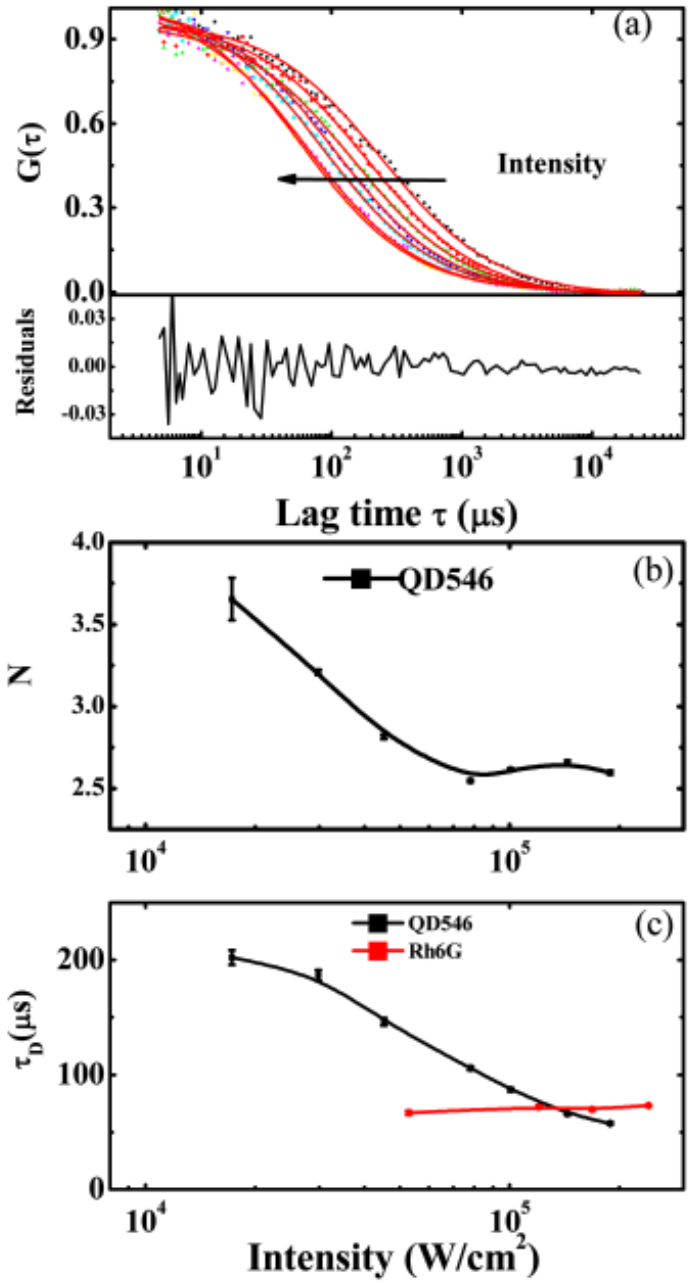

Figure 3.3: Autocorrelation curves fitted to equation 3.1 to determine N and τ_D at different excitation intensities. The continuous lines are best fits and dotted lines are data. The lower inset shows residuals of a representative fit at 145 kW/cm^2 to show quality of the fit. b) The dependence of parameter N, the average number of QDs in the detection volume on excitation intensity. We attribute the reduction in N for higher intensities to blinking. (c) The dependence of average residence time τ_D on excitation intensity. For larger intensities, τ_D for QDs is smaller than Rh6G.

approximation to its excitonic absorption spectrum [36]. Note that effective mass approximation gives the QD core size, while hydrodynamic radius using FCS also includes thickness of capping ligands. The above result suggests that blinking does not affect measurement of hydrodynamic radius of these CdTe QDs using FCS at lower intensities.

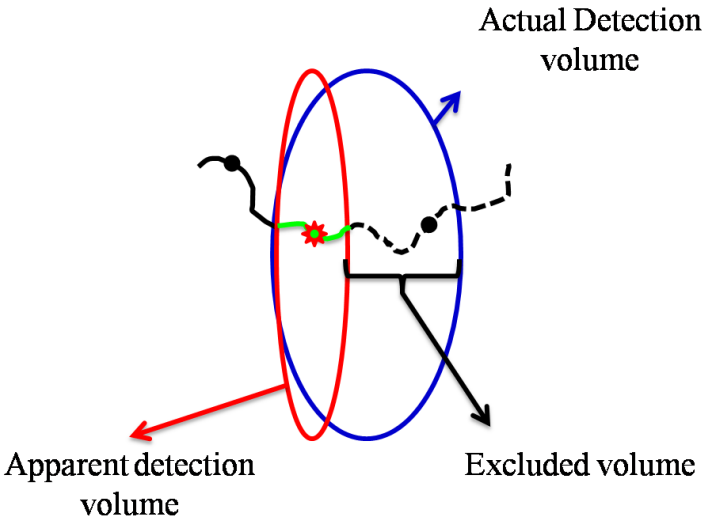

Figure 3.4: The schematic describing the "apparently reduced detection volume" for blinking QD. The continuous line represents trajectory of QD in its luminescent state, whereas the dotted line represents trajectory of QD in dark state. The apparent detection volume in FCS measurement is the volume traversed by QDs while they are luminescent. Excluded volume is the volume traversed by QDs while they are dark. The actual detection volume is measured by non-blinking organic fluorphore, Rh6G. Although equation 3.1 fits to intensity autocorrelations of blinking QDs, due to "apparently reduced detection volume", τ_D is less than the actual average residence time.

3.3.2 Addition of thiols-suppression of blinking

Eventhough there is no direct solution for removal of blinking effects from QDs, researchers has found that addition of thiols such as β-mercaptoethanol(BME) will suppress blinking to a great extent. We used addition of BME to avoid blinking effects in the FCS measurement and hence to verify the concept of "apparently reduced detection vol-

ume" in blinking QDs. It should not appear in FCS measurements on non-blinking QDs. Moreover, the diffusion time τ_D should provide correct hydrodynamic radius. Since thiol addition is known to suppress blinking, we added 1 ml of 100 μM BME to aqueous solution of QDs. Figure 3.5 shows autocorrelation curves before and after addition of BME at 145 kW/cm^2 (high intensity) and at 3.3kW/cm^2 (low intensity). At 145 kW/cm^2, the equation 3.1 (simple 3D diffusion fit) does not fit to autocorrelation curve after addition of BME. Instead an analytical expression of equation 3.2 describing a single "on-off" rate including diffusion kinetics fits to autocorrelation data. This equation is typically used in FCS analysis where a chemical reaction involving luminescence "on-off" state along with diffusion contributes to the equilibrium intensity fluctuations [28-30].

$$G(\tau) = \frac{1}{N}\left(1+\frac{\tau}{\tau_D}\right)^{-1}\left(1+(r/l)^2\frac{\tau}{\tau_D}\right)^{-1/2}\left(1+\frac{F}{1-F}exp\left(\frac{-\tau}{\tau_r}\right)\right) \tag{3.2}$$

Here luminescence fluctuations are caused due to a) fluorophores moving in and out of the detection volume because of diffusion, b) switching between "on" and "off" luminescence states of fluorophores with a single rate to attain equilibrium. This rate is reaction rate $k_r = 1/\tau_r$, where τ_r is characteristic time needed to reach equilibrium number of dark and bright populations. The k_r is sum of forward and backward rates in reaction causing luminescence . F is equilibrium dark fraction in dark-bright conversion. Table 3.1 shows various parameters obtained by fitting equation 3.1 and 3.2 to measured autocorrelations in figure 3.5a. As mentioned above, equation 3.1 fits to autocorrelation curves without BME addition whereas equation 3.2 fits to autocorrelations with BME addition. Both these measurements are performed at 145 kW/cm^2 excitation intensity. From fit parameters it is clear that diffusion time after addition of BME is recovered and now determines the hydrodynamic radius reasonably well. This supports the concept of "apparently reduced detection volume" presented in the previous section.

Additionally, the fitting of equation 3.2 means that luminescence after addition of BME fluctuates with a single rate k_r, $k_r = 30\mu s$ in the present experiment. The fit value of 0.4 for F also suggests that 40% of the QDs are dark in equilibrium dark-bright

Sample	fit parameters at 145 kW/cm^2 Intensity			
	N	$\tau_D(\mu s)$	$\tau_r(\mu s)$	F)
QDs	2.96 ±0.01	40.96 ±0.67	-	-
QDs+BME(above 70 μM)	4.74 ±0.02	160.96 ±11	28.3±1.67	0.426 ±0.01

Table 3.1: N - Average number of particles, τ_D - Diffusion time, $k_r(= 1/\tau_r)$ - Relaxation rate F - Equilibrium dark fraction

conversion at any given time, yet all of them contribute to N. A non-zero value for k_r indicates that addition of BME does not suppress luminescence fluctuations at all time scales. This does not contradict the previous evidence of blinking suppression using BME since those measurements employ millisecond binning times [21].

Average number of QDs in the detection volume increases from 2.96±0.01 to 4.74±0.02 after addition of BME (Table 3.1). Assuming all the blinking QDs are recovered from their dark state with thiol addition, the actual number of QDs in the detection volume $N_{actual} = 4.74 \pm 0.02$, So far, there is no evidence that BME addition recovers the luminescence of long-lived non-radiant QDs and therefore N_actual does not include them. $\Delta N = N_{actual} - N_{app} = 4.74 - 2.96 = 1.78$ The dark fraction due to blinking is f = $\Delta N/N_{actual} = 0.37$. It should be noted here that F, the equilibrium dark fraction and f, the photo-darkened fraction due to blinking, are different.

At 3.3kW/cm^2, addition of BME does not have any effect on FCS measurements. Figure 3.5 (b) shows autocorrelations for both before and after addition of BME at 3.3 kW/cm^2. The two curves overlap with each other and analytical expression of equation 3.1 describing diffusion alone fits to measured autocorrelations before and after BME addition.

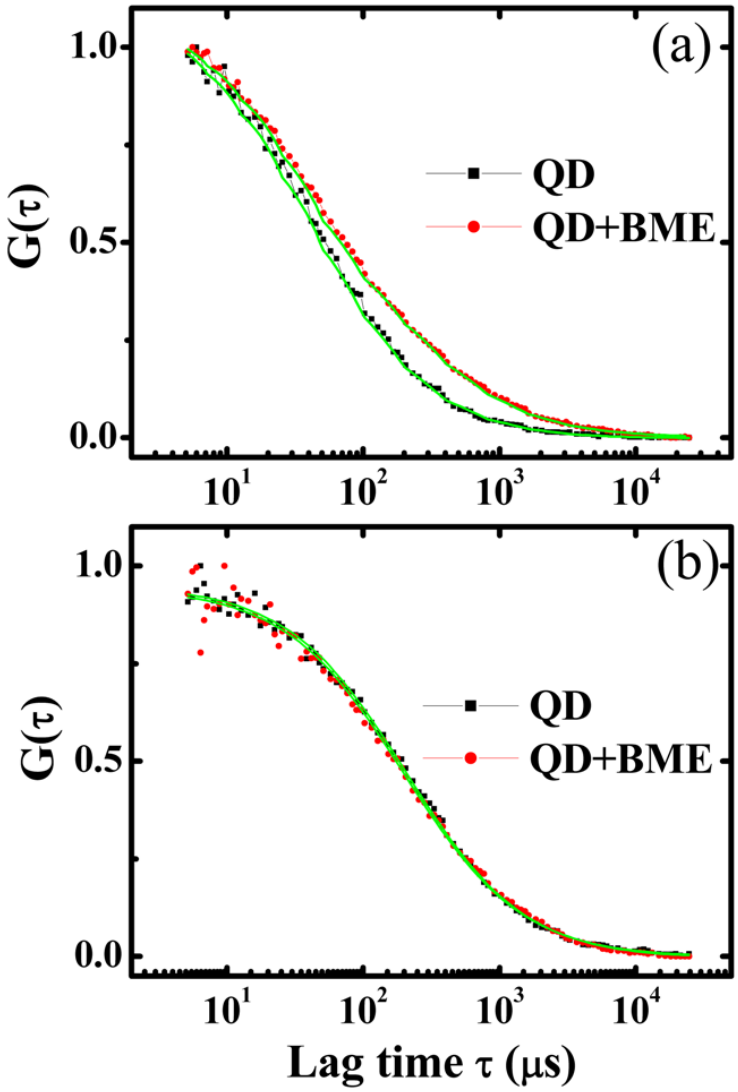

Figure 3.5: Autocorrelations without addition of BME and with addition of BME at 145 kW/cm^2. The continuous lines are fits with equation 3.1 and 3.2 for without and with BME addition respectively. b) Autocorrelations without and with BME addition for excitation intensity of 3.3 kW/cm^2. Both curves overlap each other and equation 3.1 fits to both curves yielding τ_D of 200 $\pm 5\mu$s. The hydrodynamic radius corresponding to this τ_D is 3 nm. This matches reasonably well with radius determined from effective mass approximation.

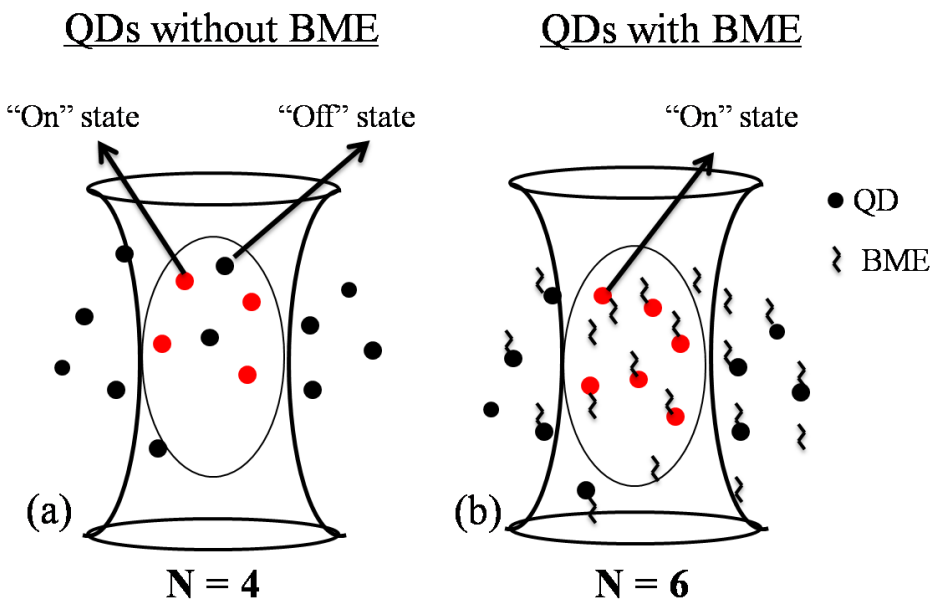

Figure 3.6: A schematic for measurement of dark fraction due to blinking using FCS. Since some of the QDs are dark at any given time due to blinking, the average number of QDs measured using FCS is less than the actual value. For instance in (a) there are 6 QDs in the detection volume, but FCS measures only four. Two QDs are dark due to blinking. The addition of thiol molecules to QD solution suppresses blinking and one can measure actual number of QDs. The difference in N divided by total number is dark fraction.

3.3.3 Photo-darkened fraction and Photo-darkening probability

We measured photo-darkened fraction due to blinking at different photo-excitation intensities(Figure 3.7). The measured photo-darkened fraction and this is linearly varying with excitation intensity suggests that it is a one-photon process.

$$f = (N_{actual} - N_{app})/N_{actual} = \Delta N/N_{actual}$$

From data in figure 3.7 we compute the probability of QD becoming dark after absorption of a photon. We refer to this as photo-darkening probability. The photo-darkened fraction measured in our experiments $f = \Delta N/N_{actual}$ must be the product of photo-darkening probability P and the number of photons absorbed "n" while the QD is illuminated with excitation light; $f = P \times n$ The number of photons absorbed "n" can be computed if we know the absorption cross section ρ, excitation intensity I in kW/cm^2, frequency of excitation υ and illumination time t; $n = I\rho t/h\upsilon$ [18]. The plot in figure 3.7 is photo-induced dark fraction f versus excitation intensity. According to aforementioned discussion, $f = P \times I\rho t/h\upsilon$ Then theoretically, the slope of straight line in figure 3.7 is $P\rho t/h\upsilon$. From figure 3.7 the slope is 1.2$\times$ 10^{-6} cm^2/W.

From the slope, we compute P to be 9 $\times 10^{-6}$. We used hυ = photon energy for 532 nm wavelength which is excitation wavelength of our laser, measured absorption cross section $\rho = 2X10^{-16}cm^2$. We have taken illumination time "t" to be the average diffusion time τ_D measured at intensity 3.3 kW/cm^2. It is 210 μs. The photo-darkening probability of 9×10^{-6} implies that, typically a QD needs to absorb 10^5 to 10^6 photons before it enters into a photo-darkened "off" state.

We now explain the result in figure 3.5 in the light of value obtained for photo-darkening probability. We note that in figure 3.5(b), there is no discernible effect of BME addition on autocorrelation curves at I = 3.3 kW/cm^2. The autocorrelations overlap with each other and equation 3.1 fits to both correlation curves. For excitation intensity of 3.3 kW/cm^2, the average number of photons absorbed by a QD in its transit through the detection volume is $I\rho\tau_D/h\nu \approx 1.0 \times 10^3$. The QDs rarely photo-darken since the

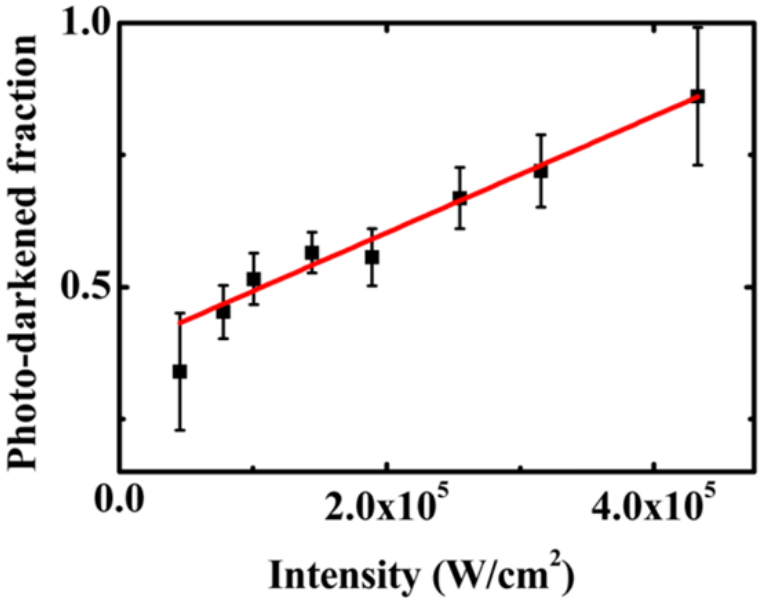

Figure 3.7: Photo-darkened fraction versus excitation intensity. The slope of straight line fitted to data is $P\rho t/h\upsilon$. It gives probability of the QD becoming dark after absorption of a photon 10^{-6}.

probability of photo-darkening is 9×10^{-6}. There are no photo-darkened QDs to recover after addition of BME. Since QDs do not enter into a dark state while in transit, there is no "apparently reduced detection volume" effect discussed in figure 3.4. At excitation intensity I = 145 kW/cm^2 in figure 3.5(a) the average number of photons absorbed by a QD while in transit in the detection volume is 1.6×10^5. Since probability of photo-darkening is around 10^{-5} to 10^{-6}, QDs are likely to enter into photo-induced dark state while in transit. This explains result in figure 3.5 that the blinking starts to affect FCS measurements only at higher intensities and correctly determines hydrodynamic radius of QDs at lower intensities.

The number of BME molecules required per QD to suppress blinking: In order to determine the minimum number of BME molecules needed per QD to suppress blinking, we add a controlled amount of BME to the dilute solution of QDs. We use excitation intensity of 145 kW/cm^2 and QD546. BME is added to the 1 ml aqueous solution of QDs in steps and autocorrelations are measured after each such addition. Figure 3.8

shows diffusion time τ_D and average number of QDs N versus BME concentration. figure 3.8(a) shows that after enough BME addition, τ_D nearly saturates. figure 3.8(b) shows N versus BME concentration. The number of fluorescent QDs at fixed laser intensity gradually increases with BME addition. The growth is initially slow, then changes rapidly and finally saturates. The growth in N with respect to BME concentration is modeled with a sigmoid growth given by Hill equation,$\theta = \theta_{max}(x^n/(x^n + \kappa^n))$ [37]. Here θ is the number of QDs recovered from photo-darkened state by BME addition and "x" is BME concentration. The parameter κ gives concentration of BME molecules needed to recover half of QDs from the photo-darkened state. The value of κ for experiments with different excitation intensities is in the range of 10 to 20 μM. As shown in figure 3.8(b), we need BME concentration of around 70 μM. The detection volume in our measurement is 0.95 fL. This translates into 4×10^4 BME molecules in our detection volume. As seen in figure 3.8(b), there are 4 QDs in the detection volume. This implies that we need 10^4 BME molecules per QD to suppress blinking under dilute conditions.

Photo-ionization of QDs and physical meaning of k_r: Do charged QDs have no photo-luminescence at all? Recently the charging model for loss of luminescence is challenged by Zhao et al. [20]. The present FCS measurement of photo-induced dark fraction and photo-darkening probability does not answer this question in a direct way. However, it is remarkable that the measurement of photo-ionization (charging) rate using Electrostatic Force Microscopy (EFM) suggests a one-photon process of photo-ionization [8]. The linear dependence of photo-induced dark fraction on intensity in our FCS measurements suggests that photo-darkening is also a one photon process (figure 3.7). Moreover, the ionization probability measured using EFM for band-edge excitation is of the same order as photo-darkening probability measured in our experiments (10^{-5} to 10^{-6}) [8]. Therefore, it is tempting to suggest that the photo-darkening is caused by photo-ionization. However, it is difficult to gather a direct evidence of charging on an individual QD in the solution. In this section we attempt to understand the relation between photo-ionization and photo-darkening purely through FCS analysis. In conventional FCS measurement of chemical kinetics, the k_r in equation 3.2 is associated with reaction rate causing "on" and

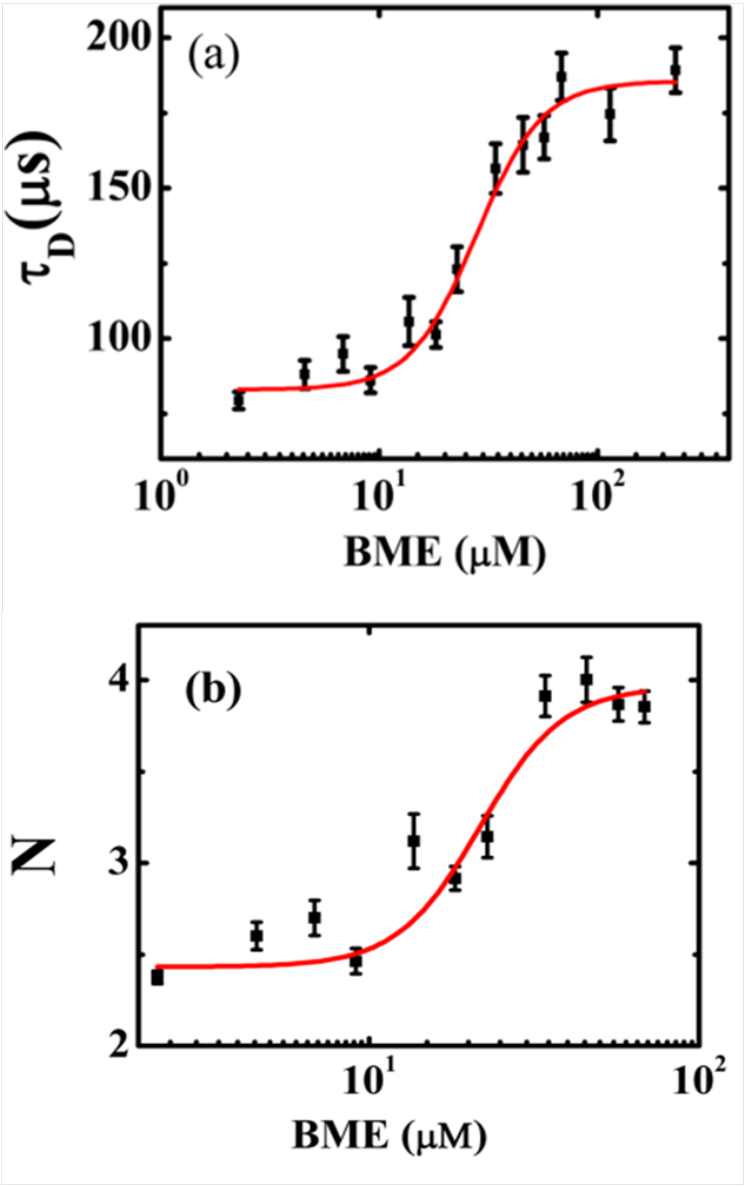

Figure 3.8: The effect of gradual addition of BME on diffusion time τ_D and average number of QDs (N) in the detection volume. a) τ_D versus BME concentration. As blinking slowly disappears with addition of BME, τ_D starts to recover. b) The average number of QDs in the detection volume versus the BME concentration. All blinking QDs which were not contributing to total average number of luminescent QDs are recovered with gradual BME addition. Dissociation constant $\kappa = 70\mu$M. At 70 μM BME concentration N starts to saturate, indicating a total recovery of QDs. At 70 μM, there are 4×10^4 number of BME molecules in our detection volume of 0.95 fL. This implies that roughly 10^4 BME molecules per QD are required to suppress blinking.

"off" luminescence states; $k_r = 1/\tau_r$. We have seen that after addition of enough BME to suppress blinking, equation 3.2 fits well to autocorrelations. What does k_r represent in present experiments? Two mechanisms are possible. First possibility is that k_r represent the association-dissociation of BME molecules with QDs. In this picture a BME molecule attaches itself to a QD and if it is in dark state it will be turned "on". Here k_r should depend on concentration of BME. We found that once the BME concentration to recover all photo-darkened QDs is reached then k_r does not depend on BME concentration. If k_r is association-dissociation rate between BME and QD then it is expected to depend on temperature. However, we found no dependence on temperature. We measured k_r in the temperature range of 25 to 65 ^{o}C. Figure 3.9 (a) shows k_r versus temperature. The temperature range is somewhat limited because the experiment is performed in aqueous phase with water immersion objectives. The second possibility for the interpretation of k_r is as follows. In the charging model of blinking, a charged QD core loses luminescence and recovers it after charge neutralization. The addition of BME is thought to neutralize, or render the electron-accepting traps inactive, by its electron-donating ability. It is well known that BME addition prevents the long-lived charged state and enhances neutralization rates. Such suppression of blinking is experimentally measured with millisecond binning times and the luminescence from QDs appears continuous [21]. The ionization-neutralization can happen at a much faster rate than can be captured in millisecond binning times. We interpret k_r as the ionization-neutralization (electron transfer) rate. The k_r describes the rate of electron transfer between the core and surface trap states.

The above-mentioned interpretation of k_r suggests that it should depend on QD core diameter and also on excitation rate, the number of photons absorbed per second. Figure 3.9(b) shows dependence of k_r on QD core diameter. We measured auto-correlations for four different QDs; QD456, QD535, QD546 and QD565. The data point indicated with an arrow is for QD456 having absorption peak at 456 nm. It is excited with a blue laser of 446 nm. The calibration for blue excitation is performed using standard dye Coumarin. The other three points represent QDs excited with a green (532 nm) laser. The QD core diameters are estimated using effective mass approximation as described in materials and

methods section. The k_r depends on QD core diameter and decreases for larger QD sizes. Figure 3.9(c) shows dependence of k_r on excitation rate. The excitation rate is computed as discussed in ref.18. The linear dependence on excitation rate suggests that electron transfer from core to surface states is a one photon process. A similar conclusion about charging is reached using EFM measurements in ref. 18. In general, the FCS measurements support the charging model of luminescence blinking proposed by Nirmal et al. and others [12, 13, 17].

Does photo-ionization occur via tunneling? The ejection of an electron from QD core is a complex process and many mechanisms have been proposed to explain this phenomenon [12-14, 20]. Tunneling is thought to be a dominant process of ionization[12-14]. If k_r represents the electron exchange rate between core and surface trap states, then its measurement becomes a useful experimental tool to reveal the process of photo-ionization. In case where the photo-generated electron tunnels through to surface states, the well width affects attempt frequency. The tunneling rate then has inverse square dependence on well width [38, 39]. The effective well width for electrons in the QD core diameter of the core itself. The linear dependence of k_r on excitation rate, its inverse dependence on QD core diameter and its insensitivity towards temperature in a modest range in our experiments suggests that tunneling is likely mechanism of electron exchange between core and surface trap states. Figure 3.10 shows a schematic describing the photo-ionization process. It is based on results using FCS to explore photo-physical properties of QDs reported in this thesis. In absence of BME, the ionization rate (core to surface states) is more compared to the neutralization rate (surface states to core). The probability of electron transfer after absorption of photon in the presence of BME, the slope of the line in figure 3.9(c) is found to be $\approx 10^{-4}$. This is roughly ten times more than the photo-darkening (photo-ionization) probability of 10^{-5} calculated from figure 3.7. Therefore we infer that addition of BME enhances the neutralization rate and this in turn increases the ionization rate as well. The k_r is addition of both ionization and neutralization rate, $k_r = k_i + k_n$ [30]. However, it should be noted that the equilibrium dark fraction, the fraction of QDs remaining dark at any given time, is still around 40 percent even

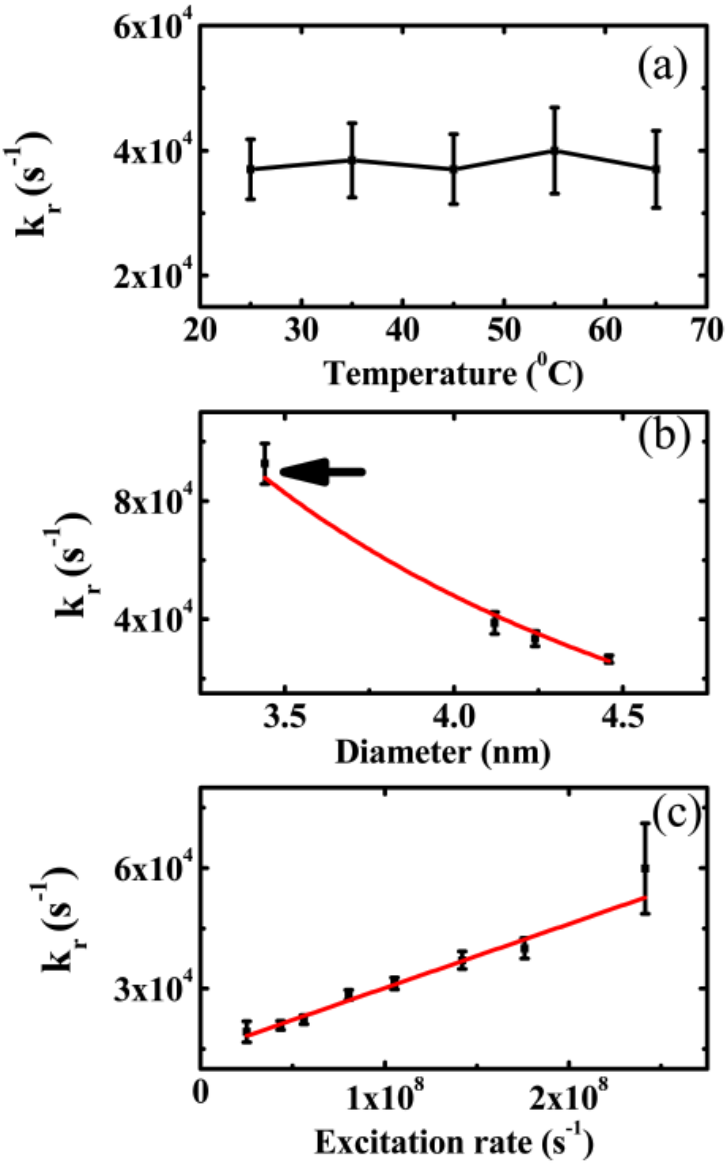

Figure 3.9: Dependence of k_r on temperature. For modest range of temperatures allowed in this experiments, k_r does not depend on temperature. This excludes the possibility of interpreting k_r as association-dissociation rate of BME molecules and QDs. b) Dependence of k_r on QD diameter estimated using effective mass approximation. The arrow indicates a data point measured using blue laser. The dependence strengthens the interpretation of k_r as electron transfer rate between core and the surface trap states. The continuous line is a guide to the eye. c) Dependence of k_r on excitation rate. This suggests a one-photon process for electron transfer. The slope of this line is probability of electron transfer after a photon is absorbed in presence of BME molecules. It is roughly 10^{-4}

after BME addition. This indicates that the appearance of continuous luminescence after BME addition on millisecond time-scales is not continuous on microsecond time scales.

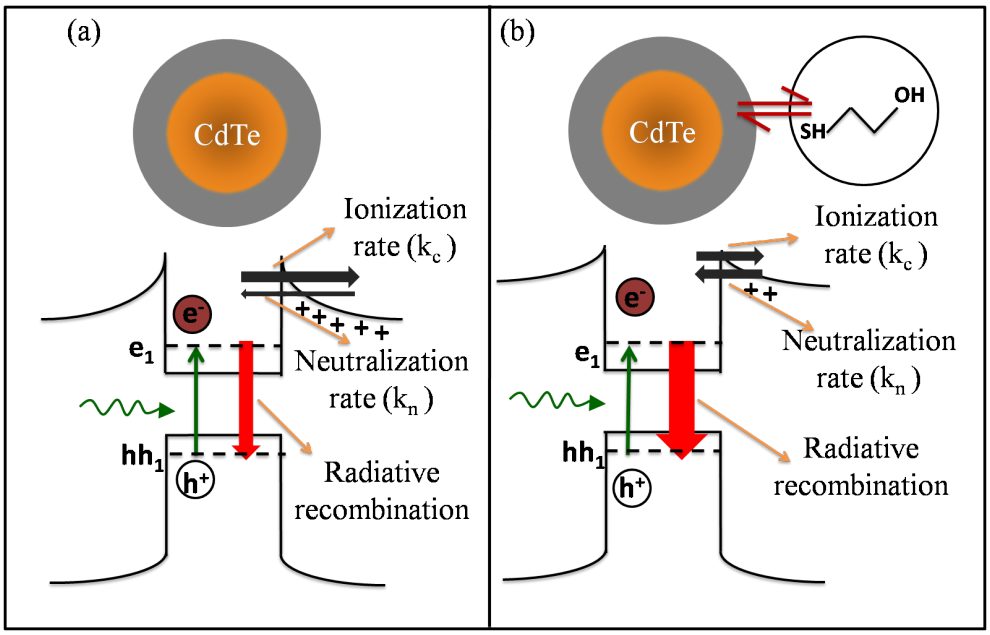

Figure 3.10: A schematic describing the findings in this paper regarding photo-physics of QDs using FCS. It describes electron transfer process in photo-excited QD in aqueous solution. a) A photo-excited electron-hole pair and its recombination give photo-luminescence. This radiative recombination rate is represented with thick red arrow. Occasionally, an electron is transferred to surface trap states with probability of $\approx 10^{-6} to 10_{-5}$. The neutralization rate k_n (thin black arrow) is negligibly small compared to ionization rate k_i (thick black arrow). b) After addition of BME both ionization and neutralization rate (thick black arrows) increase and the probability of electron transfer becomes $\approx 10^{-4}$. The QD luminescence now fluctuates due to this single and fast ionization-neutralization rate in microsecond time-scale.

3.4 Summary

To summarize, we found that blinking of colloidal CdTe QDs does not play a significant role in FCS measurements below threshold intensity for band-edge photo-excitation.

This threshold is actually related to the number of photons absorbed by a QD under illumination. Above this threshold excitation intensity, we measured the photo-induced dark fraction of QDs by recovering their luminescence with BME addition. The linear dependence of this fraction on intensity of band-edge photo-excitation suggests a one-photon photo-darkening process. This fraction is also used to calculate the probability of photo-darkening. The chemical kinetics rate in the reaction-diffusion model used in conventional FCS analysis is interpreted as the electron exchange rate that causes the "on-off" states of luminescence. The insensitivity of this rate towards temperature and its strong dependence on QD size supports the tunneling theory of electron exchange between core and surface trap states.

Bibliography

[1] M. Bruchez Jr., M. Moronne, P. Gin, S. Weiss, A. P. Alivisatos, Science 1998, 281, 2013.

[2] D. R. Larson, W. R. Zipfel, R. M. Williams, S. W. Clark, M. P. Bruchez, F. W. Wise, W. W. Webb, Science 2003, 300, 1434.

[3] J. Yao, D. R. Larson, H. D. Vishwasrao, W. R. Zipfel, W. W. Webb, Proc. Natl. Acad. Sci. (U.S. A.) 2005, 102, 14284.

[4] I. L. Medintz, H. T. Uyeda, E. R. Goldman, H. Mattoussi., Nat. Mater. 2005, 4, 435.

[5] M. Han, X. Gao, J. Z. Su and S. Nie, Nat. Biotechnol. 2001, 19, 621.

[6] A. Anas, H. Akita, H. Harashima, T. Itoh, M. Ishikawa, and V. Biju, J. Phys. Chem. B 2008, 112, 10005.

[7] W. C. W. Chan and S. M. Nie, Science 1998, 281, 2016.

[8] M. Michalet,F.F. Pinaud, L.A. Bentolila, J. M. Tsay, S. Doose, J. J. Li, G. Sundaresan, A. M. Wu, S.S. Gambhir, and S. Weiss, Science 2005, 307, 538.

[9] X. Y. Wu, H.J. Liu, J.Q. Liu, K. N. Haley, J.A. Treadway, J. P. Larson, N. F. Ge, F. Peale and M. P. Bruchez, Nat. Biotechnol. 2003, 21, 41.

[10] V. I. Klimov, A. A. Mikhaelovsky, S. Xu, A. Mlko and J. A. Hollingsworth, Science 2000, 290, 314.

[11] V. L. Colvin, M. C. Schlamp and A. P. Alivisatos, Nature, 1994, 370, 354.

[12] M. Nirmal, B.O. Dabbousi, M. G. Bawendi, J. J. Macklin and J. K. Trautman, T. D. Harris, and L. E. Brus, Nature 1996, 383, 802.

[13] M. Kuno, D. P. Fromm, H. F. Hamann, A. Gallagher, and D. J. Nesbitt, J. Chem. Phys. 2001, 115, 1028.

[14] K. T. Shimizu, R. G. Neuhauser, C. A. Leatherdale, S. A. Empedocles, W. K. Woo, and M. G. Bawendi, Phys. Rev. B, 2001, 63, 205316 (1).

[15] M. Dahan, S. Levi, C. Luccardini, P. Rostaing, B. Riveau and A. Science , 2003, 302, 442.

[16] S. Jeong M. Achermann, J. Nanda, S. Ivanov, V.I. Klimov, and J. A. Hollingsworth, J. Am. Chem. Soc., 2005,127, 10126.

[17] D. E. Gomez, M. Califano, and P. Mulvaney, Phys. Chem. Chem. Phys., 2006, 8, 4989.

[18] T. D. Krauss, S. O'Brien, L. E. Brus, J. Phys. Chem. B., 2001, 105, 1725.

[19] S. Li, M. Steigerwald, L. E. Brus, ACS nano 2009, 3, 1267.

[20] J. Zhao, G. Nair, B. R. Fisher, M. G. Bawendi, Phys. Rev. Lett., 2010, 104, 157403 (1).

[21] S. Hohang, T. Ha, J. Am. Chem. Soc. 2004, 126, 1324.

[22] Jay, L. N.; Carlini, L.; Suffern, D.; Ivanova, O.; Bradforth, S. E J. Phys. Chem. C, 2012, 116 (4), 2728.

[23] S. Doose, J. M. Tsay, F. Pinaud, and S. Weiss, Anal. Chem. 2005, 77, 2235.

[24] S. Ito, N. Toitani, L. Pan, N. Tamai, and H. Miyasaka, J. Phys. Condens. Matter., 2007, 19, 486208 10pp.

[25] C. Dong, J. Ren, Analyst, 2010, 135, 1395.

[26] C. Dong, H. Qian, N. Fang, J. Ren, J. Phys. Chem. B, 2006, 110, 11069.

[27] J. M. Tsay, S. Doose and S. Weiss, J. Am. Chem. Soc., 2006, 128, 1639.

[28] P. Zhang, L. Liang, C. Dong, H. Qian and J. Ren, Analytica Chimica Acta, 2005, 546, 46.

[29] Rochira, J. A.; Gudhti, M. V.; Gould, T. J.; Laughlin, R. R.; Nadeu,J. L.; Hess, S. T., J. Phys. Chem. C 2007, 111, 1695.

[30] D. Magde, E. Elson, W. W. Webb, Phys. Rev. Lett., 1972, 29, 705.

[31] D. Magde, E. Elson, W. W. Webb, Biopolymers 1974, 13, 1.

[32] O. Krichevsky, and G. Bonnet, Rep. Prog. Phys. 2002, 65, 251.

[33] P. Sengupta, J. Balaji, S. Maiti, Methods, 2002, 27, 374.

[34] E. Ying, D. Li, S. Guo, S. Dong, and J. Wang, Plos One, 2008, 3, e2222, 1.

[35] C. A. Leatherdale, W.-K. Woo, F. V. Mikulec, and M. G. Bawendi, J. Phys. Chem. B, 2002, 106, 7619.

[36] L. E. Brus, J. Chem. Phys. 1984, 80, 4403.

[37] A.V. Hills, J. Physiol., 1910, 40, iv.

[38] A. M. Fox, A.B. David, J. Livescu, J. E. Cunningham, and W. Y. Jan, IEEE journal of quantum electronics, 1991, 27, 2281.

[39] A. Larsson P. A. Anderkson, S. T. ENG, and A.Yariv, IEEE journal of quantum electronics, 1988, 24, 787.

Chapter 4

Diffusion Dynamics of π-conjugated polymers

4.1 Introduction

Conjugated polymers are important class of materials for electronic devices such as light emitting diodes, photovoltaics and field effect transistors [1-4]. In general, π-conjugated polymers have very strong tendency for aromatic π - stacking via inter or intra chain interactions which lead to the aggregated species [5-8]. One of the important conjugated polymer is Poly(phenylene-vinylene) (PPV) (shown in Figure 4.1). These molecular aggregates typically exist as low energy non-emissive species in which the excitation energy of highly luminescent excimers get trapped during radiative decay process. As a consequence, highly emissive polymers show low quantum efficiency or unwanted emission from aggregated species both in solution and in solid state (in films). Recently, there has been significant effort to understand the formation of these π-stack induced molecular aggregation in the development of highly emissive π-conjugated polymers [9, 11, 12]. A few synthetic approaches such as confinement of conjugation using cis-vinylene linkages [13-18] or separation of polymer chains through the introduction of bulky anchoring groups [19-23] were developed to address the aggregation phenomenon.

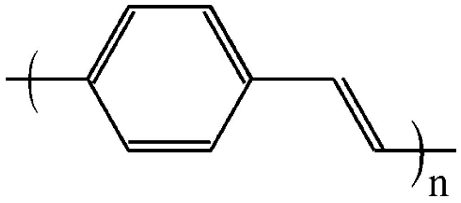

Figure 4.1: Molecular structure of PPV

Among various conjugated polymers, poly(p-phenylenevinylene)s (PPV) based polymers such as poly (2-methoxy- 5(2-ethylhexyl)-1,4-phylenevinylene) (MEH-PPV) is one of the most thoroughly studied electroluminescent polymer [24]. MEH-PPV structure is very unique in the sense that the branched ethylhexyloxy unit enhances the solubility of the polymer chain in common solvents and also shows improved luminescence properties by molecular aggregation via the branched chain. In our efforts to understand the aggregation in conjugated chains, we reported new bulky PPV homopolymers,[25] random copolymers, [26, 27] and bulky oligophenylenevinylenes [28, 29] based on tricyclodecanemethanol. Dependence of the role of solvent polarity, annealing temperature and molecular weight in chain aggregation of the MEH-PPV were also reported [30]. Though, these photophysical studies provide insight into the bulk properties of the polymers in solution or in film, it is very difficult to rationalize the role of polymer chain length on the molecular aggregation. Fluorescence correlation spectroscopy(FCS) is a single molecule technique to trace diffusion dynamics and can be used to study a single or a few polymer chains in extreme dilution at nano-molar concentrations. As discussed in Chapter 2, FCS determines the rate kinetics as well as the diffusion dynamics using minute fluctuations in the intensity at thermal equilibrium [31, 32, 33]. Such deviations occur both due to the motion of particles or chains as well as inter or intra-molecular chemical interactions. It is straightforward to measure the local concentrations, diffusion coefficients and rate kinetics of molecular interactions using FCS.

Recently Lin et al. [34] and Summers et al. [35] independently reported the fluorescence characteristics of commercially available MEH-PPV polymers (molecular weights of 37 kDa and 1,400 kDa) and tetrahedral phenylenevinylene oligomers using FCS. In both

cases, non-fluorescent conjugated polymers like poly(methylmethacrylate) (PMMA) or polystyrene were used to optimize or facilitate the uniform diffusion of conjugated chains in solution. Though the fluorescent decay dynamics of pure MEH-PPV chains were found comparable to that of the MEH-PPV/PMMA blends, a large difference in the collapsing of the chain conformations were noticed. The difference in the conformational change of the π-conjugated chains in association with PMMA chains was attributed to the presence of non-emissive PMMA (or polystyrene) as a dark matter. This limits the understanding of the diffusion properties of pure π-conjugated chains in solution. Investigating the diffusion dynamics of π-conjugated polymer chains is important as it provides more insight into the inter-chain interaction while processing these materials in electronic devices. There has not been a systematic effort to study the influence of chain length and their molecular weight distribution on the diffusion dynamics of π-conjugated polymers at single molecular or chain level. Therefore, it is very important to develop new approaches for conjugated polymers alone (without blending with other non-emissive polymers such as PMMA or polystyrene) to study their solution dynamics by single molecule technique such as FCS.

In the present investigation, we address this problem by using Fluorescence Correlation Spectroscopy(FCS), Size Exclusion Chromatography (SEC) techniques in freshly synthesized MEH-PPV polymers. We also address the following important fundamental questions: (i) what are the effects of the chain length (or molecular weight) and then molecular weight distribution on the diffusion dynamics of the π-conjugated polymers?, (ii) what is the effect of molecular weight on the inter-chain interactions of conjugated polymers and (iii) the effect of external stimuli such as temperature and concentration on the diffusion dynamics of polymer chains.

4.2 Materials and Methods

Materials 4-Methoxyphenol, 2-ethylhexylbromide, potassiumt-butoxide (1 M in THF), and Rhodamine 6G were purchased from Aldrich Chemicals. HBr in glacial acetic acid, paraformaldehyde, and KOH were purchased locally. Solvents were also purchased locally and were purified by standard procedures.

General Procedures 1H and 13C NMR spectra were recorded using a 400 MHz JEOL NMR spectrometer. All NMR spectrawere recorded in CDCl3 containing TMS as the internal standard. Infrared spectra were recorded using a Thermo-Scientific Nicolet 6700 FT-IR instrument in solid state in KBr. For the photophysical studies, all the solvents were purified according to the purification procedures prior to use. The polymer samples were completely dissolved by heating, and the homogeneous solutions thus obtained were used for further studies. The absorption spectra were recorded by a Perkin-Elmer Lambda 45 UV-visible spectrophotometer. The emission studies were done using a Florolog HORIBA JOBIN VYON fluorescence spectrophotometer with a 450 W Xe lamp as the excitation source using the reverse face mode. The quantum yields of polymer samples were determined using rhodamine 6G in water ($\phi = 0.95$). TCSPC fluorescence lifetime measurements were done by using a HORIBA JOBIN YVON Nano-LED source with a 460 nm wavelength to excite all the samples, and emission was collected at 560 nm. Fluorescence lifetime values were determined by deconvoluting the data with exponential decay using DAS6 decay analysis software. The quality of fit was judged by fitting parameters such as $\chi^2 \approx 1$, as well as the visual inspection of the residuals. The molecular weight determination and fractionation of MEH-PPV was done by the size exclusion chromatography (SEC) (or gel permeation chromatography, GPC) technique. A Viscotek GPC setup with mixed bed columns was utilized, and the signals were detected using RI, UV, and light scattering detectors. HPLC grade tetrahydrofuran was employed as a solvent for the samples, and the GPC setup was calibrated with polystyrene standards. An atomic force microscope from JPK instruments, Nanowizard III, was used for imaging the MEHPPV aggregates on the mica substrate. The sample was prepared by the drop-cast method on mica substrates. The cantilevers from budget sensors having a

stiffness of 40 N/m were used, and the imaging was performed in tapping mode.

4.2.1 Synthesis of MEHPPV polymer

Synthesis of 1-(2-ethylhexyloxy)-4-methoxybenzene: 4-Methoxyphenol (9.92 g, 0.08 mol) and KOH (8.96 g, 0.16 mol) were taken in DMSO (200 mL) and the mixture was refluxed at 80 ^{o}C for 2 h. Ethylhexylbromide (22.6 mL, 0.12 mol) was added dropwise to the reaction mixture and it was refluxed for 24 h. It was poured in 500 mL of water, extracted in dichloromethane, washed with 5% NaOH, brine solution, and dried over anhydrous sodium sulphate. The solvent was removed to obtain the product as brown coloured solid. It was purified by passing though silica gel column using 0.5% ethyl acetate in hexane as eluent. Yield= 9.4g (49 %). 1H-NMR (CDCl3, 400MHz) : 6.8 ppm (s, 4H, Ar-H); 3.7 ppm (dd, 2H, -OCH2-CH), 3.7 (s, 3H, OCH3), 1.4 (m, 1H, OCH2-CH), 1.4-0.9 ppm (m, 14H, alkyl).13C-NMR (CDCl3,100 MHz) : 153.5, 153.5, 115.3, 114.5 (Ar-C), 71.08 (Ar-OCH2), 55.7, 39.4, 30.8, 29.1, 23.8, 23, 14.1 and 11.05 ppm. FT-IR (KBr, cm^{-1}): 2936.8, 2361.2, 2066.9, 1596.8, 1510.2, 1465.2, 1384.1, 1108.4, 1037, 821.2, 742.1 and 521.5.

Synthesis of 1,4-bis(bromomethyl)-2-(2-ethylhexyloxy)-5-methoxybenzene: 1-(2-Ethylhexyloxy)-4-methoxybenzene (2.36 g, 0.01 mol) and p-HCHO (1.20 g, 0.04 mol) were taken in 30 mL of glacial acetic acid. HBr in glacial acetic acid (5.0 mL, 0.01 mol) was added using a pressure equalizing funnel. The reaction mixture was refluxed for 8 h, cooled to room temperature and the contents were poured in large amount of water. The product precipitated as a white solid and the filtered solid was crystallized from hot acetone. Yield = 2.7g (95 %). M.p = 82 C. [36] H-NMR (CDCl3, 400 MHz) : 6.8 ppm (s, 2H, Ar-H), 4.5 ppm (s, 4H, -CH2Br), 3.8 ppm (s, 3H, -OCH3), 3.8ppm (dd, 2H, OCH2-CH), 1.5-.8ppm (m, 15H,aliphatic-H). 13C-NMR (CDCl3, 100 MHz) : 150.9, 150.9, 127.4, 127.2, 114.2, 113.7(Ar-C), 70.8 (Ar-OCH2-CH), 56.2, 39.5, 29.0, 28.6, 23.9, 23.2, 14.0 and 11.2 ppm (aliphatic-C). FT-IR (KBr, cm^{-1}): 2933.3, 2871.6, 1726.4, 1513.1, 1459.9, 1400.9, 1312.7, 1106.4, 1033.6, 871.6, 675.0, 542.4, and 446.1.

Synthesis of MEH-PPV:

1,4-Bis(bromomethyl)-2-(2-ethylhexyloxy)-5-methoxybenzene (0.84 g, 2.0 mmol) was dissolved in dry THF (80 mL) and the reaction mixture was cooled to 5^oC. Potassium tert-butoxide (12.0 mL, 1M THF solution) was added drop-wise to the reaction mixture under nitrogen atmosphere. It was stirred at 30 C for 24 hours and the resultant orange-red solution was poured into large amount of methanol. The red precipitated polymer was dissolved in THF and re-precipitated again in methanol. The polymer was dried in vacuum oven overnight. Yield: 0.2 g (38%). 1H-NMR (CDCl3, 400MHz) : 7.5 ppm (b, 2H, Ar-H), 7.1 ppm (s, 2H, CH=CH), 3.9 ppm (m, 5H, OCH3 and -OCH2-), 1.8 - 0.8ppm (m, 15H, aliphatic). FT-IR (KBr, cm^{-1}): 3757.2, 3447.6, 2936.4, 2860.6, 2364.1, 2152.6, 1712.4, 1632.9, 1508.5, 1462.6, 1411.1, 1351.9, 1039.02, 968.9, 863.7, and 722.1.

Poly[2-methoxy-5-(2-ethylhexyloxy)-1,4-phenylenevinylene] (MEH-PPV) was synthesized by Gilch-route from the bis-bromomethylated monomer using potassium tert-butoxide as base catalyst at 30 ^oC in THF as shown in figure 4.2 [25, 26]. The monomer synthesis is involved in sequence of reactions starting from 4-Methoxyphenol to give the required monomer. The structure of polymers and monomers were confirmed by NMR, FT-IR spectroscopy. 1H-NMR and 13C-NMR of monomer and polymer samples are shown in supporting information. 1H-NMR spectrum of MEH-PPV polymer showed two broad peaks at 7.4 ppm and 7.1 ppm corresponding to phenyl aromatic protons and vinylene protons, respectively. The peaks for all other protons appeared below 4.00 ppm and the intensities of all the protons matched with that of the expected structure. This MEHPPV polymer was synthesized by Ms. Mahima Goel from Dr. Jayakannan group at Chemistry Division, IISER Pune.

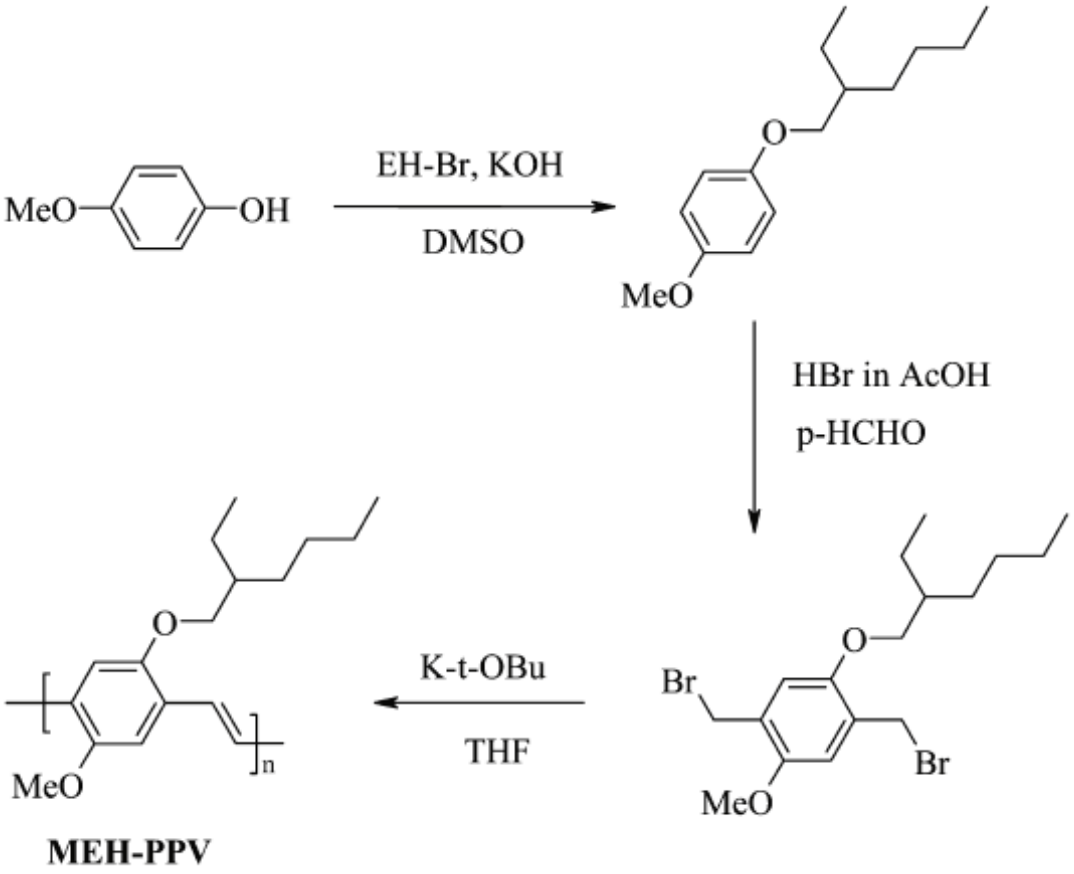

Figure 4.2: Synthesis scheme for MEH-PPV polymer

4.2.2 Size Exclusion Chromatography of MEHPPV polymer

The molecular weight of the synthesized polymer was determined by SEC. SEC chromatograms are given in figure 4.3. The synthesized sample showed broad distribution (see figure 4.3a) with M_n= 38,700 and M_w = 1,83,000 with polydispersity of 4.7. The broad SEC chromatogram showed large elution time from 12 to 18 minutes. This provides opportunity to fractionate the sample into narrow dispersed fractions. About 100 μL of 0.5 mg/mL of the sample in THF was injected into the SEC column and samples were collected at every 30 seconds after 12 minutes of the elution time. Total of 10 fractions were collected and the process was repeated at least for 10 times to collect more amounts of samples in each fraction. SEC chromatograms of all fractions were determined and are shown in figure 4.3(b). In the further discussion we use the following convention that the un-fractionated MEH-PPV sample is referred as uf-PPV and all fractionated samples are referred as Fn where "n" represents the SEC - fraction number as mentioned in the figure 4.3(b). Molecular weight, polydispersity, absorption and emission peaks are mentioned in the table 4.1.

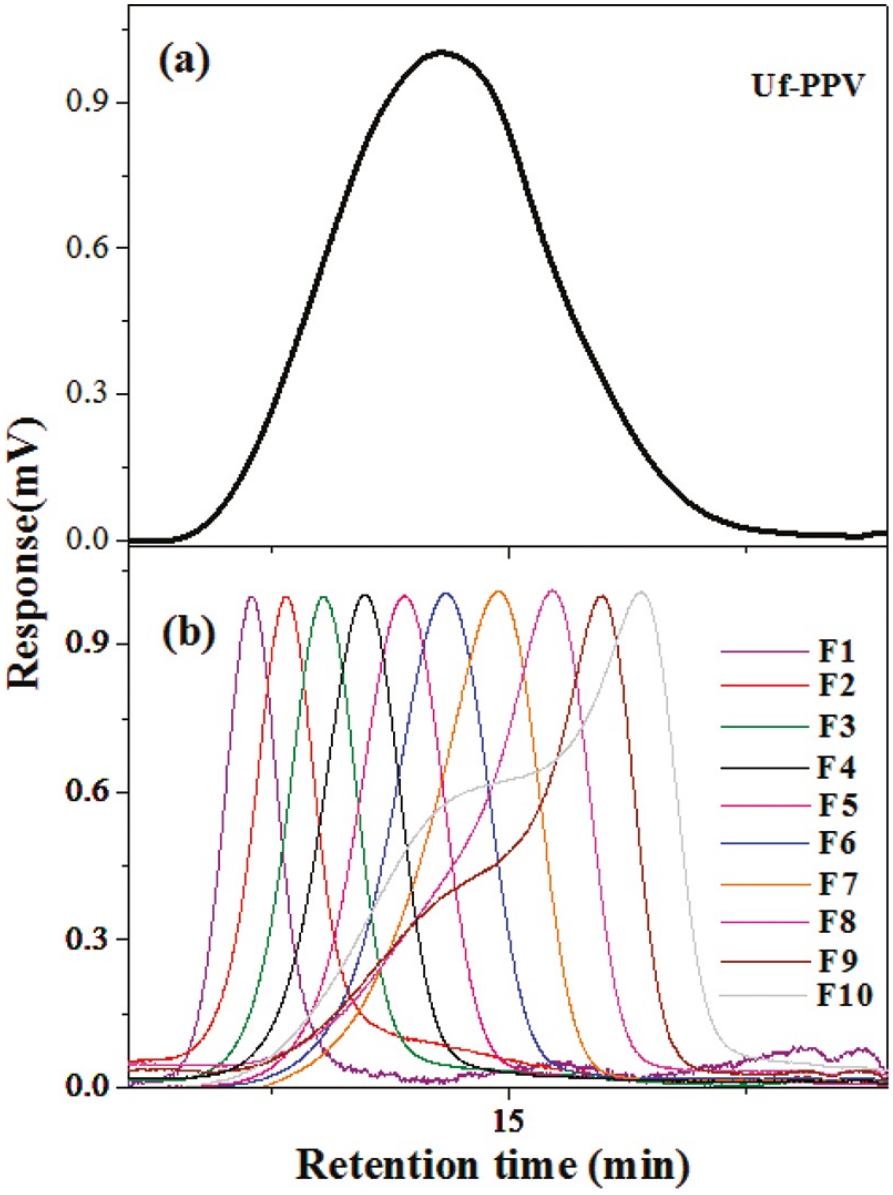

Figure 4.3: Size Exclusion Chromatograms of MEH-PPV and its fractionated samples (a) unfractionated MEH-PPV with a broad retention time (corresponds to molecular weight of the polymer) distribution.(b) fractionated samples (F1-F10) with narrow distribution. Values of molecular weights obtained are shown in the table

Sample	M_n	M_w	M_w/M_n	R_{fwhm}	$\lambda_{Max.}(abs)$	$\lambda_{Max.}(Emission)$
uf-PPV	38700	183000	4.7	158	498	556
F2	524000	688000	1.3	46	490	554
F3	386000	467000	1.2	50	489	552
F4	231000	307000	1.3	55	487	552
F5	144000	198000	1.3	61	490	551
F6	86000	129000	1.5	69	491	554
F7	52000	90000	1.7	76	490	553
F8	31600	73000	2.3	80	489	553

Table 4.1: M_n - Number averaged molecular weight, M_w - Weight averaged molecular weight, M_w/M_n - Polydespersity, R_{FWHM} - Full width at half-maximum of SEC chromatogram, $\lambda_{max}(Abs)$ - Absorption maxima, $\lambda_{max}(Emission)$ - Emission maxima

The fractions F1, F9 and F10 were obtained in very small quantities and they were not used for any further analysis. Molecular weights of polymers may be overestimated due to the difference in the polystyrene standards generally used for calibration.Hence, the polydispersity of the samples calculated based on M_w/M_n values may be little different from the actual distribution of the chains. Full width at half maximum of the retention time (R_{FWHM}, R=Retention time) of the SEC- chromatogram is another important quantity which directly provides the distribution of the polymer chains in fractionated samples irrespective of the standards used for calibration of the SEC. The R_{FWHM} for all the fractions were determined and the data are provided in table 4.1. For instance, the narrow dispersed sample (F2) has lower R_{FWHM} compared to that of its broad molecular weight counterpart (F8). It is evident that the fractionated samples are found to show much narrow distribution as compared to that of the un-fractionated sample (uf-PPV). The polydispersity data (see table 4.1) shows a non-linear trend and the values are almost invariant up to F5 and appeared little broad from F6 to F8. Though all chromatograms are mono-disperse (for F2 to F8, see figure 4.3b), the R_{FWHM} values increase with decrease in the molecular weights (towards low fraction number). It indicates that the polydispersity of the fractionated samples increase with decrease in the molecu-

lar weights. It may be summarized that all the fractionated samples are mono-dispersed; however they vary in their chain length (or molecular weight) as well as distribution. This facilitates the investigation on the role of polymer chain length (also distribution) on the diffusion kinetics and luminescent characteristics on wide range of narrow distributed of MEH-PPV samples.

4.2.3 Photophysical properties

The photophysical properties of the fractionated samples were studied in toluene. Toluene is chosen as solvent for spectroscopic studies due to high boiling point, low vapor pressure and not hygroscopic under atmospheric conditions. Further, toluene is also suitable solvent for studying chain interactions in conjugated polymers, specifically MEH-PPV[30]. For this purpose, fractionated samples were dried and then re-dissolved in HPLC grade toluene. The molar extinction coefficient of MEH-PPV was determined as 1.9×10^4 $mol^{-1}cm^{-1}$ and it is used for determination of the concentration of polymer samples employed for photophysical studies. Polymer solution (in toluene) with optical density of 0.1 (concentration = 5.3×10^{-6} M) were prepared for photophysical studies. The absorption and emission spectra of the F2 to F8 and uf-PPV samples are shown in figure 4.4a and 4.4b respectively. The emission spectra were recorded by exciting at 490 nm and Rhodamine 6G was used as standard to determine the quantum yield of the samples using following equation $\phi_s = \phi_r(F_s A_r / F_r A_s)(n_s/n_r)^2$, where ϕ_s is the fluorescent quantum yield, F is the area of the emission curve, n is the refractive index of the solvent, and A is the absorbance of the solution at the exciting wavelength. The subscripts r and s denotes the reference and sample respectively.

The un-fractionated sample, uf-PPV has absorbance maxima at 498 which is almost 10 nm red shifted compared to that of the fractionated samples (see table4.1). The red shift in the un-fractionated sample indicates that the sample has more aromatic π-stacking in solution through strong polymer chains interactions. Interestingly, the photophysical properties and quantum yields of the fractionated samples were almost uniform for wide range of molecular weights ranging from 500 kDa to 32 kDa. The quantum yield of the

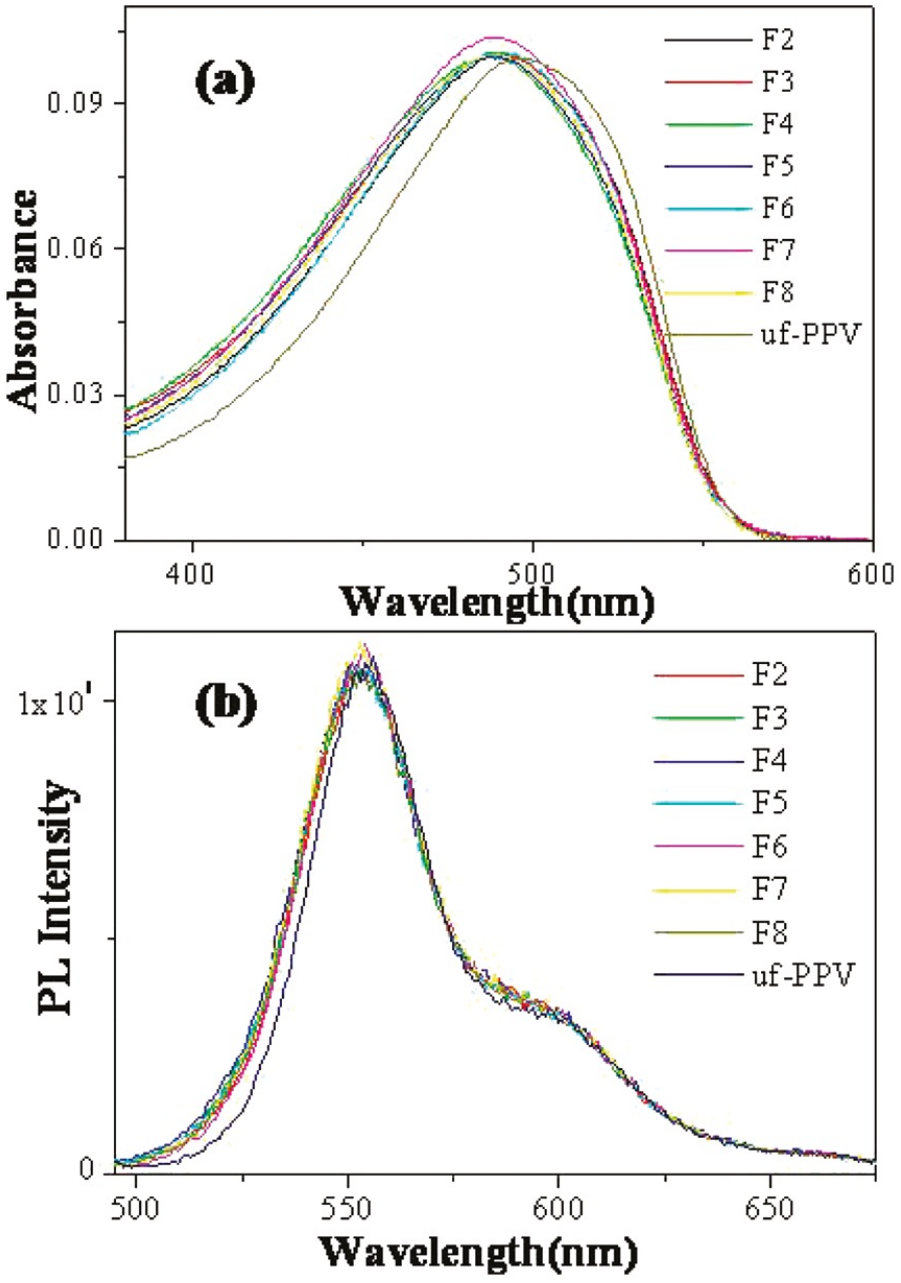

Figure 4.4: a)Absorption and b)Emission spectra of polymer fractions in toulene solution at room temperature

samples was obtained in the range of 0.22 - 0.25, which are in accordance with earlier reports for MEH-PPV samples [39, 40]. Photophysical studies of all fractions determined and are consistent with the literature reports. This also indicates suitability of the sample for FCS studies

4.3 Results and Discussion

4.3.1 FCS analysis of MEH-PPV polymer

Since the dynamics of the polymer chains is expected to be heterogeneous with a distribution of diffusion time-scales, we use MEMFCS fitting algorithm to obtain the correct diffusion coefficients of the polymer chains [37, 38]. The auto-correlation curve for 144 kDa (for F5) is shown in figure 4.5. The data was fitted using conventional single component fit (see figure 4.5a) as well as MEMFCS fitting algorithm (see figure 4.5b). MEMFCS fitting shows less residue compared to conventional fitting. This suggests that heterogeneous distribution is present in polymer chain diffusion. Hence, in the present work the MEMFCS fitting is used for FCS data analysis.

To optimize the experimental conditions for measurement of diffusion dynamics of MEHPPV chains in toluene, we choose fraction 5 (M.W. 144 kDa) and performed experiments in various directions namely, measurement time, temperature and concentration of chain chromophores. Autocorrelation curves were recorded upto 900 s with regular time interval of 200 s. This is to establish the stability of the luminescent chromophores with respect to time under laser illumination. Figure 4.6a shows that no systematic change in diffusion coefficient with time up to 700 seconds. This indicates stability of polymers are upto 10-12 minutes for FCS measurements. Further, the effect of temperature on the diffusion coefficient was investigated from 30 - 80 ^oC (with 10 ^oC interval) and is shown in figure 4.6b. The diffusion coefficients decreased with increase in temperature and this can be due to the expansion of polymer chains. Therefore, the diffusion measurements were restricted to room temperature (at 30 ^oC). We further studied the effect of concentration

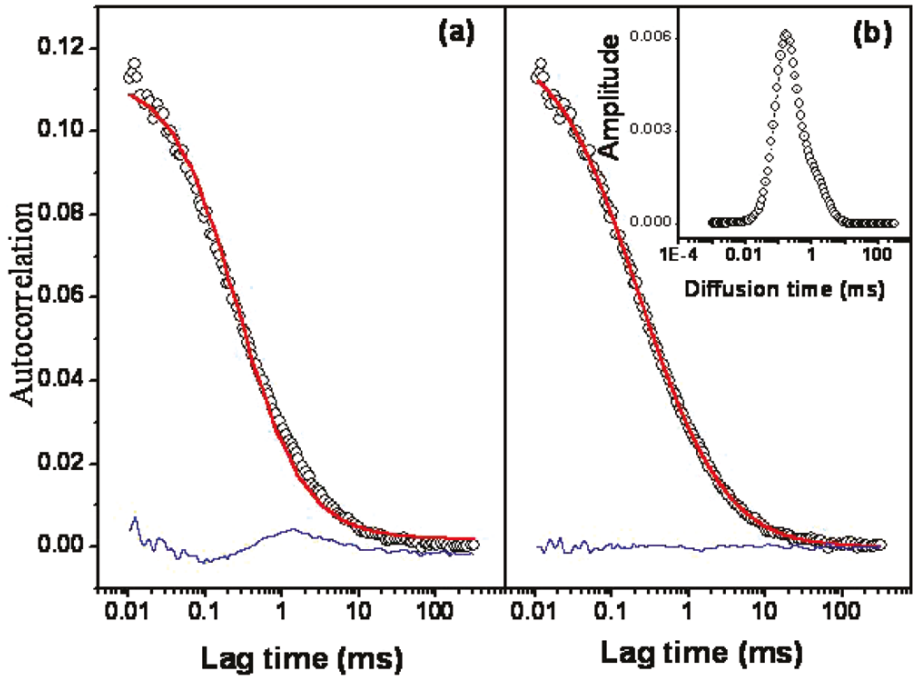

Figure 4.5: Autocorrelation data of fraction F5 fitted with (a)conventional single component fit and (b)MEMFCS fit. Inset shows the distribution of diffusion time

of polymer samples of diffusion measurements. It was found that concentration in the range of 10 to 20 nM were appropriate for experiments. Based on the above analysis of fraction-5, we have optimized the system with concentration of 10 nM and measurement time of 100 s at room temperature for further diffusion studies of other fractions. Eventhough, the polymer sample is stable for approximately 10 min, we have chosen only 100 s measurement time as this time is sufficiently larger time (10^4 orders of magnitude) than the polymer diffusion diffusion time (μ s range). Therefore, the recorded autocorrelations are well-averaged with in this measurement time.

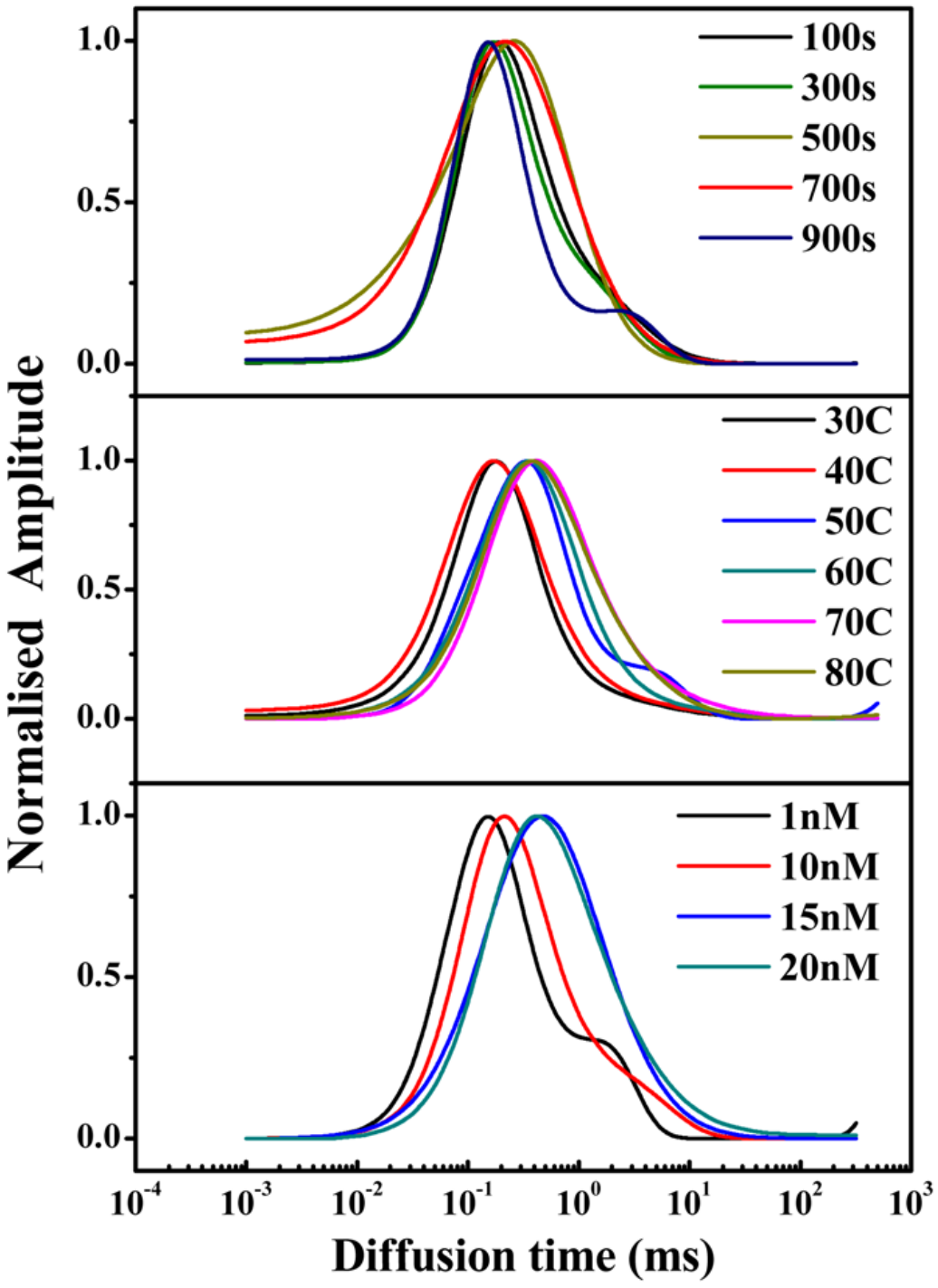

Figure 4.6: MEMFCS fits of fraction F5 at various a)time intervals, b)temperatures and c)concentrations

4.3.2 Role of the chain length on molecular aggregation of MEH-PPV

To trace the role of π-conjugated chain length (or molecular weight) on the diffusion dynamics, four narrow dispersed fractionated samples (F3, F4, F5 and F7) with molecular weights 386, 231, 144, and 52 kDa and a broad un-fractionated uf-PPV sample were chosen. Diluted solution of 10 nM of all these fractions in toluene were used to record auto-correlation curves. figure 4.7 shows the autocorrelation curve and MEMFCS plots of all fractions (see also Table 4.2). The autocorrelation curve of the uf-PPV showed multiple diffusion characteristics with two shoulders at $\tau_D = 0.02$ and 3.0 ms. The two shoulders either side of the main peak are may be due a larger aggregates and a very short polymer chains in the uf-PPV sample and these should be avoided in the fractionated samples. As expected, all fractionated samples show single peak with certain Full Width at Half Maximum D_{FWHM}.

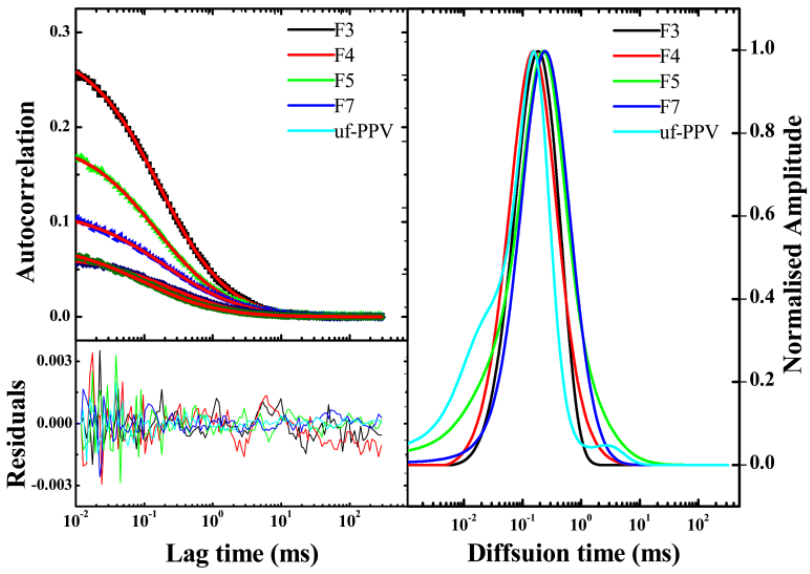

Figure 4.7: a)Autocorrelation curves and b)MEMFCS fits of different fractions. Parameters obtained are listed in the following table.

Sample	$\tau_D(peak)(ms)$	$D_{FWHM}(ms)$	N	Diff. Coeff($\mu m^2/s$)	Size(nm)
F3	0.190±0.03	0.415	3.89	75.3±11.8	130±30
F4	0.147±0.01	0.448	5.9	88.8±6.0	120±20
F5	0.190±0.01	0.566	9.2	68.2±3.5	940±130
F7	0.246±0.02	0.692	17.4	57.6±4.6	640±140
uf-PPV	0.147	0.280	15.86	96.8	film

Table 4.2: $\tau_D(peak)$ - peak value of the diffusion time, D_{FWHM} - Full width at half-maximum of diffusion time, N - Average number of chromophores, D - Diffusion coefficient, Average size of polymer chain aggregates obtained form AFM images

Following quantities are extracted from above result, 1)average number of polymer chains (N) in the detection volume(1/G(0)), D_{FWHM} and diffusion coefficient and are plotted with molecular weight as shown in figure 4.8. The D_{FWHM}, N decreases with increasing molecular weight. Unlike other fluorescent molecules, in conjugated polymers, the concentration of the species are typically calculated based on the repeating unit mass of the chromophores. Thus, for a given concentration, higher molecular weight polymer have fewer chains in solution compared to that of lower molecular weight counterpart. Therefore, the increase in N-value for lower molecular weight fractions is the consequence of more number of shorter chains appeared in detection volume (see figure 4.8a, b). The diffusion coefficient increases with increase in the molecular weight. This means the higher molecular weight chains (longer chain) diffuse much faster than shorter ones (see figure 4.8c). At very large molecular weight (F3), the diffusion coefficient attains plateau. The comparison of data of D_{FWHM}, diffusion coefficient and 'N' of unfractionated sample uf-PPV with narrow fractionated samples revealed the following points (see also table 4.2): (i) the diffusion coefficient of the uf-PPV chains are almost similar to the high molecular weight polymer chains of M_n = 400 kDa (F3) (ii) the average number of fluorophores in the focal volume (N) for uf-PPV is very close to that of low molecular weight chains of M_n = 52 kDa (F7). These results of uf-PPV are in contradiction with the observation in the narrow dispersed samples. This indicates that the diffusion is not uniform in the un-fractionated samples and their diffusion coefficient is predomi-

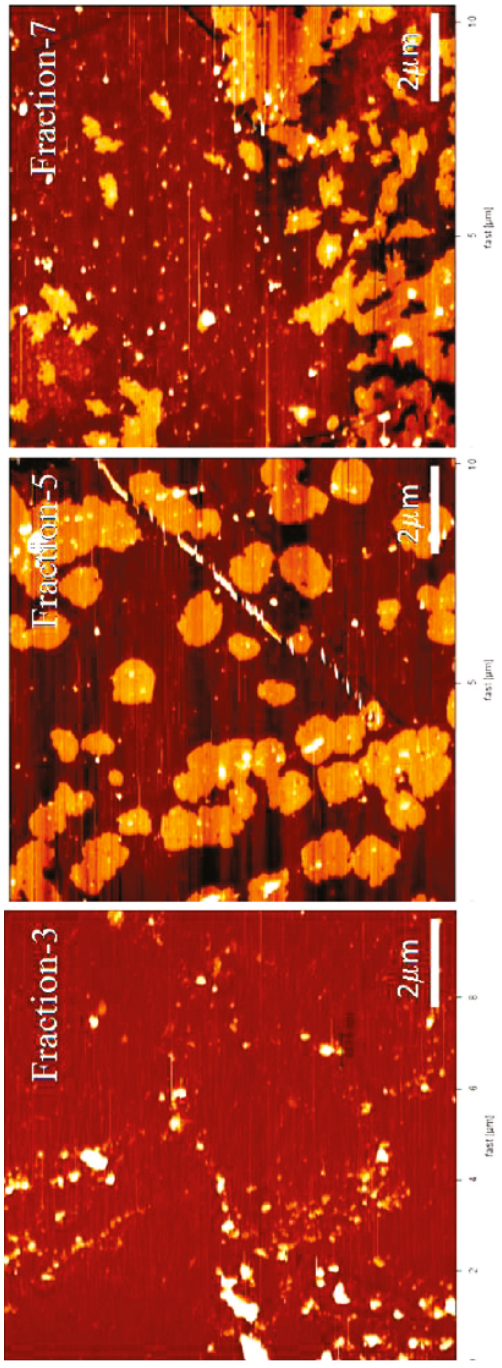

Figure 4.8: AFM images of fractions 3,5 and 7

nantly determined by the longer chains present in the broad distribution (see figure 4.3a). Therefore, it is clearly evident that FCS data for the un-fractionated samples alone is not enough to establish the correlation between the molecular weight of the chains with their diffusion dynamics. It is important to fractionate the samples in order to obtain the correct diffusion coefficients using the MEMFCS algorithm. The trends in figure 4.8 indicate that the diffusion dynamics of the chains is predominantly influenced by the chain length rather than molecular weight distribution. All the fractions have identical chemical structure with trans-vinylene linkage. Therefore, the polymer chains in the fractions are expected to have stiff backbone structure. The number average molecular weights of the fractions have minimum 30 kDa and it accounts for at least 100 repeating units in the backbone. Typical persistence lengths for the polymer are constituted by 8-10 repeating units. Therefore, the chain lengths of fractionated samples are much longer than that of expected persistence length for MEH-PPV chains. Further, toluene is very good and highly preferred solvent for MEH-PPV chains and it keeps the chain in most expanded conformation. Therefore, the difference in the diffusion dynamics of the polymer chains having different molecular weights is a consequence molecular aggregation phenomenon rather than other structural parameters like persistence length.

In order to understand the chain length dependent diffusion dynamics, the fractionated samples were subjected to AFM analysis. Typically, polymer chains exists either as expanded or collapsed globular particles in solution depending on their chain length (or molecular weight) [41]. At higher molecular weight, the strong intra-chain interactions result in the formation of globular (or tightly packed) particles [42]. On the other hand, lower molecular weight chains have hairy structures (like in the expanded conformation) and possess high possibility for inter-chain interactions. Among the various available techniques to analyze the existence of chain interactions and their particulate nature, AFM images of the films cast from the dilute solutions are highly reliable. AFM images of samples F3, F5 and F7 are shown in figure 4.9. Evaporation of solvent molecules from a drop of polymer solution increases the local concentration of the polymer chains and promotes their chain-interactions. Strong intra-chain interactions produce tiny par-

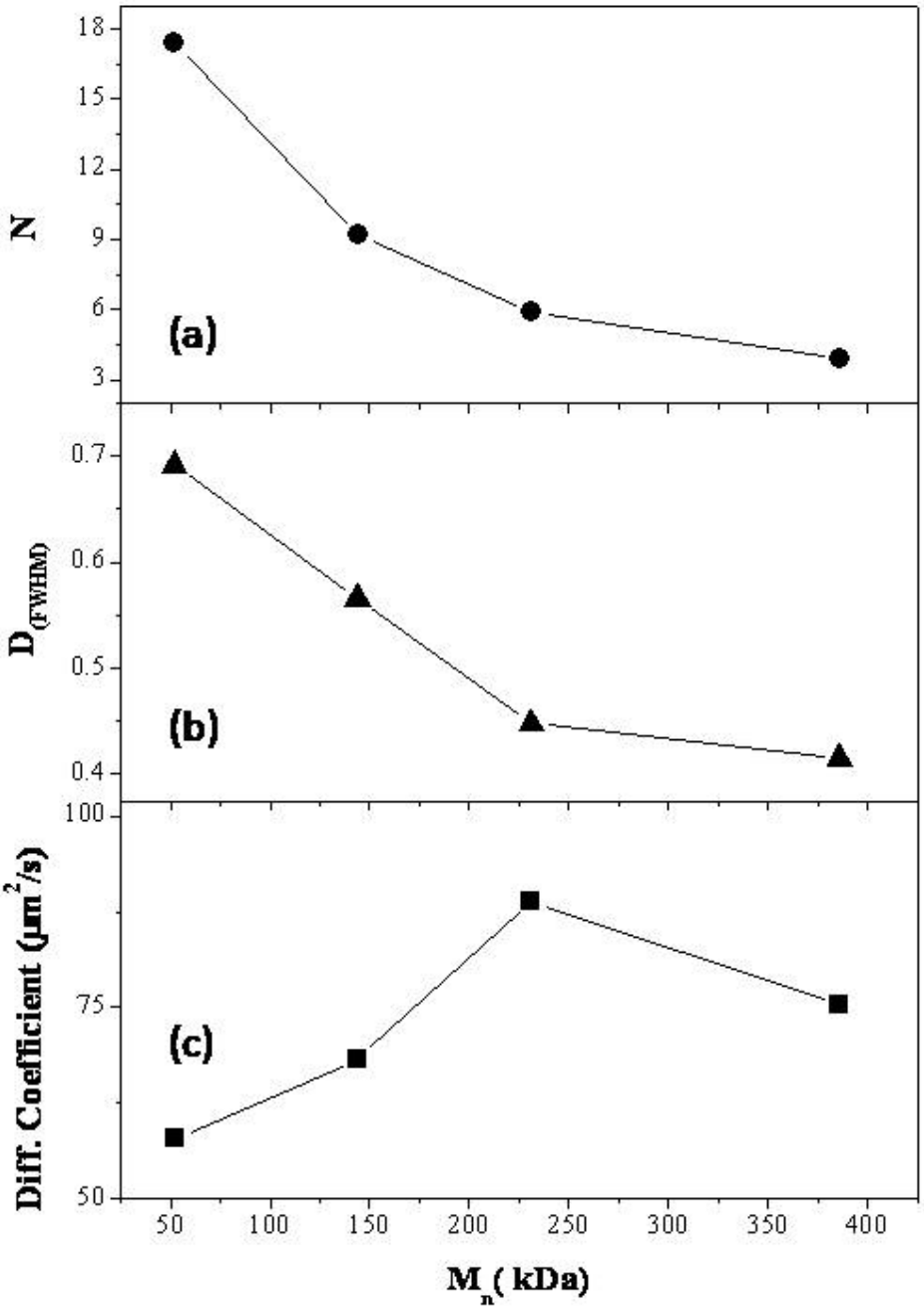

Figure 4.9: plots of N, D_{FWHM}, Diffusion coefficient versus Molecular weight M_n

ticles whereas larger particles are produced via inter-chain interactions. Higher molecular weight sample F3 produced 130 nm tiny particles whereas micrometer sized larger particles were formed by F5. At very low molecular weight polymers (in the sample F7), the particulate nature is lost and it appeared as film via strong inter-chain interactions. The size of the structures formed in the dilute solutions inferred from the hydrodynamic radius in FCS data is much smaller compared to the aggregates in AFM images. This is because AFM images are taken after the aggregates settled down after evaporation of solvents. It should be noted that the AFM shows smaller aggregates for longer chains compared to shorter chains indicating the beginning of aggregation and inter-chain interactions in solution itself. Based on the above experimental evidence, a model has been proposed for the diffusion dynamics of the conjugated polymers in solution in figure 4.10. There are two important factors that affect the mobility of the chains in dilute solutions: (i) size of the polymer chain aggregates (or particles) and (ii) the inter-particle interactions. In a dilute solution, the globular tiny molecules move fast and have relatively less probability for the inter-particle interactions. Low molecular weight chains possessed hairy structures, which inherently enhance the inter-particle interaction. As a consequence, the diffusion became slow in the low molecular weight chains. Hence, the larger polymer chain lengths experience fast diffusion in solution compared to their low molecular weight counterparts. In a nut shell, in the present investigation, we have clearly proved that the isolation of narrow polydisperse conjugated sample is very much crucial in establishing the correlation between diffusion dynamics and chain length (or molecular weights) of π -conjugated polymers using FCS.

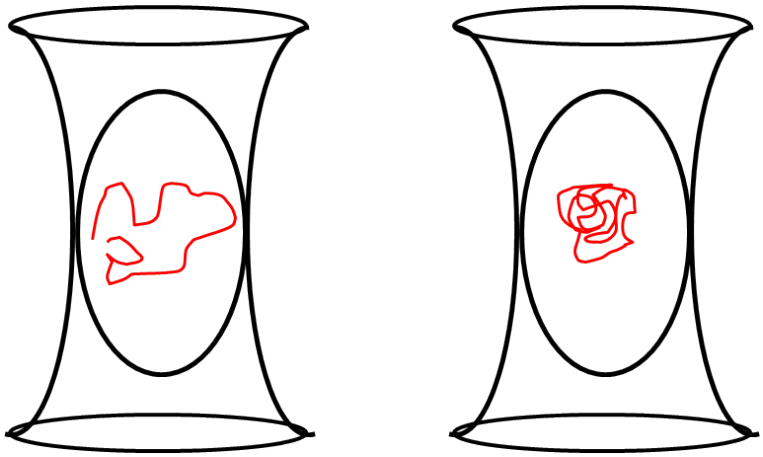

Figure 4.10: Model for the diffusion of different molecular weight polymers

4.4 Summary

In conclusion, the diffusion dynamics of the π-conjugated polymer was investigated for freshly synthesized and narrow molecular fractionated MEHPPV using FCS. The important outcome of the present investigation may be summarized as follows: (i) narrow polydispersed samples of molecular weights ranging from 500 to 20 kDa were obtained by the fractionation techniques, (ii) the retention time based R_{FWHM} of SEC chromatogram is found to be a more suitable representation for the distribution of the fractionated samples, (iii) the photophysical properties of the fractionated samples are almost identical for the entire molecular weight range of 500 to 20 kDa, (iv) the maximum entropy based fitting (MEMFCS) method is used to determine the diffusion time from the FCS data and this method is particularly useful in such situations where the diffusion dynamics is strongly heterogeneous, (v) three parameters obtained from FCS such as D_{fwhm}, diffusion coefficient, and average number of particles in excitation volume (N) are used to trace the diffusion dynamics of the polymer chain, (vi) D_{fwhm} and N decrease with the increase in the molecular weight of the chains, whereas the diffusion coefficient showed the opposite trend, (vii) AFM studies revealed the formation of tiny nanoparticles at higher molecular chains, and (viii) the high molecular weight chains possessed globular structure and diffused faster in solution, whereas the low molecular weight chains possessed inter-particle interaction and show slow diffusion in solution. The approach demonstrated here may

be very useful for establishing the role of the π-conjugated chain length (or molecular weight) while processing them from dilute solution in electronic devices such as light emitting diodes and photovoltaics.

Bibliography

[1] Burroughes, J. H.; Bradley, D. D. C.; Brown, A. R.; Marks, R. N.; Mackay, K.; Friend, R. H.; Burns, P. L.; Holmes, A. B. Nature 1990, 347, 539.

[2] Friend, R. H.; Gymer, R. W.; Holmes, A. B.; Burrouges, J. H.; Marks, R. N.; Taliani, C.; Bradley, D. D. C.; Dos Santos, D. A.; Gredas,J. L.; Longlund, M.; et al. Nature 1999, 397, 121.

[3] Sheats, J. R.; Antoniadis, H.; Hueschen, M.; Leonard, W.; Miller,J.; Moon, R.; Roitman, D.; Stocking, A. Science 1996, 273, 884.

[4] Kraft, A.; Grimsdale, A. C.; Holmes, A. B. Angew. Chem., Int. Ed.1998, 37, 402.

[5] Traiphol, R.; Charoenthai, N.; Srikhirin, T.; Kerdcharoen, T.;Osotchan, T.; Maturos, T. Polymer 2007, 48, 813.

[6] Hsu, J. H.; Fann, W.; Tsao, P. H.; Chuang, K. R.; Chen, S. A.J. Phys. Chem. A 1999, 103, 2375.

[7] Jakubiak, R.; Collison, C. J.; Wan, W. C.; Rothberg, L. J.; Hsieh, B. R. J. Phys. Chem. A 1999, 103, 2394.

[8] Chen, S. H.; Su, A. C.; Chou, H. L.; Peng, K. Y.; Chen, S. A.Macromolecules 2004, 37, 167.

[9] Huang, W. Y.; Matsuoka, S.; Kwei, T. K.; Okamoto, Y. Macromolecules 2001, 34, 7166.

[10] Setayesh, S.; Grimsdale, A. C.; Weil, T.; Enkelmann, V.; Mullen, K.; Meghdadi, F.; List, E. J. W.; Leising, G. J. Am. Chem. Soc. 2001, 123, 946.

[11] Becker, H.; Spreitzer, H.; Kreuder, W.; Kluge, E.; Schenk, H.; Parker, I.; Cao, Y. Adv. Mater. 2000, 12, 42.

[12] Nguyen, T. Q.; Doan, V.; Schwartz, B. J. J Chem. Phys. 1999,110, 4068.

[13] Cyriac, A.; Amrutha, S. R.; Jayakannan, M. J. Polym. Sci., Polym.Chem. 2008, 46, 3241.

[14] Padmanabhan, G.; Ramakrishnan, S. J. Am. Chem. Soc. 2000,122, 2244.

[15] Liao, L.; Pang, Y.; Ding, L.; Karasz, F. E.; Smith, P. R.; Meador, M. A. J. Polym. Sci., Polym. Chem. 2004, 42, 5853.

[16] (a) Liao, L.; Pang, Y.; Ding, L.; Karasz, F. E. Macromolecules 2002, 35, 3819. (b) Pang, Y.; Li, J.; Hu, B.; Karasz, F. E. Macromolecules 1999, 32, 3946.

[17] Liao, L.; Pang, Y.; Ding, L.; Karasz, F. E. Macromolecules 2001,34, 6756.

[18] Zheng, M.; Sarker, A. M.; Gurel, E. E.; Lahti, P. M.; Karaz, F. E. Macromolecules 2000, 33, 7426.

[19] (a) Chou, C. H.; Hsu, S. L.; Dinakaran, K.; Chiu, M. Y.; Wei, K. H. Macromolecules 2005, 38, 745. (b) Xia, C.; Advincula, R. C.Macromolecules 2001, 34, 5854.

[20] (a) Yang, J. S.; Swager, T. M. J. Am. Chem. Soc. 1998, 120, 5321. (b) Yang, J. S.; Swager, T. M. J. Am. Chem. Soc. 1998, 120, 11864.

[21] Wang, H.; Song, N.; Li, H.; Li, Y.; Li, X. Synth. Met. 2005,151, 279.

[22] Tang, R.;Chuai, Y.;Cheng,C.; Xi, F.; Zou,D. J. Polym. Sci., Part A: Polym. Chem. 2005, 43, 3126.

[23] Bao, Z.; Amundson, K. R.; Lovinger, A. J. Macromolecules 1998, 31, 8647.

[24] Akcelrud, L. Prog. Polym. Sci. 2003, 28, 875.

[25] Amrutha, S. R.; Jayakannan, M. J. Phys. Chem. B 2006, 110, 4083.

[26] Amrutha, S. R.; Jayakannan, M. Macromolecules 2007, 40, 2380.

[27] Resmi, R.; Amrutha, S. R.; Jayakannan, M. J. Polym. Sci., Polym. Chem. 2009, 47, 2631.

[28] Amrutha, S. R.; Jayakannan, M. J. Phys. Chem. B 2009, 113, 5083.

[29] Goel,M.; Jayakannan,M. J. Phys. Chem. B 2010, 114, 12508.

[30] Amrutha, S. R.; Jayakannan, M. J. Phys. Chem. B 2008, 112,1119.

[31] (a) Krichevsky, O.; Bonnet, G. Rep. Prog. Phys. 2002, 65, 251.

[32] Magde,D.; Elson, E.;Webb,W. Phys. Rev. Letts. 1972, 29, 705.

[33] (a) Magde, D.; Elson, E. Biopolymers 1974, 13, 1.

[34] Lin, H.; Person, G.; et al. Nano Lett. 2009, 9, 4456.

[35] Summers, M. A.; Robinson, M. R.; Bazan, G. C.; Buratto, S. K. Chem. Phy. Lett. 2002, 364, 542.

[36] Neef, C. J.; Ferraris, J. P. Macromolecules 2000, 33, 2311-2314.

[37] Sengupta, P.; Balaji, J.; Maiti, S. Methods 2002, 27, 374-387.

[38] Sengupta, P.; Garai, K.; Balaji, J.; Periasamy, N.; Maiti, S. Biophys. J. 2003, 84, 1977-1984.

[39] Fu, L.; Ferreira, R. A. S.; Silva, N. J. O.; Fernandes, A. J.; Ribeiro- Claro, P.; Goncalves, I. S.; Bermudez, V. Z.; Carlos, L. D. J. Mater. Chem. 2005, 15, 3117.

[40] Fakis, M.; Anestopoulos, D.; Giannetas, V.; Persephonis, P. J. Phys. Chem. B 2006, 110, 24897.

[41] Odian, G. Principles of polymerization, 4th ed.; John Wiley Sons: India, 2007.

[42] Wang, P. S.; Lu, H. H.; Liu, C. Y.; Show, A. C. Macromolecules2008, 41, 6500.

Chapter 5

Conclusions and Future Outlook

5.1 Summary

In this thesis, we presented theory and instrumentation of Fluorescence Correlation Spectroscopy technique. We used FCS to address the fluorescent intermittency or "blinking" behavior in quantum dots and Molecular aggregation in π-conjugated polymers.

Our results suggest that blinking in colloidal CdTe QDs affects the FCS measurements. Excitation intensity dependence of "blinking" is unusual. Below threshold intensity, blinking is negligible and does not affect the diffusion measurements. Above this threshold, it alters number of molecules in the detection volume due to photo darkening in QDs. We measured the photo-induced dark fraction and photo darkening probability of QDs by recovering their luminescence by adding anti-blinking agent such as β-Mercaptoethonal. The chemical kinetics rate in the reaction-diffusion model used in conventional FCS analysis is interpreted as the electron exchange rate that causes the "on-off" states of luminescence. The insensitivity of this rate towards temperature and its strong dependence on QD size supports the tunneling theory of electron exchange between core and surface trap states

In π-conjugated polymers work, we presented FCS experiments along with maximum entropy based (MEMFCS) analysis of narrow dispersed samples. We observed diffusion

dynamics of these polymers is heterogeneous and strongly dependent on the chain morphology. Our analysis suggests that high molecular weight chains possessed globular structure and diffused faster in solution, whereas the low molecular weight chains possessed inter-particle interaction and show slow diffusion in solution.

Besides the presented work in this thesis, we present the following research proposal as an future outlook of this thesis.

5.2 Future Outlook

The proposed picture of light-QD interaction is that an absorbed photon may cause ionization by transferring the electrons to surface trap states with a small probability $\approx 10^{-6}$ [1, 2]. Once charged, the QD does not emit light and emission quantum yield is reduced. Therefore, the charged QD turns dark or enters to "off" state also called as photo-darkening. Even though the photo-ionization probability and the photo-darkening probability which was estimated in FCS measurements are in the same order of magnitude, it is not sufficient to prove the hypothesis that photo-ionization directly causes photo darkening. A possible experiment to establish this hypothesis is measurement of charge and luminescence simultaneously from a single QD under continuous illumination. Such measurement is possible by combining Electrostatic Force Microscopy (EFM) along with single molecule fluorescence detection. Here, we provide a brief introduction to EFM and progress towards the integration of EFM with fluorescence for simultaneous charge and photo detection.

Electrostatic Force Microscopy

Electrostatic force microscopy (EFM) is dynamic non-contact atomic force microscopy where the electrostatic force is probed. This force arises due to the attraction or repulsion of separated charges. Electrostatic force is a long-range force and can be detected 100 nm from the sample. During EFM measurements, scans are conducted twice along the same line in order to minimize the topography effects on the electrostatic force gradient

signal. In the first scan, topographical profile of the specimen is obtained in intermittent contact mode. Then, the tip is lifted to a predetermined height, and the second scan is performed at a constant separation between the biased tip and the sample surface. The tip-sample separation is maintained constant by following the topographical profile of the sample. The conductive tip is biased during the second scan, and the interaction between the biased tip and the sample influences the oscillation phase of the vibrating cantilever. These oscillations in phase shifts are detected and processed by the external lock-in amplifier to generate electrostatic force gradient signals [3, 4, 5]. Schematic of EFM measurement is shown in figure 5.1.

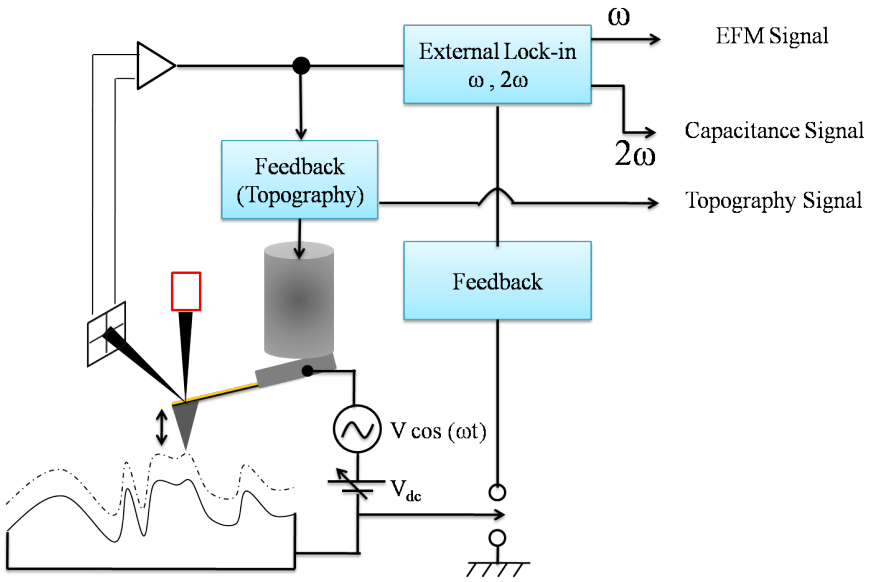

Figure 5.1: Schematic diagram of the electrostatic force microscope based commercial AFM set up. External Lock-in amplifier are used for the detection of ω and 2ω signal

When a voltage V occurs between the sample and the EFM Tip the electrostatic force F can be written as

$$F = \frac{1}{2}\frac{dC}{dz}V^2 \tag{5.1}$$

where C is the tip to sample capacitance. The voltage V is composed of the applied dc (V_{dc}) and sinusoidal voltages ($V_{ac}sin(\omega t)$). In addition to this, voltage induced between the tip sample (V_s) also contribute the V. Therefore, substituting the $V = V_{dc} + V_s + V_{ac}sin(\omega t)$ and rearranging the terms, force can be decomposed in the following three

terms. First term is

$$F_{dc} = \frac{1}{2}dC/dz[(V_{dc} + V_s)^2 + \frac{1}{2}V_{ac}^2] \tag{5.2}$$

This term represents bending of the cantilever and difficult to detect.
Secondly,

$$F_\omega = dC/dz[(V_{dc} + V_s)V_{ac}sin(\omega t)]. \tag{5.3}$$

This term has a linear dependence on the capacitive coupling and sample voltage. So capacitive coupling and the voltage contrasts can be seen in the force signal F_ω.

If second feedback loop is injected with proper value of external voltage to fulfill the condition such that $F_\omega = 0$. Then the surface voltage variations can be measured. This is called Kelvin Probe Microscopy. The third term is

$$F_{2\omega} = \frac{-1}{4}dC/dzV_{ac}^2cos(2\omega t). \tag{5.4}$$

This force term is used to measure the work function of the surfaces at atomic scale.

If charges are involved instead of voltages, this can be observed in the F_ω signal [6]. Let the tip sample separation z and the static charge on the surface is Q_s then the induced Coulomb force on the tip is CV_{ac}. Now, F_ω term can be written as the following

$$F_\omega = [dC/dzV_{dc} - Q_sC/4\pi\epsilon_0 z^2]V_{ac}sin(\omega t). \tag{5.5}$$

So the sign and position of charges Q_s can be obtained but their measurement strongly depends on the tip and sample configuration. Thus by using EFM non-contact method the topography and the surface charge can be measured.

Central hypothesis of photo ionization causes photo darkening which has no direct evidence yet can be measured using combination of EFM and fluorescence. The schematic of this measurement shown in figure 5.2.

The proposed experimental procedure is as following. QDs are immobilized on a conducting surface such as ITO coated glass coverslip and are optically excited. Firstly, a

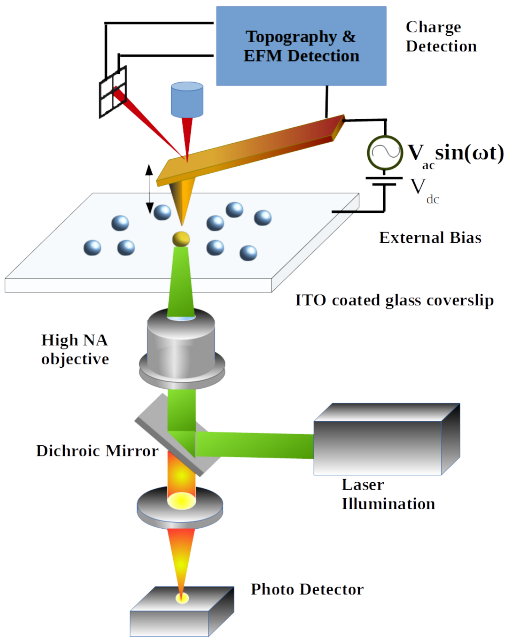

Figure 5.2: Schematic diagram of the proposed measurement

normal topographic image of the sparse QDs will be recorded and then deliberately a conducting cantilever will approached on to a single QD or a few QDs. Now, the charge signal from the external lock-in $F(\omega)$ and the time trace of fluorescence are simultaneously recorded under continuous laser illumination. We expect that performing such measurement can directly provide the relation between the photo charging and photo darkening. We are currently developing this technique to test the hypothesis. Till now, we have been able to integrate the fluorescence detection with the commercial AFM setup from JPK instruments which has a capability of electrostatic force measurement. Illumination port of inverted optical microscope (Zeiss) has been modified for the laser excitation. The side port of the camera port has been modified to pinhole to detect the photons. Here, we use similar confocal detection geometry for photon detection. Figure 5.3 shows the picture of experimental setup designed for proposed measurement.

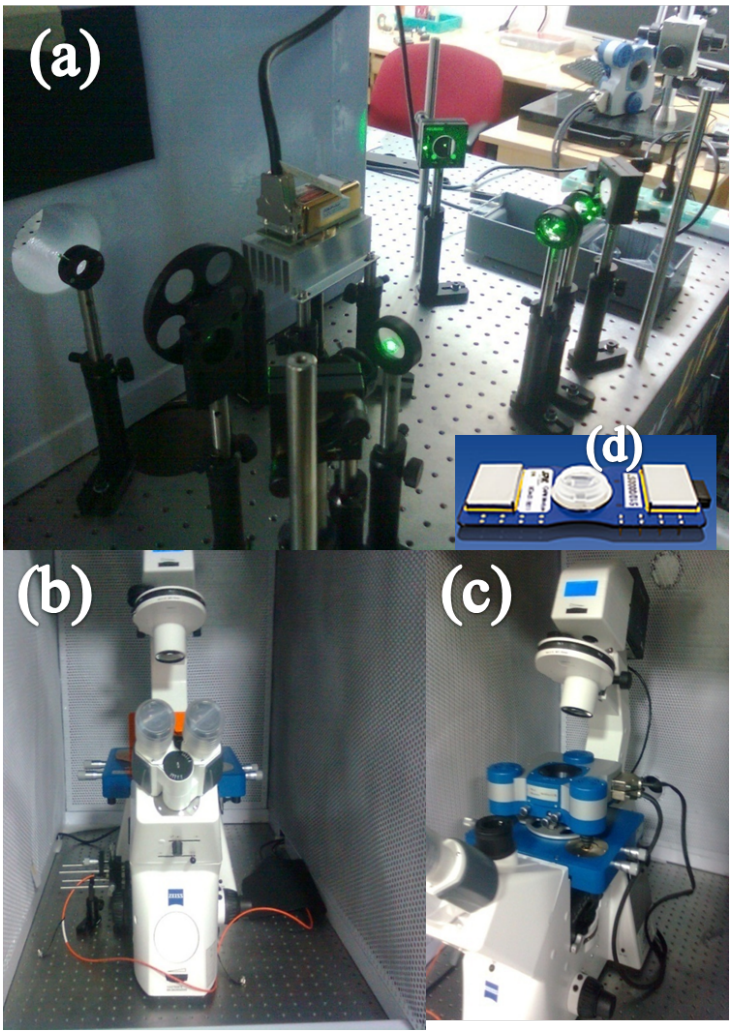

Figure 5.3: Images of the Experimental set up a) Laser excitation optics b) Detection at the side port of Zeiss inverted microscope c) AFM head placed on the integrated stage. d) Cantilever holder along with circuit component to perform EFM measurements

5.3 Other future plans

Some of the other possible experiments are to synthesize novel QDs such as core/shell QDs with varying shell/core thickness can prevent blinking. The methodology that we have developed using FCS can be a quick tool to quantify the amount of blinking in these novel QDs. Such experiments are currently in progress [7-11].

The field of conjugated polymers and semiconductor nanocrystals had been developing in parallel, with little overlap and interactions. As the both semiconducting organic/inorganic nanomaterials are appealing optoelectronic materials[8, 9]. There is a possibility of combining and create a hybrid of these two materials to obtain the desired properties from both materials complimented the downside of individual materials. In particular, blends of conjugated polymers and semiconductor quantum dots (QDs) have interesting applications in light-emitting diodes photovoltaics, and biosensing [12-15]. The interaction between the excited states of these two materials, can determine the optoelectronic properties of the resulting hybrid material and needs to be understood. Specifically, charge separation and electron transfer are present in both photo-excited conjugated polymers and QDs and are crucial light emitting and biosensing applications. Therefore, one of our future plans is also to focus on such hybrid materials along with above mentioned sensitive measurements to nurture the fundamental scientific understanding and to deliver cutting edge technologies.

Bibliography

[1] M. Nirmal et al., Nature, 1996, 383, 802.

[2] T. D. Krauss et al., J. Phys. Chem. B., 2001, 105, 1725.

[3] Y. Martin, H. K. Wickramasinghe, Applied Physics Letters, 1987, 50, 1455.

[4] Girad P, Nanotechnology, 2001, 12, 485.

[5] Gil A, Colchero J, Gomez-Herrero J and Baro A M, Nanotechnology, 2003, 14, 332.

[6] Romain Stomp, Yoichi Miyahara, Sacha Schaer, Qingfeng Sun, Hong Guo, and Peter Grutter, 2005, 94, 056802-1.

[7] Zhihua Xu, Corey R. Hine, Mathew M. Maye, Qing ping Meng, and Mircea Cotlet, ACS Nano, 2012, 6, 4984.

[8] J. H. Burroughes, D. D. C. Bradley, A. R. Brown, R. N. Marks,K. Mackay, R. H. Friend, P. L. Burns and A. B. Holmes, Nature, 2009, 347, 539.

[9] C. B. Murray, D. J. Norris and M. G. Bawendi, J. Am. Chem. Soc., 1993, 115, 8706.

[10] V. L. Colvin, M. C. Schlamp and A. P. Alivisatos, Nature, 1994, 370, 354.

[11] Dabbousi, B. O.; Bawendi, M. G.; Onitsuka, O.; Rubner, M. F. Appl. Phys. Lett., 1995, 66, 1316.

[12] Tessler, N.; Medvedev, V.; Kazes, M.; Kan, S. H.; Banin, U. Science, 2002, 295, 1506.

[13] Koktysh, D. S.; Gaponik, N.; Reufer, M.; Crewett, J.; Scherf, U.; Eychmuller, A.; Lupton, J. M.; Rogach, A. L.; Feldmann, J. Chem. Phys. Chem 2004, 5, 1435.

[14] Huynh,W. U.; Dittmer, J. J.; Alivisatos, A. P. Science 2002, 295, 2425.

[15] Campbell, I. H.; Crone, B. K. Adv. Mater., 2006, 18, 77.

List of Publicatoins

1. Fluorescence Correlation Spectroscopy of Gold Nano particles
   Sri Balaji, ***A. V. R. Murthy****, Neha Tiwari and Sulabha Kulakarni*
   Spectroscopy Letters, 45:1, 22-28 (2012)

2. Probing the Role of Chain Length on the Diffusion Dynamics of p-Conjugated Polymers by Fluorescence Correlation Spectroscopy
   A. V. R. Murthy*, Mahima Goel, Shivprasad Patil, and M. Jayakannan*
   J. Phys. Chem. B, 115, 10779-0788

3. Photo-induced dark fraction due to blinking and photo-darkening probability in aqueous CdTe Quantum Dots
   A. V. R. Murthy*, Padmashri Patil, Shouvik Datta and Shivprasad Patil*
   J. Phys. Chem. C, 117, 13268-3275